Antifouling Biocides
Leaching, Degradation and Fate

Table of Contents

Preface

The project about the leaching, degradation and fate of antifouling biocides has been conducted between 2016 and 2020 and was founded by the Danish Environmental Protection Agency - Pesticide Research Programme. The project was performed at Aarhus University, Department of Environmental Science. Key persons in the project were Kai Bester, Ulla E. Bollmann, Jasper T. Koning and Yi Cai. Additionally, Burhard Waterman (LimnoMar) was involved as a consultant.

The progress of the project has been followed and discussed by the working group EXPOSURE consisting of: Henrik F. Brødsgaard, Anne Mette Madsen, Niels Lindemark, Carsten Suhr Jacobsen, Jesper Johannesen, Kristian Brandt, Kai Bester, Jes Vollertsen, Marja Koski, Hanne Ingmer, Nina Gregersen, Henrik Wennermark and Stine Nørgaard Schmidt.

The report is split into three main topics (1) occurrence, (2) degradation and fate, and (3) leaching. Parts of this project report have been published in international scientific journals. Additionally, the project results have been presented at several international conferences.

J.T. Koning, U.E. Bollmann, K. Bester. The occurrence of modern organic antifouling biocides in Danish marinas. Marine Pollution Bulletin, 2020, 158, 111402.

J.T. Koning, U.E. Bollmann, K. Bester. Biodegradation of third-generation organic antifouling biocides and their hydrolysis products in marine model systems. J. Haz. Mat., 2021, 406, 124755.

Y. Cai, J.T. Koning, K. Bester, U.E. Bollmann. Abiotic fate of tolylfluanid and dichlofluanid in natural waters. Sci. Total Environ., 2021, 752, 142160.

Y. Cai, J. Apell, N.C. Pflug, K. McNeill, U.E. Bollmann. Photochemical fate of medetomidine in coastal and marine environments. Water Research, 2021, 191, 116791.

Summary

Antifouling biocides are used to keep the underwater boat hulls free of barnacles, algae and other microorganisms and thereby reduce roughness of the surface to give you higher speed and lower fuel consumption. Already with the increasing substitution and finally ban of tributyltin (TBT) products, huge changes of the antifouling market happened. Within the implementation of the Biocidal Products Regulation (The European Parlament and the Council of the European Union, 2012) also antifouling products (product type 21) underwent reassessments; some compounds were prohibited as no dossiers were submitted and other new products came into the market.

A market survey showed that currently mostly inorganic antifouling ingredients and Pyrithion based antifouling products are used. It seems like Dichlofluanid, Tolylfluanid, Tralopyril and Medetomidine will be upcoming items.

In the framework of this project new analytical protocols were tested to determine these new antifoulings including metal-organic compounds such as Zinc-Pyrithion. While the organic compounds a priori produced little analytical problems, Zinc-Pyrithion proved to hydrolyse very rapidly (within hours)..Chemical markers were suggested to trace inputs of this compound. Generally it can be outlined that currently or upcoming antifouling compounds hydrolyse rapidly but seem to produce relatively stable metabolites. E.g., Dichlofluanid and Tolylfluanid hydrolyse to DMSA and DMST respectively. DMST and DMSA are then both biodegraded and photodegraded to DMS, which is already known from other contexts to be persistent. In a monitoring study, both DMST and DMSA were detected in nearly all samples from and around marinas in Denmark. However the concentrations were comparatively low, which is probably due to the (currently) low market penetration of these solutions. Interestingly, relative high concentrations of Irgarol (Cybutryn) were determined in sediments of marinas. A more detailed comparison with the concentrations in the water showed the water/sediment was not in equilibrium concerning Irgarol, Indicating towards a transport of Irgarol from the sediments to the aqueous phase, which indicates that the Irgarol concentrations are due to older usages and not contemporary emissions.

The hydrolysis experiments showed, that results obtained in pure water cannot easily be transferred to brackish or sea water. Hydrolysis is especially relevant for the metal-organic compounds as well as Tolylfluanid, Dichlofluanid and Tralopyril. For all these compounds, the hydrolysis leads to defined hydrolysis products. In the biodegradation experiments and photodegradation experiments, these hydrolysis products had to be included.

Photodegradation of DMST and DMSA gave kinetics in the expected range resulting in a multitude of photodegradation products. Opposite to the assessment report, medetomidine proved to be photodegradable. – In the assessment report only a comparison of sunlight and UV-vis spectrum of Medetomidine is presented and as no overlap was seen it was concluded it cannot be photodegraded.- In reality indirect photodegradation is relevant and leads to several identifiable photodegradation products.

Biodegradation leads to a multitude of metabolites that are to some extent known from other contexts. Especially the formation of DMS from Tolyfluanid and Dichlofluanid and the formation of BCCPCA from Tralopyril needs mentioning. Medetomidine is metabolized to medetomidine acid.

Leaching of antifouling compounds from antifouling paints seems considerably reduced in comparison to paints such as used on facades. It was not 100% possible to reveal the mechanism of the release in the framework of this project.

All the biodegradation and photodegradation products found in this project indicated towards a gap in the biocidal product regulation, as this is not covering the assessment of transformation products.

Sammenfatning

Antifoulingbiocider anvendes i bundmaling af skibe og både for at forhindre, at alger og muslinger sætter sig fast på skiber og både og dermed mindsker deres fart og øger forbruget af brændstof. Markedet for bundmalingstyper er ændret gradvist med introduktionen af nye biocider og senere et forbud mod tributyltin (TBT)-produkter. Med implementering af Biocidforordningen (The European Parlament and the Council of the European Union, 2012) blev antifouling-midler (produkttype 21) revurderet; salget af nogle stoffer ophørte, mens nye kom på markedet. I dette projekt skal der udvikles en ny analysemetode, til at måle koncentrationer af pt. markedsførte antifoulingbiocider i vand og sediment. Ud over monitorering af antifoulingbiocider i det danske vandmiljø, skal der udføres nogle udvasknings- og nedbrydningsforsøg. Disse vil generere vigtige data om emission af antifoulingbiocider fra moderne bundmalinger og deres skæbne i vandmiljøet. Til sidst, skal laboratorie-resultaterne sammenlignes og verificeres med data fra monitoreringsstudiet.

Inden for rammerne af projektet blev nye analytiske protokoller testet for at bestemme de nye antifoulingbiocider, inklusiv metalorganiske forbindelser som Zink-Pyrithione. De organiske antifoulingbiocider havde *a priori* få analytiske problemer, der var nemt at løse. Zink-Pyrithione, på den anden side, viste sig at hydrolysere hurtigt (inden for et par timer). Derfor blev det foreslået at analysere nedbrydningsprodukter i stedet for Zink-Pyrithione selv. Generelt var det klart, at de nuværende antifoulingbiocider hydrolyserer hurtigt, men det resulterer i relativt stabile nedbrydningsprodukter. Eksempelvis hydrolyserer Dichlofluanid og Tolylfluanid til DMSA og DMST med en halvt liv under seks timer. DMSA og DMST nedbrydes derefter videre gennem biologisk nedbrydning og fotodegradering til DMS, hvilket allerede (fra andre sammenhænge) er kendt for at være persistent. I en overvågningsundersøgelse blev både DMST og DMSA fundet i næsten alle prøver fra og omkring lystbådehavne i Danmark. Koncentrationerne var dog forholdsvis lave, hvilket sandsynligvis skyldes, at disse løsninger (for øjeblikket) har lav markedsindtrængning. På samme tid blev relativt høje koncentrationer af Irgarol (Cybutryn) fundet i sedimenter fra disse lystbådehavner. En mere detaljeret sammenligning af Irgarol koncentrationerne i vand viste, at vandet og sedimentet ikke var i ligevægt med hensyn til Irgarol. Dette var en indikation for transport af Irgarol fra sediment til den vandige fase, og det betyder at Irgarol koncentrationerne skyldes ældre anvendelser og dermet ikke kommer fra nye emissioner.

Hydrolyseexperimetnerne viste, at resultater opnået i rent vand ikke let kan overføres til brakvand eller havvand. Hydrolyse er især relevant for metalorganiske forbindelser såvel som Tolylfluanid, Dichlofluanid og Tralopyril. For alle disse forbindelser fører hydrolyse til definerede hydrolyseprodukter. I eksperimenterne med biologisk nedbrydning og fotonedbrydning måtte disse hydrolyseprodukter medtages. Fotonedbryning af DMST og DMSA gav kinetik i det forventede interval, hvilket resulterede i et multitud af fotodegradationsprodukter. Modsat vurderingsrapporten viste sig medetomidine som fotodegradabelt. - I rapporten præsenteres kun en sammenligning af sollys og UV-vis spektrum af Medetomidine, og da der ikke blev set nogen overlapning, blev den konkluderet, at den ikke kan fotodegraderes. - I virkeligheden er indirekte fotodegradering relevant og fører til adskillige identificerbare fotodegraderingprodukter.

Biologisk nedbrydning fører til en række nedbrydningsprodukter, der til en vis grad er kendt fra andre sammenhænge. Især dannelsen af DMS fra Tolylfluanid og Dichlofluanid samt dannelsen af BCCPCA fra Tralopyril skal nævnes. Medetomedin metaboliseres til medetomedinesyre.

Udvaskning af antifoulingforbindelser fra bundmaling synes at være betydeligt reduceret i sammenligning med maling som brugt på facader. Det var ikke 100% muligt at afsløre mekanismen for frigivelsen inden for rammerne af dette projekt.

Alle de biologiske nedbrydnings- og fotodegradationsprodukter, der findes i dette projekt, indikerer et hul i reguleringen af biocidholdige produkter, da denne ikke dækker vurderingen af transformationsprodukter.

1. Introduction

1.1 Antifouling biocides – definition and legal status

Antifouling (AF) biocides are defined as "products used to control the growth and settlement of fouling organisms (microbes and higher forms of plant or animal species) on vessels, aquaculture equipment or other structures used in water" (PT21 of the Biocidal Products Regulation (European Parliament and Council 2012)). AF biocides are needed to keep the underwater boat hulls free of algae and other microorganisms, thus reducing the transport of non-indigenous species, and thereby reduce roughness of the surface to give you higher speed and lower fuel consumption.

A previously popular antifouling biocide, tributyltin (TBT), has been banned internationally by the International Maritime Organization since 2008 for its adverse effects on non-target organisms (IMO, 2001). In response, the antifouling market has changed in Europe also due to the implementation of the Biocidal Products Directive (98/8/EC) in which product type 21 covers antifouling biocides.

Currently, dossiers have been submitted for twelve active ingredients (Table 1) for the approval as product type 21. Besides cybutryn (irgarol 1051), which was not approved, as well as Zinc-Pyrithione for which the decision is outstanding, all remaining AF biocides were approved for PT21. As no dossiers were submitted for chlorothalonil [2,4,5,6-tetrachloro-isophthalonitrile], diuron [3-(3,4-dichlorophenyl)-1,1-dimethylurea], TCMTB [2-(thiocyano methylthio) benzothiazole] or TCMS pyridine [2,3,5,6-tetrachloro-4-(methyl sulphonyl) pyridine], they are prohibited to be used in AF products after 2008.

TABLE 1: Substances with dossiers submitted for the approval in product type 21 (Approval status by 08/11/2020).

Compound	IUPAC name	CAS No	Formula	Approval PT21
Cybutryn Irgarol 1051	2-methylthio-4-tertbutyl-amino-6-cyclopropyla-mino-s-triazine	28159-98-0		no 2016/107
DCOIT SeaNine 211 Kathon 5287	4,5-dichloro-2-n-octyl-4-isothazolin-3-one	64359-81-5		√ (01/01/2016) 437/2014
Dichlofluanid	N-dimethyl-N-phenylsulph-amide	1085-98-9		√ (01/11/2018) 2017/796
Tralopyril Econea	4-bromo-2-(4-chloro-phenyl)-5-(trifluorome-thyl)-1H-pyrrole-3-car-bonitrile	122454-29-9		√ (01/01/2015) 1091/2014
Tolylfluanid	N-[dichloro(fluoro)me-thyl] sulfanyl-N-(dime-thylsulfamoyl)-4-methyl-aniline	731-27-1		√ (01/01/2016) 2015/419
Medetomidine	5-[1-(2,3-dimethylphe-nyl) ethyl]-1H-imidazole	86347-14-0		√ (01/01/2016) 2015/1731
Zinc-Pyrithione ZnPT	zinc complex of 2-mercaptopyridine-1-oxide	13463-41-7		decission outstanding
Copper pyrithione CuPT	copper complex of 2-mercaptopyridine-1-oxide	14915-37-8		√ (01/01/2016) 2015/984
Zineb	zinc ethylene bis dithio-carbamate	12122-67-7		√ (01/01/2016) 92/2014
Copper flakes (coated with aliphatic acid)		7440-50-8	Cu	√ (01/01/2018) 2016/1088
Copper Thiocyanate		1111-67-7		√ (01/01/2018) 2016/1090
Copper(I)oxide		1317-39-1	Cu_2O	√ (01/01/2018) 2016/1089
Free radicals generated in situ from ambient air or water				decission outstanding

1.2   Analytical methods

While analytical methods for pure organic AF biocides as SeaNine 211 (DCOIT), Irgarol 1051 (cybutryn) or diuron are well established for detection of low concentrations (down to ng L^{-1}) (e.g. Bollmann et al. 2014), the analysis of metal containing AF biocides as ZnPT and Zineb are rare. Especially, for the zinc and copper complexes of 2-mercaptopyridine-1-oxide (pyrithione) problems in the analytical procedure have been reported widely and no standard analytical method is developed so far (Bones et al., 2006; Caren Anja Doose et al., 2004; Thomas, 1999, 1998; Yamaguchi et al., 2006). Most promising for the pyrithiones seems to be the transchelation from ZnPT into the more stable CuPT and analysis via HPLC-MS with atmospheric pressure chemical ionization (APCI) (Bones et al., 2006). However, this restricts from analyzing CuPT and ZnPT in parallel. Also, several interactions with the stationary phase in chromatographic systems have been described (Doose et al., 2004).

1.3   Sources and concentrations

Usually in winter and spring, old paints are removed from the boat hulls before repainting to reduce build-up of old paint over the years (Figure 1). This causes usually the formation of AF paint particles (Turner, 2010) and pollution of boatyards with AF biocides (Eklund and Eklund, 2014). Methods to reduce the environmental pollution with the removal of the old paint have been studied and suggested. (Højenvang, 2003).

FIGURE 1: Removal of old AF paint (left) and repainting of the underwater boat hull (right).

The freshly painted boats are launched and slowly release biocides to the marine environment. A study on a ship equipped with DCOIT (Dichloroctylisothiazolinone) AF paint showed that the water concentration decreased rapidly within the first 10 m from the source, from several hundred ng L^{-1} to below 50 ng L^{-1} further away (Steen et al., 2004).

Also, several other studies have shown that marinas are hot spots for AF contamination, with the antifoulings being detected at relatively high concentrations in both water and sediments(Konstantinou and Albanis, 2004). Especially in harbors with low water exchange and high boat density considerably higher irgarol concentrations (300-440 ng L^{-1}) have been measured than in harbors with tidal water exchange or open harbors (<100 ng L^{-1}) (Biselli et al., 2000).

In general, many studies focused on the environmental occurrence and fate of globally used AF biocides, namely irgarol, copper or diuron. A summary of the data can be found in Thomas and Brooks (2010) review (Thomas and Brooks, 2010). For other AF biocides as DCOIT, CuPT and ZnPT only very little data is available on their occurrence. For the other AF biocides no data is available at all.

1.4 Biocide release from antifouling paints

An optimal antifouling biocide needs to be effective, while simultaneously limiting its environmental impact (Thomas and Brooks, 2010). Antifouling biocides have to dissolve in order to reach their desired effect (Kiil et al., 2003). As such controlling dissolution of the biocide is the key mechanism 1) maintaining the effective concentration, while 2) reducing input to the environment.

Several different AF paints are on the market (Figure 2): hard AF paints meaning hard polymer matrix where the biocides are supposed to leach out, and on the opposite soft/soluble/controlled depletion polymers/self-polishing paints (depending on the producer) generally using the principle of a water soluble polymeric matrix, where the biocides are released when the surrounding paint matrix is dissolved (Figure 2). Very few studies on leaching kinetics from AF biocides from paints are available (Grunnet and Dahllöf, 2005) and none of them included the different paint polymer principles within their study approach (Ryuji Kojima et al., 2016; Yebra et al., 2006, 2004).

The antifouling paint matrix has a major influence on the leaching rate of the biocides. In general, there are two types of paint matrices: insoluble and soluble paint matrix. An insoluble paint matrix, often called hard paints, relies on water entering pores to solubilize the biocide (Almeida et al., 2007; Styszko and Kupiec, 2016). For these paints, the initial biocide release is high and the leaching rate decreases exponentially over time (Kiil et al., 2003). The soluble paint matrices, on the other hand, often incorporate the biocides into a water-soluble polymer (Chambers et al., 2006). Here, the biocides will also leach into water that enters pores in the matrix. However, the depth of the pores is regulated by the matrix itself dissolving, which leads to a release rate that is more controlled than the insoluble matrix paints (Falaye and Oyewumi, 2011; Hellio and Diego Meseguer, 2009).

The leaching process itself entails multiple processes. A painted surface, once submerged, will start to absorb water. This absorption process is paired with the release of a relatively large quantity of biocides, as the biocides at the upper surface layer are easily dissolved (Uhlig et al., 2019). The leaching process then continues with the remaining biocides that lie deeper inside the paint film or are more strongly adsorbed to the paint matrix (Uhlig et al., 2019). There are two mechanisms underlying further leaching, dissolution, and diffusion (Erich and Baukh, 2016; Schoknecht et al., 2013). Dissolution occurs when the biocides desorb from the paint matrix and enter water-filled pores (Erich and Baukh, 2016). Then, diffusion is the process that transports the biocides out of the pores and towards the paint surface (Erich and Baukh, 2016).

Either mechanism, dissolution or diffusion, can limit the leaching rate of biocides from paint. If dissolution is the limiting process, then the cumulative biocide release is linear with time (Erich and Baukh, 2016). Diffusion limited leaching, on the other hand, shows a linear relationship with the square root of time (Erich and Baukh, 2016; Saltzman, 2001). However, this linear relationship is only valid until 60% of the biocides have leached, hereafter, the leaching dynamics change as the concentration gradients driving diffusion change (Vergnaud, 1993).

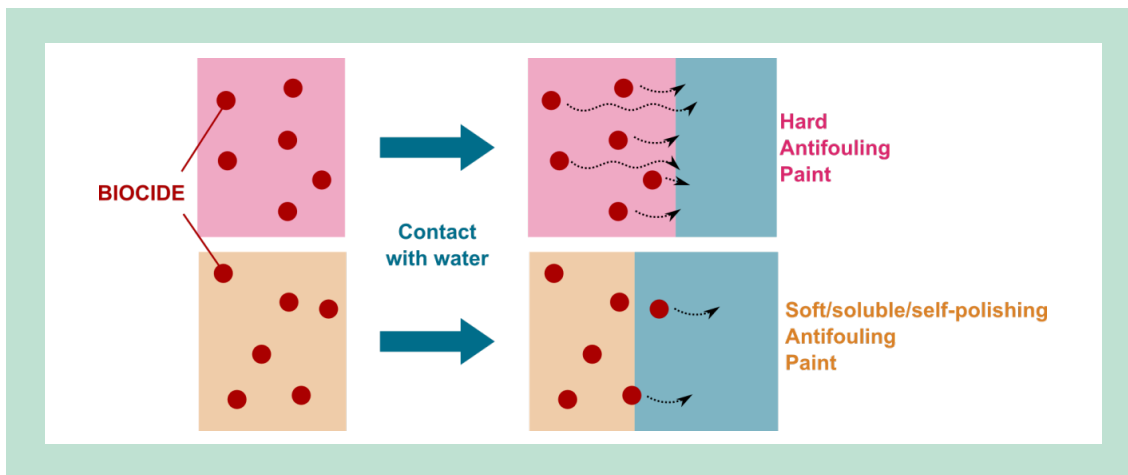**FIGURE 2:** Different types of AF paint and the assumed leaching behavior of biocides. While for the hard antifouling paints, the polymer is unchanged and the antifouling ingredient needs to migrate through the polymer, for the self-polishing paints it is assumed that the polymer is removed from the surface and there is thus always "fresh" antifouling ingredient at the surface without it migrating through the paint.

2. Hypotheses and Objectives

Several studies on AF biocides are from the early 2000-years (Biselli et al. 2000, Thomas 1998, Thomas et al. 2000, Thomas et al. 2002, Voulvoulis et al. 1999, Albanis et al. 2002) within the framework of the ban of tributyltin (TBT). However, since then the AF market has changed due to the approval and disapproval of active compounds. Hence, reliable updated data are needed on occurrence and fate of currently used AF biocides in the marine environment. The knowledge on transformation products (TPs) is limited and in comparison to pesticide registration the requirements on data on TPs is considerably lower under the Biocidal Products Regulation (European Parliament and Council 2012). Moreover, modern AF paint technologies with self-polishing polymer matrices (SPCs) or eroding matrices in so-called CDPs (Controlled Depletion Polymers) are predominantly in use. Hence, leaching performance might differ considerably from that of hard AF paints.

The project had the following objectives:
- Establish a standard analytical method for present-day antifouling biocides
- Monitoring of AF biocides in selected harbors (predominantly marinas), open water, and sediment
- Identification of degradation products and their fate in the environment
- Determining leaching from antifouling paint including hard paints and soft/soluble/CDPs, self-polishing paints (SPCs)
- Comparing and verifying the predictions from the laboratory measurements with the monitoring data from Danish recreational marinas.

3. Market survey

An online survey was conducted, where material safety data sheets (MSDS) were scanned and scored for which biocide is in use. A selection was made so that only antifouling paints available for purchase in Denmark were used, which led to a total of 145 MSDS documents from 9 different manufacturers, sold in the period 2015-2019. The paints were divided into two groups: one group for use on recreational vessels and one for commercial vessels. This way 104 paints ended up in the recreational group, while 45 paints were in the commercial group (Table 2).

About 43 % of all paints in the recreational group contained one of the antifouling biocides, the remaining 57% of antifouling paints did not contain organic biocides, but only inorganic copper or zinc. The most common biocide found in the MSDS data sheets was the metal-organic Zinc-Pyrithione, applied in 23 % of the paints (Table 2). The second most abundant biocide was dichlofluanid found in 7% of the paints. Other biocides found were: copper pyrithione at 5%, irgarol also at 5%, zineb at 4% and tralopyril in 3% of the cases. Moreover, the biocides tolylfluanid, DCOIT and medetomidine were not found (Table 2).

Biocides seeed more commonly added to commercial antifouling paints, where 68% of the assessed MSDS sheets indicated the use of organic biocides. In these paints about 52% used copper pyrithione and 34% used Zineb. DCOIT was also found in only 2% of the paints. The biocides, dichlofluanid, tolylfluanid, tralopyril, irgarol, medetomidine and Zinc-Pyrithione were not found in the scanned MSDS sheets.

Therefore, there seems to be a big difference between antifouling paints used for recreational or commercial vessels. The commercial paints contain to a higher degree metal-organic biocides. Moreover, the commercial paints seem to favor copper pyrithione, while recreational paints tend to rely on Zinc-Pyrithione.

TABLE 2: Market survey of organic antifouling biocide containing paints on the market in Denmark during 2015-2019.

Biocide	Recreational	Commercial
Dichlofluanid	7	0
Tolylfluanid	0	0
Tralopyril	3	0
Irgarol*	5	0
DCOIT	0	1
Medetomidine	0	0
Copper pyrithione	5	21
Zinc-Pyrithione	24	0
Zineb	4	14
Sum biocides	45	28
Total paints surveyed	104	45

* only in MSDS from 2015

4. Materials and methods

4.1 Organic biocides and transformation products

An overview over the organic biocides and their relevant hydrolysis products, which are covered by this project, can be found in Table 3. Additional transformation products are discussed in the respective chapters (Phototransformation products in Tables 8 and 9, Biodegradation products in Figure 31). Compounds were used as received from the suppliers, without any further purification.

TABLE 3: Supplier of organic biocides covered by this project and relevant hydrolysis products.

Compound	IUPAC name	Parent compound	CAS No	Supplier
Cybutryn (Irgarol)	2-methylthio-4-tertbutyl-amino-6-cyclopropylamino-s-triazine		28159-98-0	Dr. Ehrenstorfer
DCOIT	4,5-dichloro-2-n-octyl-4-isothazolin-3-one		64359-81-5	Thor GmbH Speyer
Dichlofluanid	N-[dichloro(fluoro)methyl] sulfanyl-N-(dimethylsulfamoyl)aniline		1085-98-9	Dr. Ehrenstorfer
Tralopyril	4-bromo-2-(4-chlorophenyl)-5-(trifluoromethyl)-1H-pyrrole-3-carbonitrile		122454-29-9	AKoS
Tolylfluanid	N-[dichloro(fluoro)methyl] sulfanyl-N-(dimethylsulfamoyl)-4-methylaniline		731-27-1	Sigma-Aldrich
Medetomidine	5-[1-(2,3-dimethylphenyl) ethyl]-1H-imidazole		86347-14-0	Toronto Research Chemicals
DMSA	(dimethylsulfamoylamino) benzene	Dichlofluanid	4710-17-2	Sigma-Aldrich
DMST	1-(dimethylsulfamoyl amino)-4-methylbenzene	Tolylfluanid	66840-71-9	Toronto Research Chemicals
BCCPCA	3-bromo-5-(4-chlorophenyl)-4-cyano-1H-pyrrole-2-carboxylic acid	Tralopyril		In-house synthesis

In-house synthesis of the Tralopyril-hydrolysis product BCCPCA

The hydrolysis product of Tralopyril, BCCPCA, is not available commercially. As such, the decision was made to synthesize the compound in the laboratory to be able to quantify Tralopyril in the environment. A previously reported method was used (Downs et al., 2017) with small adaptions to reduce complexity of the operation. The procedure was as follows: 500 mg of Tralopyril was added to 30 mL of methanol. Hereafter, 30 mL of a 5M NaOH-solution was added. This mixture was left standing for 48 hours, after which the methanol was evaporated using a Büchi multiport evaporator (40 degrees, 240 rpm, 100 mBar). Precipitation starts occurring with decreasing methanol content; however, a 38% HCl solution was added dropwise to precipitate all of the compounds remaining in solution. The collected precipitate was then filtered and washed using 250 mL water. The washed precipitate was dried at 80 degrees overnight.

A fraction of the collected precipitate was dissolved in methanol and analyzed using the LC-MS/MS using a Q1 scan as well as targeted MRM analysis (appendix 1.2). In the targeted analysis both the Tralopyril and the BCCPCA could be detected. However, an additional peak was

identified in the Q1 scan. This peak corresponds to BCCPCA with an added methyl group, which could be a residual from using methanol during the synthesis. Nevertheless, the analysis has shown that the compounds can be chromatographically separated. BCCPCA was purified further using a fraction collector in order to produce a clean analytical standard for quantitative analysis.

4.1.1 Water extractions

H2O-philic speedisks (J.T. Baker, Deventer, The Netherlands, P/N 8072-06) were mounted on a vacuum manifold prior to the experiment. The cartridges were then conditioned with 20 mL of methanol (LCgrade, Lichrosolv, Merck). Hereafter, the cartridges were conditioned using 20 mL of deionized water (containing 0.5% phosphate buffer), before loading the 1 L samples via a suction system (vacmaster 10, biotage, Uppsala, Sweden). Then, the cartridges were washed using another 20 mL of phosphate-buffered deionized water. Finally, the biocides were eluted from the cartridges using 20 mL of methanol and 20 mL of acetonitrile, successively (isocratic LC grade, Lichrosolv, Merck). The combined eluates were evaporated to 1 mL using a Büchi Syncore® multiport condenser (Büchi, Flawil, Switzerland) at 50 °C, 240 rpm, and 100 mbar for about 90 min. The remaining extracts were transferred to 1.5 mL autosampler vials and analyzed using HPLC-MS/MS. The entire sets of extractions for the transects were performed over several days due to space limitations on the vacuum manifold. Blank extractions (deionized water) were performed along with each set of samples to control for cross-contamination between samples. Recoveries were tested in spiked deionized water (range from 3 ng/L to 1000(ng/L). Absolute recoveries ranged from 31% to 91%, relative recoveries (IS-corrected) were around 106% ± 24%.

4.1.2 Sediment extractions

Sediment samples were stored in the freezer at −20 °C. The samples were thawed prior to freeze-drying overnight and were then extracted using accelerated solvent extraction (ASE 350, ThermoFisher, United States). For each sample, 10 g of freeze-dried sediment was mixed with 10 g of Hydromatrix (Varian, Palo Alto, CA, USA), this mixture was then added to the ASE-cells, and spiked with the internal standard solution (10 ng/ g). Free space in the 40 mL cells was filled up using Ottawa sand. Extraction was then performed at 80°C, 1000 psi, and using methanol as a solvent. Two cycles were performed with 1 min preheating time, 5 min static time, flushed and purged at 60%. Recoveries were tested by spiking freeze-dried sediment in a range from 0.1 ng/g to 300 ng/g. Absolute recoveries ranged from 15% to 33%, while relative recoveries ranged from 52% to 100%.

4.1.3 HPLC-MS/MS analysis

An HPLC system (Ultimate 3000, Dionex, United States) was used to separate the biocides before detection by MS/MS. The column used for reverse-phase chromatography was a Synergi column (Polar-RP, 4 µm particle size, 80 Å pore size, 150 × 2 mm, Phenomenex, Torrance, CA, USA). Two mobile phases were prepared for reverse-phase chromatography: water (Gradient grade, LiChrosolv, Merck, Darmstadt, Germany) and methanol (HPLC-MS grade, LiChrosolv, Merck, Darmstadt, Germany), both containing 0.2% of formic acid (LiChrosolv, Merck, United Stated). Chromatography for the reverse phase method started with 100% water during the first minute. Afterwards, a linear gradient with methanol started, reaching 60% methanol after 4 min. Hereafter, the fraction of methanol was increased further in a linear gradient to reach 100% at 12 min, where it stayed until 12.5 min. Finally, from 12.5 min to 13.0 min the column was brought back to 100% water, where it stayed until the end of the method at 15.5 min. A flow rate of 300 µL/min was applied for the entire duration. The eluate of the first 3 min of the run was sent to waste to prevent salts from entering into the mass spectrometer and interfering with ionization. The column temperature was maintained at 20 °C during the run. Detection was performed employing an API 4000 (SCIEX, Framingham, MS, USA) triple quadrupole mass spectrometer utilizing electrospray ionization in positive mode. Data treatment was performed in Analyst 1.6.3 (Sciex, Framingham, United States). A calibration line (0.3 ng/mL – 1000 ng/mL(extract)) was

used to calculate concentrations, where internal standards were used to correct for recovery and matrix effect. Limits of detection (LOD) and quantification (LOQ) were determined as 3 times signal to noise and 10 times signal to noise, respectively.

N,N-Dimethylsulfamide (DMS) was added to the project in a later phase. Based on a method described by (Bollmann and Badawi, 2020) a method was established using a Hypercarb column (100 mm × 2.1 mm, particles = 3 µm; ThermoFisher Scientific, Waltham, MA, USA). The following gradient of water and methanol (both with 0.2% formic acid) was used: 0-1 min 1% B; 1-4 min 1 to 100% B; 4-4.1 min 100 to 1% B; 4.1-10 min 1% B. Pyridine-D_5 was used as internal standard.

4.2   Metal-organic biocides

Standards of the metal-organic antifouling biocides were acquired, an overview is presented in Table 4. Two different experiments have been performed to explore how to best analyze the metal-organic antifouling biocides.

For the first experiment Zinc-Pyrithione was dissolved in dichloromethane (DCM) at a concentration of 1 mg/mL. This dissolved Zinc-Pyrithione was spiked into 10 mL water to reach a concentration of 50 µg/mL. This 10 mL solution was split up into fractions, where each fraction consisted of 1 mL in an autosampler vial. Internal standards were added to each 1 mL fraction, to a concentration of 100 ng/mL. The 1 mL fractions were placed in the autosampler tray of the HPLC-MS/MS where they were repeatedly injected into the system. The repeated injections were performed in such a way that 10 injections of 50 µL each were taken from one fraction, before taking 10 injections out of the next fraction and so on until all fractions were injected 10 times. Detection was achieved using a different set-up on the HPLC-MS/MS. For this experiment, a shorter Synergi column (Polar-RP, 2.5 µm, particle size, 100 Å pore size, 50 x 3 mm, Phenomenex, Torrance, CA, United States) was installed on the HPLC. The chromatographic method used the same buffers as the common method (water 0.2% formic acid, methanol 0.2% formic acid), but in a different program. This program was started with 100% water up to the 1st minute. Then a methanol gradient was applied reaching 100% methanol at the 2nd minute. The methanol remained at 100% until 3.5 min, after which water was set to 100% again until the end of the run at 5 min. The flow rate during the experiment was set to 750 µL/min. Parameters such as temperature were maintained according to the common HPLC method. The ion source was also replaced in this experiment, as an Atmospheric-pressure chemical ionization (APCI) source was installed and operated with the following conditions CAD 10, CUR 10, GS1 25, NC5, TEM 400.

In the second experiment, Zinc-Pyrithione and Zineb were suspended into different water types in order to establish their stability in the natural environment. Four different water types were tested: deionized water, artificial seawater (1.2% sea salts (Sigma-Aldrich)), natural water (collected Roskilde fjord July 2018), and filter sterilized natural water (0.22 µM, Whatman syringe filter). Fresh stocks for Zinc-Pyrithione and Zineb were added to each water type to a final concentration of 250 µg/L. These treatments remained as suspensions since the metal-organic biocides do not dissolve in water. The suspensions were homogenized as much as possible and 1 mL was transferred to an HPLC-MS/MS autosampler vial. From here 10 µL was repeatedly injected into the HPLC-MS/MS, with an injection every 15 min for the full experimental duration of 50 hours.

TABLE 4: Metal-organic biocides and their transformation products

Compound	IUPAC name	CAS No	Supplier
Zinc-Pyrithione ZnPT	zinc complex of 2-mercaptopyridine-1-oxide	13463-41-7	Sigma-Aldrich
Copper pyrithione CuPT	copper complex of 2-mercaptopyridine-1-oxide	14915-37-8	Santa Cruz Biotec
Zineb	zinc ethylene bis dithio-carbamate	12122-67-7	Sigma-Aldrich
PT	2-Mercaptopyridine-N-oxide	1121-31-9	Sigma-Aldrich
PT2			
PSA	2-Pyridinesulfonic acid	15103-48-7	Sigma-Aldrich
EU	Ethylene urea	120-93-4	Dr. Ehrenstorfer
ETU	Ethylene thiourea	96-45-7	Dr. Ehrenstorfer
EBIS	5,6-dihydroimidazol[2,1-c][1,2,4]dithiazole3-thione	33813-20-6	AKoS

4.3 Monitoring studies
4.3.1 Selection of marinas
4.3.1.1 Danish marinas

In this study 13 marinas were selected across the Danish island of Sjælland (Figure 3). In these marinas both triplicate water and sediment samples were collected, except for Sydhavnen and Langelinie were only water samples were taken as the sediments were too deep to reach. The marinas were selected for an even distribution around Sjælland, while also covering a wide range of types of harbors. The marinas ranged in size from 80 to 750 berths. Some marinas (Gilleleje, Sydhavnen, Langelinie) were also used for commercial purposes, such as fishing or transport. Several marinas (Frederikssund, Roskilde, Holbæk) were selected for their location at inland fjords. Marinas at the north and western side of Sjælland (Gilleleje, Kalundborg, Korsør) are situated at the Kattegat and have higher salinity than those on the southeastern side of Sjælland that are situated at the entrance to the Baltic Sea (Faxe Ladeplads, Vordingborg, Køge, Langelinie).

4.3.1.2 Seasonal trend and transect

Two marinas were selected for a seasonal trend and a transect study: Brøndby and Roskilde (Figure 3). For the seasonal trend study, seven triplicate water and sediment samples were taken between March 2019 and January 2020 in these two marinas. In this way, the samples cover the entirety of the sailing season, which runs from early May to late September, while most boats are on land during winter time. The transect studies were performed on the 31st of July 2019 in Roskilde and on the 3rd of October 2019 in Brøndby. The transect in Roskilde was collected at a distance of 0 m, 50 m, 120 m, 230 m, 440 m, and 820 m, where 0 m was determined as the slipway (Figure 3). In Brøndby marina, the transect was collected at the following distances: 0 m, 60 m, 230 m, 560 m, 580 m, 1480 m, 2210 m with 0 m taken as the berths closest to the mouth of the marina. Only water samples were collected during these transects, all water samples were collected at a depth of 0.5 m. Distances were determined by GPS coordinates. A different boat was used for each marina, the specific antifouling paints used on the respective boats are unknown. Roskilde marina lies open towards a large inland fjord, containing brackish water (13.06 ± 0.54 PSU). The marina has around 300 berths for boats of various sizes. In contrast, Brøndby marina lies southwards to Køge Bugt and the Øresund strait, at the Western shores of the Baltic Sea in the greater Copenhagen area. Brøndby marina also contains brackish water (8.51 ± 1.54 PSU) and has 550 berths. Moreover, Brøndby marina is surrounded by a

seawall, which may limit water exchange. Neither Roskilde nor Brøndby is separated from the sea by locks, which allows continuous water exchange.
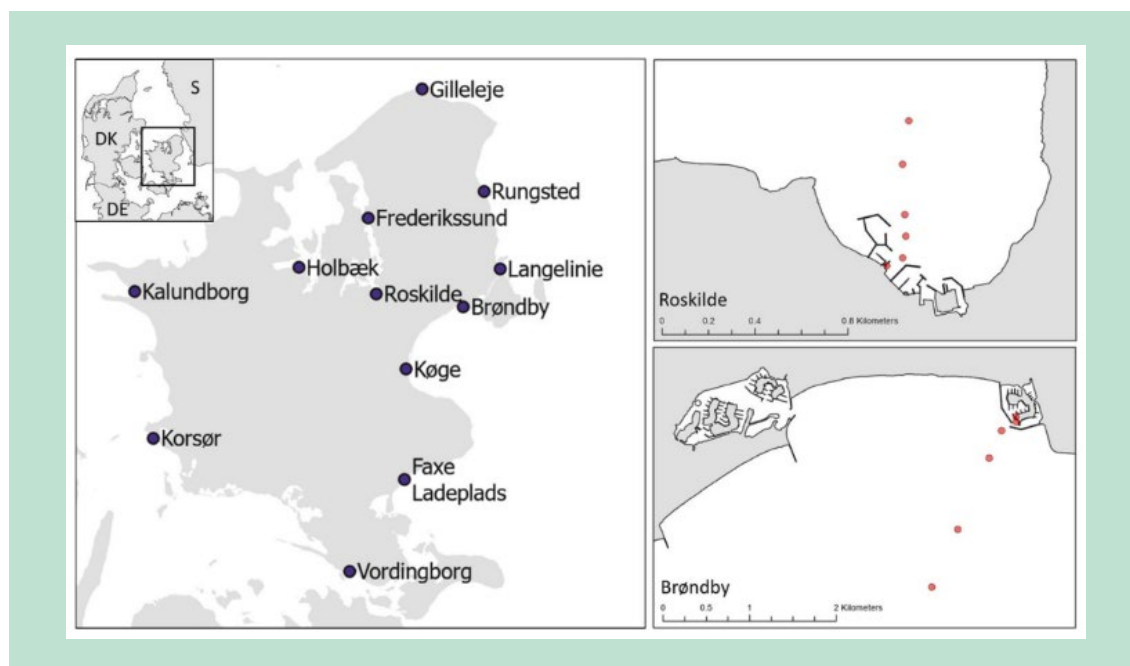

FIGURE 3: The 13 marinas selected across the Danish island of Sjælland.

4.3.2 Water sampling

Water samples were collected at a depth of 0.5 m, using a 1 L pyrex glass bottle mounted on an extendable sampling pole. Triplicates were taken for the seasonal trend and the geographical monitoring; each replicate was taken at a different location roughly in the center of the marina. All samples were transported to the laboratory in a cooled box. Water samples were stored at 4 °C in the fridge and extracted using solid-phase extraction within 24 h. A composite sample consisting of 15 mL from each replicate was used to measure pH (Orion Versa Star Pro, Thermo Scientific), salinity (Orion Versa Star Pro, Thermo Scientific), and TOC (total organic carbon, TOC-L/TNM-L, Shimadzu, Tokyo, Japan), the data can be found in the Supplementary Table 2.1. In preparation, the samples were spiked with the following internal standards: Octylisothia-zolinone-D17 (OIT)-D17, MedetomidineD3, DMST-D7, Pyridine-D5, Irgarol-D9, and Propicona-zole-D5 at a concentration of 100 ng/L. In addition, a phosphate buffer was prepared at pH 7.6 by adding 0.13 g KH2PO4 and 0.87 g K_2HPO_4 to 100 mL deionized water; the phosphate buffer was then also added to the samples at a final concentration of 0.5% v/v.

4.3.3 Sediment sampling

Sediment samples were collected by dragging an HDPE plastic scoop attached to the telescopic sampling pole across the surface of the sediment up to 1.5 m in depth. The sediment was then transferred to 40 mL glass containers and 50 mL falcon tubes. Triplicates were taken from the same spot near the slipway. The transport of samples was done in a cooled box. Sediment samples were stored in the freezer at −20 °C until extraction by ASE.

4.4   Degradation

Upon leaching to the water phase, antifouling biocides undergo transformation reactions. Both abiotic transformations (hydrolysis and phototransformation) as well as biological transformation processes are possible degradation mechanisms. Both degradation kinetics of the active compound, identification and fate of transformation products were addressed within this project.

4.4.1   Hydrolysis

Several of the organic biocides are known to hydrolyze rapidly in water. An initial hydrolysis experiments was conducted to identify those biocides that are hydrolyzing rapidly. Hydrolysis was followed over a two-weeks' time course. All organic biocides covered by this project (Tralopyril, Irgarol, Medetomidine, Dichlofluanid, Tolylfluanid and DCOIT in a methanol solution) were spiked in 1 mL deionized water to a concentration of 250 ng/mL and kept at room temperature, in the dark during the course of the experiment. Triplicate samples were spiked at respective time points prior analysis: 1 hour, 1 day, 2 days, 3 days, 4 days, 5 days, 6 days, 7 days, 9 days, 11 days and 14 days. These samples were analyzed by HPLC-MS/MS (see paragraph 4.1.3) and were only scanned for the parent compounds, not for transformation products.

A second experiment was performed for rapidly degrading compounds, i.e., Tolylfluanid, Dichlofluanid or Tralopyril. Within these experiments the hydrolysis rate constants were determined as well as those hydrolysis products identified, which needed to be considered in environmental monitoring. These experiments were performed for individual compounds (250 ng/mL) in both deionized water or in sampled fjord water (grab sample, 22/03/2018, Roskilde Fjord, 55°41'30.1"N, 12°04'56.7"E). Alternately, these samples were repeatedly injected into the HPLC-MS/MS in predefined time intervals (30 min) for 25 hours using the auto-sampler. The samples were stored at 8°C in the dark on the autosampler. Both, active compound and respective hydrolysis products (DMSA, DMST, and BCCPCA) were analyzed using HPLC-MS/MS (see paragraph 4.1.3).

4.4.2   Photodegradation
4.4.2.1   Identification of transformation products

Experiments to identify transformation products were performed in a test chamber equipped with three UVC lamps (5W each, Philips, 1.1–1.4 W m^{-2}) as described in (Minelgaite et al., 2017). Tolylfluanid, Dichlofluanid, Medetomidine and Tralopyril were spiked into deionized water with an initial concentration of 15 μM (Volume = 50 mL, MeOH content = 1%) in individual beakers. During irradiation, the solutions were stirred at 10°C. Aliquots (1 mL) were sampled at 0, 5, 10, 15, 20, 25, 30 and 48h. Afterward, samples were stored at 4°C until analysis.

Samples were analyzed on a quadrupole time-of-flight mass spectrometer (TripleToF 5600, AB Sciex, Framingham, MA, USA) equipped with electrospray ionization (ESI) according to (Schlüsener et al., 2015). An Agilent 1200 Series HPLC system with an Agilent Zorbax Elipse Plus C18 column (2.1 mm × 150 mm, 3.0 μm) was used for separation. The mobile-phase flow rate was set to 300 μL/min using a gradient of water and acetonitrile (both with 0.1% formic acid). The injection volume was 10 μL. Information dependent acquisition (IDA) was conducted on the qTOF-MS consisting of full scan (TOF scan) measurements (100-1200 Da) in both positive and negative electrospray ionization mode (ESI +/-) with product ion scans (30 1200 Da) targeted on signals with an intensity higher than 100 cps. Transformation products were proposed based on the high-resolution mass spectrometric data.

If analytical standards were available, the identity of suggested transformation products was validated (using retention time and product ion scan) and quantified using the HPLC-MS/MS (Ultimate 3000, Dionex, Germering, Germany; API 4000, AB Sciex, Framingham, MA, USA). A Synergi polar-PR column (150 mm × 2 mm, particles = 4 μm; Phenomenex, Torrance, CA, USA) was used as separation column. Most compounds (except for p-toluidine and 5A2MP) were analyzed using a multistep gradient of 0.2% formic acid in water (A) and 0.2% formic acid in methanol (B): 0-3 min 0% B, 4-12 min 60 to 80% B, 12-12.1 min 80 to 100% B, 12.1-14 min 100% B, 14-14.1 min 100 to 0% B, 14.1-17 min 0% B. To quantify Tolylfluanid, Dichlofluanid,

DMST and DMSA, the injection volume was set to be 5 µL. The injection volume was set to 100 µL while aiming to quantify the phototransformation products.

Analysis of *p*-toluidine and 5A2MP (carbendazim-D$_4$ as internal standard) was performed under neutral conditions by using a multi-step gradient of water (A) and methanol (B): 0-2 min 0% B, 2-3 min 0 to 60% B, 3-10 min 60 to 80% B, 10-10.1 min 80 to 100% B, 10.1-12 min 100% B, 12-12.1 min 100 to 0 % B, 12.1-15.5 min 0% B. Water (with 0.2% formic acid) at a flow rate of 0.03 mL/min was added into the flow path between column and ESI-source to optimize ionization.

Medetomidine was not degrading under UVC-light in deionized water. Thus, an additional degradation study to identify its transformation products was performed using a UVA-light and a photosensitizer. The photodegradation of 5 mM dexmedetomidine (Sigma-Aldrich) sensitized by perinaphthenone (200 µM, E°*(S*/S$^-$) V (SHE) = 1.03)) in 50:50 ACN: borate buffer (pH = 9.2) to gain sufficient weight for phototransformation products identification on Nuclear Magnetic Resonance (NMR) spectroscopy. Phototransformation products were measured and isolated on LC-UV with a Supelco C18 column (25 × 10 mm, 5 µm) using water and acetonitrile (both acidified with 0.1% formic acid) as gradient. Fraction solutions were dried by blowing N$_2$ first, and redissolved in CDCl$_3$ for following NMR measurement.

Identification and verification of medetomidine phototransformation products were performed in two steps: (i) Bruker AVANCE III-400 spectrometer was operated to collect proton NMR, HSQC (heteronuclear single quantum coherence), HMBC (heteronuclear multiple bond correlation) and carbon-13 NMR spectra, in which deuterochloroform (CDCl$_3$) was used as the solvent. NMR data were treated through Bruker Topspin 3.5 software; (ii) by dissolving the isolated photoproducts into acetonitrile, samples were submitted to q-TOF for product ion scan measurements. MS2 data were interpreted to support NMR analysis results.

4.4.2.2   Validation of pathways

Stock solutions of Tolylfluanid, Dichlofluanid, DMST and DMSA in methanol were spiked into four empty beakers, respectively. The solvent was evaporated overnight to exclude the contribution of methanol in the phototransformation pathways. 10 mL of deionized water was added to prepare an initial concentration of 0.6 µM. Before UVC irradiation, 5 hours of stirring was carried out in the dark to reach complete dissolution. Samples (1 mL) were taken at time points 0, 24, 48, and 72h, respectively. Pathway identification was conducted by using a multi-reaction monitoring method (described in paragraph 4.4.2.1) to compare concentrations of newly identified transformation products produced from Tolylfluanid or DMST, and Dichlofluanid or DMSA.

4.4.2.3   Indirect photodegradation

Zinc porphyrin, which has a low triplet state reduction potential E°*(S*/S$^-$) V 0.78 of SHE (Kalyanasundaram and Neumann-Spallart, 1982), can be used to determine the reaction rate constant with singlet oxygen. Lumichrome, E$_0$*(3S*/S$^-$) = 1.91 SHE (McNeill and Canonica, 2016) higher than ZnP (0.78), is applied as dissolved organic matter sensitizer. The hydroxyl radical-mediated reaction rate can be conducted using H$_2$O$_2$ and NaNO$_2$ as resources, respectively.

DMSA & DMST

The indirect photolysis of DMSA and DMST was carried out at least in duplicates. The previously described photoreactor (Minelgaite et al., 2017) was slightly modified and equipped with nine UVA lamps (Philips TL-D 8W 10 Actinic BL (MASTER), China; installation of 3 on each side of the chamber) emitting a continuous UVA-spectrum with the highest wavelength at 365 nm. A rotating holder with open borosilicate test tubes was placed in the center. 10 mL of the respective solutions were added to the tubes for irradiation and 200 µL was removed at intervals. DMST and DMSA were added using a 5 mM stock solution in acetonitrile, reaching final concentrations of 17 µM and 19.5 µM in the respective tubes. Water-soluble lumichrome (LC, 1 µM), Zinc porphyrin (ZnP, 1 µM) and H$_2$O$_2$ (3 µM) were used as photosensitizers to generate triplet state lumichrome (^{3}LC*), singlet oxygen (^{1}O$_2$), and hydroxyl radicals (·OH). Furfuryl alcohol (FFA, 40

μm) was used as probe compound for lumichrome and singlet oxygen experiments. Meanwhile, sodium benzoate (10 μm) was used as reference compound for hydroxyl radicals. Borate buffer (5 mM) was used to adjust the natural pH conditions (pH = 8.2). Concentrations of DMST, DMSA and the probes were determined using HPLC-DAD (Ultimate 3000, ThermoFisher), to reduce contamination of the mass spectrometer with borate buffer. DMST, DMSA and benzoate were determined at wavelength 229 nm. The concentration of FFA was measured at 219nm. A Synergi polar-PR column (150 mm × 2 mm, particles = 4 μm; Phenomenex, Torrance, CA, USA) was used as separation column. Flow rate was 0.3 mL/min, and the gradient was (A) water + 0.2% formic acid and (B) acetonitrile + 0.2% formic acid: 0-2 min 15% B, 2-8 min 15 to 50% B, 8-10 min 50% B, 10-10.1 min 50 to 15% B, 10.1-13 min 15% B. DMS was analyzed using HPLC-MS/MS (paragraph 4.1.3).

Medetomidine

The indirect photodegradation of Medetomidine was conducted in a photochemical reactor (Rayonet) with eight to twelve 365nm bulbs (Southern New England Ultraviolet Co., RPR-3500 Å). 8 mL samples were prepared in borosilicate test tubes, and 200 μL of aliquots was removed at certain time points for quantification.

The photochemical transformation rate constants of Medetomidine with singlet oxygen and triplet-state organic matter were measured through steady-state photolysis in the presence of photosensitizer Zinc porphyrin (ZnP) and model sensitizer lumichrome (LC), respectively. Experiments were conducted at pH 5 and 9, where Medetomidine was in protonated form (Med$^+$) or deprotonated form (Med^0), respectively. In addition, singlet oxygen experiments were conducted at pH 9.3 (borate buffer) and pH10.5 (carbonate buffer). The solutions contained Medetomidine (20 μM), furfuryl alcohol (FFA, 40 μM), acetate buffer (5 mM), and photosensitizer (LC or ZnP, 1 μM). Aliquots were taken at seven time points. Degradation of Medetomidine and FFA was measured by LC-UV (Agilent 1100 series) using a Zorbax XDB-C18 column (3 mm × 150 mm, 5 μM). The mobile phase A (water with 0.1% formic acid) and B (acetonitrile with 0.1% formic acid) were used at a flow rate of 1 mL/min. A gradient mobile phase was used as following: 0-1 min, 83% A; 1-6 min, 83 to 70% A; 6-8.5 min 70%A, 8.6 min 70 to 83% A, and 8.6-11.5 min 83% A. The injection volume was 40 μL. The monitoring wavelength was 219 nm for both Medetomidine and FFA.

Hydroxyl radical-mediated experiments were conducted containing hydrogen perioxide (2 mM) or sodium nitrite (100 μM) as sources of hydroxyl radicals at pH 5.6 and 9.2, where 97.3% and 99% medetomidine were protonated, respectively. Sodium benzoate (10 μM) was used as a probe compound. To prevent the reaction between acetonitrile and hydroxyl radicals, residual acetonitrile in Medetomidine stock solution was evaporated before making reaction solution. Aliquots (200 μL) were sampled at each half an hour. The experiments were reproduced for four times. Degradation of Medetomidine and benzoic acid was measured by high performance liquid chromatography-photodiode array (HPLC-PDA) using a Thermo Hypersil God Aq-01 column (4.6 mm × 150 mm, 5 μM). The mobile phase A (water with 0.1% formic acid) and B (acetonitrile with 0.1% formic acid) were used at a flow rate of 1 mL/min. A gradient mobile phase was used as following: 0 2 min, 80% A; 2-10 min, 60% A; 10-10.1 min 80%A, and 10.1-13.1 min 80% A. The injection volume was 40 μL. The monitoring wavelength was 219 nm for Medetomidine and benzoic acid.

Theoretical background

To determine the steady-state concentrations of singlet oxygen $[^1O_2]_{ss}$ and hydroxyl radicals $[\bullet OH]_{ss}$ in the system, the probe compounds furfuryl alcohol (FFA) and benzoate were used. According to Haag et al. (1984), the consumption rate of the probe compounds can be calculated as follows:

$$-d[FFA]/dt = k_{rxn,FFA}[\,^1O_2]_{ss}[FFA] \tag{Eq. 1}$$

$$-d[benzoate]/dt = k_{rxn,benzoate}[\bullet OH]_{ss}[benzoate] \tag{Eq. 2}$$

The second order rate constants of FFA and benzoate with $^1O_2$ and $\cdot OH$, respectively, have been determined earlier to be $k_{rxn,FFA}$ = 1x10^8 M^{-1} S^{-1} (Appiani et al., 2017) and $k_{rxn,benzoate}$ = 5.9x10^9 M^{-1} S^{-1} (Buxton et al., 1988).

Therefore, the photodegradation rate constant for the target compounds (TC) with the reactive species were calculated by plotting against probes degradation as follows:

$$\frac{k_{rxn,probe}}{k_{rxn,TC}} = \ln\left(\frac{[TC]_t}{[TC]_0}\right) / \ln\left(\frac{[Probe]_t}{[Probe]_0}\right) \qquad \text{(Eq. 3)}$$

Where $k_{rxn,probe}$ and $k_{rxn,TC}$ are the second-order reaction rate constants of the probes (FFA, benzoate) and target compounds with reactive species.

The photolysis of target compounds in natural aquatic environment is primarily considered as a combined contribution of various reactive species reactions. Therefore, the overall observed degradation rate constant k_{obs} can be calculated as a sum of the individual contributions on the degradation of the target compound TC:

$$k_{obs} = k_{TC,\,^1O_2}\left[\,^1O_2\right]_{ss} + k_{TC,\bullet OH}\left[\bullet OH\right]_{ss} + k_{TC,\,^3LC^*}\left[\,^3LC^*\right]_{ss} \qquad \text{(Eq. 4)}$$

$$\text{Contribution of } ^1O_2 = \frac{k_{TC,\,^1O_2}\left[\,^1O_2\right]_{ss}}{k_{obs}}$$

$$\text{Contribution of } \bullet OH = \frac{k_{TC,\bullet OH}\left[\bullet OH\right]_{ss}}{k_{obs}}$$

$$\text{Contribution of } ^3LC^* = \frac{k_{TC,\,^3LC^*}\left[\,^3LC^*\right]_{ss}}{k_{obs}}$$

Where $k_{TC,\,^1O_2}$, $k_{TC,\bullet OH}$, and $k_{TC,\,^3LC^*}$ are the second-order reaction rate constants of target compound (DMST, DMSA or Medetomidine) with the respective reactive species.

4.4.2.4 Natural sunlight photodegradation

Coastal water was collected in Roskilde Fjord (Risø, 55°41'30.1"N 12°04'56.7"E) and sea water was collected from the shore in the southern Kattegat (Liseleje, 56°00'59.4"N 11°57'44.5"E) in Denmark and used without further treatment. Deionized water was produced from an in-house apparatus (Reverse Osmosis Unit maxi RO (Saint-Maurice, France) equipped with an Aquada UV ultraviolet water disinfection (Herford, Germany)) and used as control. Water properties, i.e., pH (Orion Versa Star Pro, Thermo Scientific), salinity (Probe 013005MD conductivity cell, Orion Versa Star Pro, Thermo Scientific), and TOC (total organic carbon, TOC-L/TNM-L, Shimadzu, Tokyo, Japan) were measured prior to the start of the experiment (Table 5). Solar radiation during the experimental days (Figure Appendix 3.1) was measured by a weather station 730m linear distance from the experiment setup (Riedel et al., 2018).

TABLE 5: Properties of deionized water, coastal water and sea water.

	Deionized water	Coastal water	Sea water
pH	6.8	8.3	8.1
Salinity [PSU]	N.D.*	12.0	16.1
TOC [mg/L]	N.D.*	8.08	4.09

* N.D: not determined

The outdoor phototransformation experiments were conducted in a wooden box covered by a quartz glass pane (wavelength transmission ≥ 190 nm). In this box, nine 200 mL glass beakers (11 cm height and 8 cm diameter) were placed in a water bath (8°C) on a multi-position magnetic stirrer. Experiments were conducted in parallel in deionized, coastal and sea water. While two beakers of each water type were exposed to sunlight, one beaker was covered with aluminum foil, serving as dark control (Figure 4). Tolylfluanid, dichlofluanid, medetomidine and tralopyril were spiked into the respective waters as a mixture stock solution to obtain a final concentration of 5 mg/mL (MeOH content = 1.75%). The first sample was collected after stirring for 6 hours in the dark to allow for homogenization, and other aliquots were sampled after 1, 2, 3, 4, 7, 11, 14, 17, 22, 29, 41 and 45 days (25/05/2018 – 10/08/2018). Additionally, to compensate for the water loss by evaporation between sampling time points, deionized water was added to each reactor according to the weight loss between the sampling points. Afterwards, samples were spiked with

internal standards (medetomidine-D$_3$: 0.98 µM and carbendazim-D$_4$: 0.27 µM for acidic and neutral method analysis, respectively) and stored at -20°C until analysis.

Additionally, to the dissipation of the parent compounds, the formation of newly identified transformation products was evaluated. The analytical methods for the parent compounds as well as tolylfluanid and dichlofluanid are described in paragraph 4.4.2.1. As no analytical standards were available for medetomidine, a product ion scan method was used on a UPLC-qToF instrument (6600, Sciex) using a RP18 (2.1 ×30 mm, 1.7 µm) column with a water (+0.1% formic acid) and methanol (+0.1% formic acid) gradient: 0-3 min 0% B, 3-9 min 0-80% B, 9-11 min 80%-100% B, 11-16 min 100% B, 16-16.1 min 100-0% B. The eluate during the first 3 min of the run was directed to waste to prevent the accumulation of salt. Product ion scans targeting the respective m/z of identified transformation products were used to determine the peak areas.
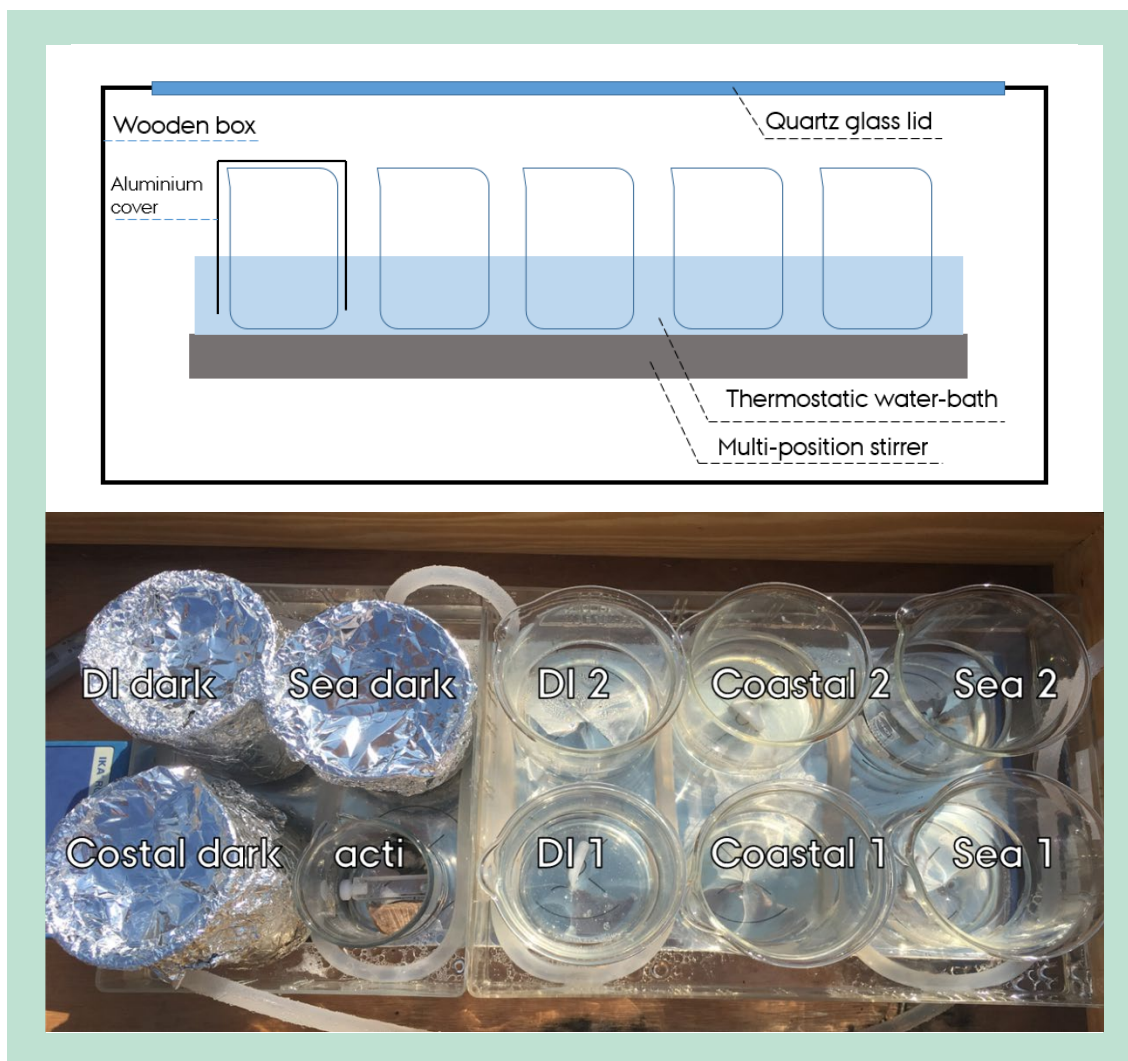

FIGURE 3: Experimental setup of the photodegradation experiments under natural sunlight.

4.4.3 Biodegradation
4.4.3.1 Sediment incubations

Sediment was collected from Roskilde fjord (coordinates: 55°41'29.8"N 12°04'56.3"E) by using a telescopic sampling pole to scrape off the top 10 cm of the sediment. The organic content of the sediment was determined by drying a fraction of the sediment (2 hours, 105 °C). Then, following a standard procedure, the dried sediment was burned at 450 °C for 2 hours, with the mass difference before and after burning taken as the organic content. For this sediment, the total organic carbon comprised 20 g/kg. Following Schwarzenbach and Westall, the expected TOC values for a eutrophic lake are around 19 g/kg, which matches the current observation

(Schwarzenbach and Westall, 1981). Control (biologically inactivated) sediments were generated by autoclaving (120 °C, 20 min) a fraction of the collected sediments.

Empty Erlenmeyers were spiked with a multi-component standard, containing 4 µg of the antifouling biocides. The methanol was allowed to evaporate overnight. Then, the collected sediment was divided into the Erlenmeyers, so that each Erlenmeyer contained 4 g wet sediment and 40 mL of deionized water. Deionized water was used in these experiments to 1) prevent the injection of salts into the HPLC-MS/MS and 2) allow for scanning of transformation products without high background levels, these results yielded no additional transformation products 3) Roskilde fjord contains DMSA and DMST (Koning et al., 2020), so additional inputs into the experiment were prevented. The biocide concentrations in the experiment were 0.46 µM DMSA, 0.48 µM DMST, 0.46 µM BCCPCA, and 0.50 µM Medetomidine. A control experiment was set up similarly but used the autoclaved sediment instead. Both, the sediment incubations and control, had a pH of 7.8 during the experiment. Both the bioactive and the inactivated control incubations were conducted in triplicate.

All Erlenmeyers were covered with aluminum foil to avoid contact with light, and the Erlenmeyers were set on a shaker table (Unimax 2010, Heidolph, USA) at 120 rpm, at room temperature. Samples were then collected by taking out 1 mL at selected time intervals (0, 1, 2, 7, 10, 14, 17, 24, and 27 days). The sample at time-point 0 was taken 1 hour after the start of the experiment, to allow the biocides to dissolve in the water. Right after taking samples, they were spiked with internal standards at a concentration of 100 ng/mL. Hereafter, the samples were centrifuged to remove particles and were then injected into the HPLC-MS/MS system.

4.4.3.2 Degradation kinetics and partitioning
Zero and first-order kinetic models were fitted to the acquired data using GraphPad Prism (v5.04, GraphPad Software, USA). The appropriate models were selected using Akaike's information criterion (AIC) to avoid over-fitting (Hirotogu Akaike, 1973). The AIC estimates the information that is lost using a model while taking the simplicity of a model into account. Therefore, for a given data set the zero or first-order model with the lowest AIC was reported. Comparisons between the K values of first-order models were made using an extra sum-of-squares F test, where appropriate.

The expected fraction of a biocide in sediment was also calculated for the sediment incubations. For this the reported log K_{ow} values were used to calculate the partitioning of the respective compound between sediment organic matter and water (log K_{oc}), using equation 1 (Schwarzenbach and Westall, 1981):

$$\log Koc = 0.72 * \log Kow + 0.49 \qquad (1)$$

with 0.72 and 0.49 being empirical parameters following Schwarzenbach and Westall (1981): K_{oc} and K_{ow} were found correlated, with 0.72 representing lower lipophilicity of the natural sorbents than octanol and 0.49 being the resulting y-intercept. The log K_{oc} was then used to calculate the fraction of the biocide in water (F_w) using equation 2 (Schwarzenbach et al., 2002):

$$Fw = \frac{Vw}{Vw + Koc * Moc} \qquad (2)$$

where V_w represents the total volume of water, which was 42.73 mL in the experiments. M_{oc} represents the mass of the organic carbon of the sediment, which was 0.43 g for the used sediments. The amount in sediment was then calculated for the samples taken after 1 day, as the partitioning process was expected to have reached equilibrium at that moment.

4.5   Leaching
4.5.1   Experimental design
Two antifouling paints were used for the experiments. Hempel Hard Racing White 76300 (Hempel, Lyngby, Denmark) was selected as a representative for the insoluble matrix antifouling paint (hard paints), while Hempel Mille NCT 7188W (Hempel, Lyngby, Denmark) was used as a soluble matrix paint (self-polishing). The paints were prepared by transferring 250 g wet paint to a 500 mL Schott Duran glass bottle. Then, the biocides were spiked using 30 mL methanol into the paint, to reach a final concentration of 0.06 mg/g wet paint. The mixture was blended by a

paddle paint stirrer attached to a power drill, which was lowered into the paint and set to stir at 240 rpm for 1 hour.

After stirring, the paints were applied on ceramic tiles (Cement It Grey Mosaik, Class Tile, Maranello, Italy, 5 x 5 cm) by using a paint roller for extra smooth surfaces. The tiles were weight controlled after applying each paint layer. Paint layers were applied with 10 min intervals as the thin layers dried fast. The average layer weight was 0.20 ± 0.04 g and was similar for the different paints. Each paint was used to paint a triplicate set of two-layer and a triplicate set of five-layer painted tiles. The tiles were then stored at room temperature and in the dark, until the start of the experiment (1 week later).

The experiment was started by filling 100 mL of tap water into 500 mL glass beakers. The painted tiles were suspended in a custom made hanger, which was then lowered into the water. The hangers and tiles were positioned at the surface, so that just the painted side of the tile was underwater, while the non-painted side remained dry. A magnetic stir bar was added and was set to stir at 120 rpm. Samples were taken every hour by taking out 1 mL by pipette and transferring it to autosampler vials. All water in the beakers was replaced immediately after sampling, to maintain a concentration gradient, and to prevent an equilibrium being reached between paint matrix and water.

4.5.2 Calculating diffusion coefficients

Diffusion coefficients are constants that describe mass flux driven by a concentration gradient through a surface over time (Saltzman, 2001; Vergnaud, 1993). The formulas by which diffusion coefficients are derived were summarized by Urbanczyk et al. (Urbanczyk et al., 2019). The fraction of leached biocide per unit of time can be calculated by taking the cumulative amount of biocide that is leached (M_t) and dividing by the original amount of biocide (M_0). In this study, M_t represents the concentration in water, while M_0 represents the amount of biocides in the applied paint. These values were plotted against time in hours and against the square root of time, to determine linearity. Diffusion coefficients were calculated if leaching was linear against the square root of time (Erich and Baukh, 2016).

The resulting slope (s), together with the painted area (A), and the specific paint density (p), and the mass of the paint (m) were used to calculate the diffusion coefficient (D) with the following formula:

$$D = \frac{s^2 \left(\frac{m}{A \times p}\right)^2 \pi}{16}$$

5.   Method development

5.1   Organic biocides

Extractions were performed using a concentrations series (following paragraph 4.1.1). Three replicates were present for each concentration in the series, including for a blank extraction control. The compounds were spiked into 1 L of deionized water at the following concentrations: 1 ng/L, 3 ng/L, 10 ng/L, 30 ng/L, 100 ng/L, 300 ng/L and 1 µg/L. Each of these samples were also spiked with the following internal standards: OIT-D17, Medetomidine-D3, DMST-D7, Pyridine-D5, Irgarol-D9 and PPZ-D5 at a concentration of 100 ng/L. In addition, a phosphate buffer was prepared at pH7.6 by adding 0.13g KH2PO$_4$ and 0.87g K$_2$HPO$_4$ to 100 mL deionized water. This buffer was then added to the sample to reach 5 v/v%.

Solid phase extractions (SPE) were performed on a concentration series basis, to identify the quantitation limits of the current extraction method. The relative recovery (to internal standards) for all compounds, at all concentrations, was 106% ± 24%, the absolute recoveries are described below.

However, there were a few compounds that could not be recovered at all. These undetected compounds are: PSA, PT2, PT, EU, ETU and EBIS (transformation products of the metal-organic biocides). This was, in fact, expected for these compounds, due to their high polarity or through interactions with water. Therefore, these compounds could not be retained on the cartridges. However, this does not mean that these compounds cannot be analyzed; they can still be analyzed through direct injections without the need for SPE. This will likely lead to high detection and quantitation limits, but this will have to be determined.

Most other compounds could be recovered without further issues. A few compounds are known to be sensitive to pH changes, which is why the phosphate buffer was included during extractions. These compounds are Medetomidine and 3OH-Medetomidine. Medetomidine and 3OH-Medetomidine could be recovered well and even up to a 100% in the higher concentrations, meaning that the addition of a buffer seems to lead to stable results.

DMSA and DMST are structurally similar and were, therefore, expected to behave similarly during SPE. This is also what we determined. Both compounds had a recovery rate around 50% on the lowest concentration, which increases up to a 100% qin the three highest concentrations.

Irgarol and its transformation products, TB-DesS-DesE, TB-OH-DesB, TB-OH-DesE and M1, can also be recovered with the current method. Irgarol itself can be well extracted from the sample and follows a gradual increase from 50% recovery to 100% from low to high concentrations. The transformation products, however, do not seem to exceed 50% recovery, with the exception of M1. M1 is the major transformation product and it can be extracted well, with a recovery between 75% and 100% during the experiment.

DCOIT had a decent recovery, which followed the expected pattern with lower recoveries at the lower concentrations. However, in none of the cases recovery was up to a 100%, in fact, recovery did not seem to exceed 75%. This is something that has been observed during optimization steps as well, where the recovery of DCOIT was always lower than those of the other antifouling biocides (not counting transformation products). The transformation products OMA and OOA were not recovered very well. Some signals were present in all samples, but recovery generally did not exceed 20%.

5.2   Zinc-Pyrithione and Zineb
5.2.1   HPLC-MS/MS analysis of ZnPT and Zineb

For this experiment, Zinc pyritione (ZnPT) was dissolved in DCM and then spiked into water to determine whether ZnPT can be detected when dissolved. The experiment was also analyzed using an APCI ion source, instead of the ESI. Indeed, ZnPT signals were found in the samples (Figure 5a). Signals for PT2 and PT were also detected (Figure 5b & c). ZnPT signals from

Dichloromethane (DCM) remained relatively stable during the experiment (Figure 5a). A linear regression was plotted through the data for exploratory purpose, resulting in a significant upward trend (R^2 = 0.36).

For PT2, the average signal showed an increasing trend (Figure 5b). PT2 signals start to increase more rapidly as soon as the first injection from one of the fractions is made (Figure 5b). This process repeats when the next fraction is injected for the first time.

The signals for PT fit well to previously observed results. For PT, the concentration increased for the first four hours, then a maximum was reached at an intensity if 4.0 * 10^5. The signals remain roughly at this maximum until the end of the experiment (Figure 5c).

From the experiment, it was clear that the transformations of ZnPT occurred in water. One reason for the transformation could be rapid transformation (DT_{50} < 15 min), due to the presence of light (Sakkas et al., 2007). However, light was excluded as much as possible during the experiment, with light only present during the preparation phase of the experiment. There is also a small amount of light entering the sample when the autosampler was ready to inject, as the cover of the autosampler will be opened for a few seconds.

Another reason for transformations might be reactions with the stationary phase of the column (Caren Anja Doose et al., 2004). However, the different compounds could be chromatographically separated (Figure 7). The lack of any significant peak tailing shows that the reactions occurred in the sample, instead of in the chromatographic column (Caren Anja Doose et al., 2004).

With light and chromatographic reactions excluded it can be assumed that the formation of PT2 and PT occurred in the water sample. The water sample was split into eight fractions that were analyzed consecutively. For PT2 there is a general upward trend resembling overall formation in the sample, however, each of the eight specific fractions showed its own specific PT2 formation as well. This might have been caused by contact with the autosampler, and/or by contact with air. It is understood that PT can oxidize with the stationary phase of chromatographic columns (Caren Anja Doose et al., 2004). It seems then that contact with the autosampler also induced this oxidative process, causing linear increases in each individual sample fraction. The overall increases in PT2 and PT might also be caused by the presence of air, which has also been shown to facilitate oxidation of PT (and possibly ZnPT) (Doose et al., 2004).

Normally, the formation of transformation products is linked to degradation/transformation of the parent compound. However, in this case, the signal for ZnPT was constant during the course of the experiment, seemingly showing a lack of degradation. This might be caused by the low water solubility of ZnPT since it is practically insoluble in water (and most organic solvents (Guthery et al., 2005)) (Francisco and Goka, 2005). If this is the case, then ZnPT does transform in the sample but is replenished from the undissolved fraction (or the fraction dissolved in DCM) leading to very low yet stable water concentrations.
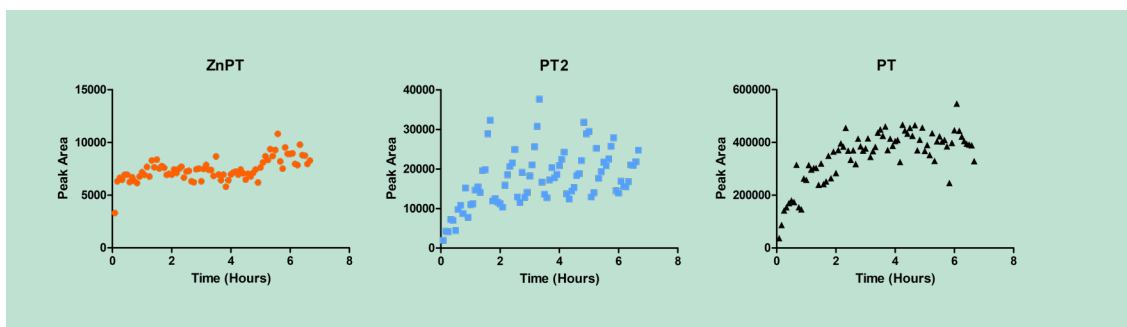
FIGURE 4: Analysis of ZnPT in deionized water by APCI. ZnPT was dissolved in DCM and spiked in water. ZnPT could be readily detected across all time points. However, PT and PT2 were also present, indicating transformation of ZnPT. ZnPT signals increased linearly in the experiment. PT signals increased nonlinearly during the experiment. PT2 signals showed a combination: the average signal increased in a similar fashion as PT, but separate vials showed a linear increase specific to that sample vial.

5.2.2 Chromatography of ZnPT and Zineb

In this experiment aimed at instrumental chemical analysis, using DCM to dissolve ZnPT before spiking into water and APCI as an ion source, each compound showed multiple chromatographic peaks (Figure 6). It was expected that chromatographic separation was based on polarity which, would be PT first, then PT2, and last ZnPT.

PT (Figure 6a) shows peaks at 2.62 min and 3.07 min. The peak at 2.62 min was chosen for the experiment, since it fits the expected retention time, and has the most intense signal. The signal at 3.07 min was assumed to be an insource product of ZnPT.

PT2 (Figure 6b) eluted with three peaks, with retention times of 2.62 min, 2.76 min, and 3.07 min. Here, the peak at 2.76 min was presented as PT2 in the experiment, since it was the only independent peak. The peak at 2.62 min matches the retention time of PT, and the peak at 3.07 min matches the retention time of ZnPT. Therefore, these two signals are considered insource fragments of PT and ZnPT.

ZnPT (Figure 6c) showed signals at both 2.62 min and 3.07 min. Here it was assumed that the signal at 2.62 min corresponds to insource fragments of PT. The peak at 3.07 min was assumed to represent ZnPT, due to the expected retention time of the ZnPT complex.

It was clear that there were many insource products. Moreover, this insource formation goes all directions, for example injecting PT also shows ZnPT signals and vice versa. This has also been observed in various literature sources (Bones et al., 2006; Sakkas et al., 2007). Chromatographic separation of ZnPT, PT, and PT2 indicates that the transformations occur in the sample, instead of in the system. However, the rapid signal changes of PT, and PT2, will make for poor calibration standards, as the signals may vary wildly between injections. Notwithstanding, that ZnPT signals were rather close to the background, with a signal to noise ratio of 30 at the concentration of 50 µg/mL ZnPT.
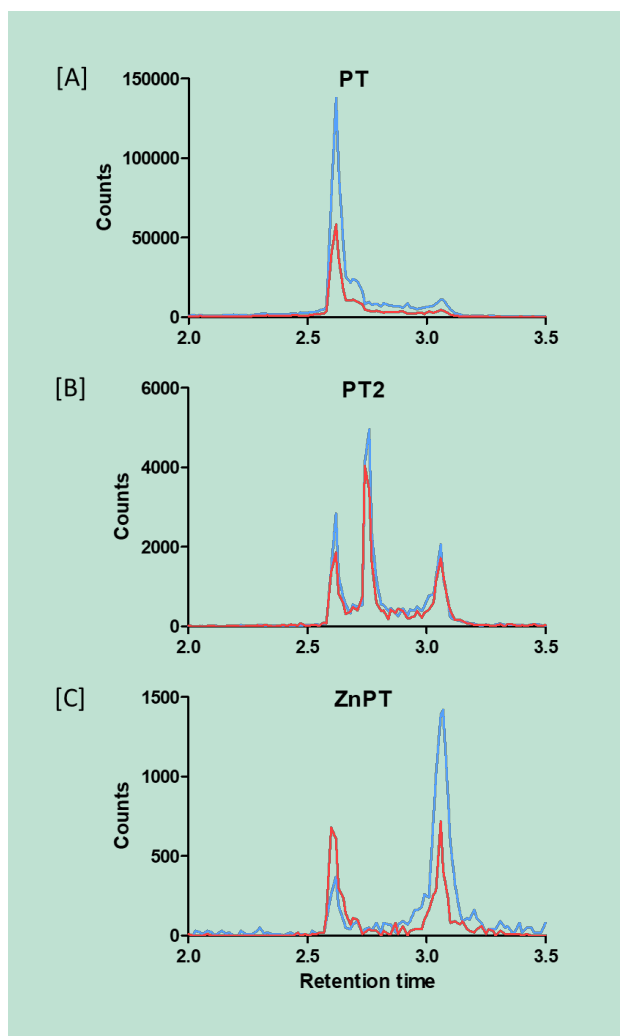
FIGURE 5: Chromatographic peaks of a ZnPT injection after 6 hours of the experiment. Detection was done by APCI-MS/MS. ZnPT was dissolved in DCM, which was then diluted in water so that effects of the water on ZnPT could be tested. The blue (quantifier) and red (qualifier) lines each represent one of the transitions. The y-axis was plotted in counts, the x-axis as the retention time in minutes. PT=Pyrithione; PT2=Dipyrithione, ZnPT=Zinc-Pyrithione.

5.2.3 APCI-MS analysis of ZnPT

Standards for PT, PT2, and ZnPT were used to scan which other insource products may be found (Figure 7). All standards were prepared in methanol. The PT standard (Figure 7a) showed the expected peak of PT at 128 m/z, but other signals were also present. The signal at 253 corresponds to the expected m/z of PT2, indicating some (insource) formation. The signal at 237 m/z would correspond to the mass of PT2(-O), while the signal at 221 corresponds to the mass of PT2(-O$_2$). Signals at 112 would correspond to the mass of PT(-O). For the PT2 standard (Figure 7b) the expected signal at 253 m/z is also the strongest signal. A signal for PT at 128 m/z was also observed. Moreover, 237 (PT2(-O)), 221 (PT2(-O$_2$)), and 112 m/z (PT(-O)) were also present. The ZnPT standard (Figure 7c) shows a clear signal for ZnPT at 317 m/z, including the expected Zn isotopes at 319 and 321 m/z. PT signals were also clearly present at 128 m/z. With the last signal at 112 m/z fitting with the expected mass of PT(-O). Between the three different spectra, it is clear that 128 m/z, corresponding to PT, is present as an insource product. Furthermore, the signal at 112 m/z was also present in all the standards, this mass to charge ratio corresponds to PT minus an oxygen (Sakkas et al., 2007). This PT(-O) has also been shown to have an insource product at 221 m/z, (Sakkas et al., 2007) which was observed in the

PT and PT2 standards, but not in the ZnPT standard. An m/z of 221 corresponds to PT2(-O_2) (Sakkas et al., 2007). There is also a signal at 237 in the PT and PT2 standards, which would correspond to PT2(-O) (Sakkas et al., 2007). The signal at 371 m/z in the PT and PT2 standards remains unexplained. Signals for other metal-PT(2) complexes, such as CuPT2 (316 m/z), MnPT2 (305 m/z), and FePT2 (308 m/z) were not detected. The Fe^{3+} complex is also described as a common product, but the mass (435 m/z (Caren Anja Doose et al., 2004)) is outside the scanned range. Another known phototransformation product of ZnPT is PSA. PSA was not detected, likely due to its polar nature so that it was not captured on the reverse phase column, moreover, PSA also works better in negative ionization mode.
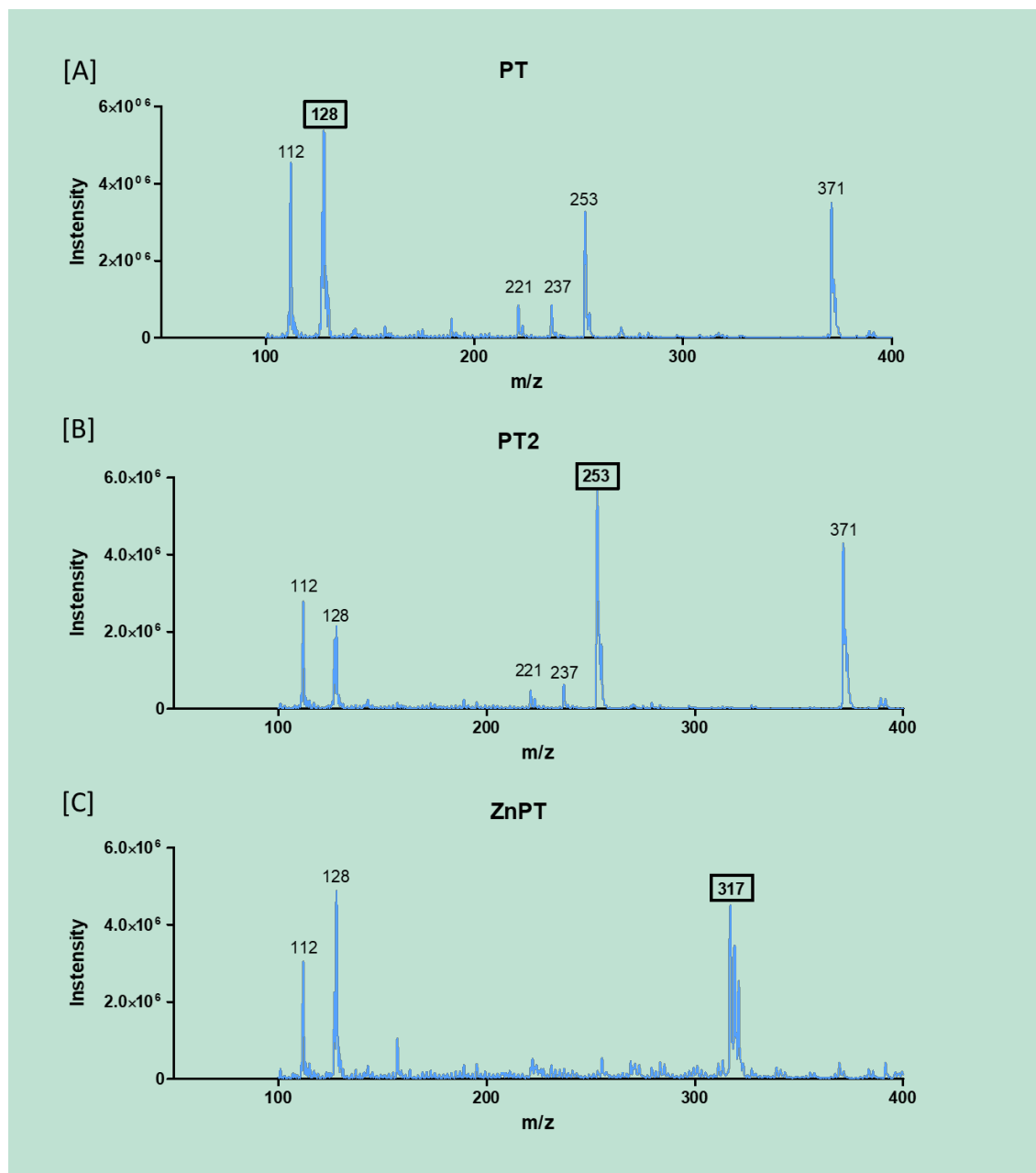

FIGURE 6: APCI-MS spectra of methanol standards from PT (A), PT2 (B), and ZnPT (C). Molecular ions are highlighted. The standards were injected using the syringe pump.

Key findings – Method recommendations

It was no problem to establish, a method to analyse the organic antifouling compounds at trace concentrations even including the hydrolysis products. It proved, however, to be a challenge to establish a method for the metal organic compounds.

This is *a priori* not due to lack of instruments or skills, but due to the rapid hydrolysis of the respective compounds (Zn Pyrithione and Zineb). Both are hydrolysing while preparing the standard solutions or running the instrumental analysis.

For Zn Pyrithione the best candidates for emission monitoring are Dipyrithione (PT2) and Pyrithione (PT). However, also these compounds can relatively rapidly be transferred into each other. As also both Copper and Zinc-Pyrithione will react to these markers, it will make sense to establish a sum of Pyrithiones as a monitoring parameter.

6. Occurrence

6.1 Danish marinas

Water and sediment samples were collected during the summer 2019. Samples were extracted and analyzed for the antifouling biocides (Table 6).

Only three of the six tested antifouling biocides were detected, either directly or indirectly as transformation products in the investigated marinas. The biocides Dichlofluanid and Tolylfluanid were not detected themselves and their use became apparent only by testing for their hydrolysis products DMSA and DMST, respectively. Furthermore, Irgarol was detected even though it has not been on the market since 2016 when it lost approval in the EU (European Comission, 2016). Neither DCOIT, Medetomidine, and Tralopyril nor the Tralopyril hydrolysis product BCCPCA were detected in any of the samples. However, the hydrolysis products DMSA and DMST of Dichlofluanid and Tolylfluanid, respectively, were found in most marinas. Moreover, Irgarol was found in all of the collected sediments, indicating its lingering presence despite it losing approval for use in 2016. DMSA was found in the water of 11 out of the 13 marinas, at an overall median concentration of 4.84 ± 6.04 ng/L. The highest concentration that was observed for DMSA at 19.78 ± 1.57 ng/L occurred in Korsør marina. DMST was detected in all marinas, except for Langelinie,with a median concentration of 0.38 ng/L. The highest concentration of DMST was 1.57 ± 0.20 ng/L, which was detected in Gilleleje marina.

Irgarol was detected in less than half of the marinas (6 out of 13). For this antifouling biocide, the highest concentration was found in Sydhavnen (1.44 ± 0.34 ng/L). The median concentration of Irgarol, between the marinas where it was detected, was 0.63 ng/L. When it comes to sediments, only 2 out of the 6 biocides were detected. These biocides were Irgarol and DMSA (the hydrolysis product of Dichlofluanid). DMSA was only found in the sediment of two marinas, Køge and Faxe Ladeplads, and only in one or two of the replicate samples. In Faxe, DMSA was detected in one replicate at a concentration of 1.53 ng/g. In Køge, DMSA was detected in two replicates, with an average of 1.98 ± 1.77 ng/g. Irgarol, on the other hand, was detected in every sample that was collected in the 11 marinas where sediment was acquired. For this biocide the median concentration was 4.53 ng/g in sediments. The highest concentration of Irgarol was observed in the sediment samples from Kalundborg marina at 20.13 ± 9.11 ng/g.

The concentrations of DMSA in this study were similar to those found in Germany during 2013, where 21 ng/L DMSA was the median concentration of 16 marinas (Daehne et al., 2017). In contrast, the currently presented concentrations for DMST were markedly lower than the 25 ng/L reported in the aforementioned study. This might reflect different representation in market shares between Dichlofluanid and Tolylfluanid. Irgarol is currently not sold on the antifouling market in Europe but has been used as an alternative to tributyltin in past years (1985–2016). Previous reports from Germany (1998) show that Irgarol was found in sediments with concentrations averaging around 21 ng/g wet weight (Biselli et al., 2000). In the present study the highest concentration of Irgarol was 21.95 ± 3.07 ng/g of dry sediment. The currently reported concentration is around three times lower when comparing to the previously reported results from wet sediments, as the wet sediments were about three times heavier.

A more recent report (Germany 2013) shows that Irgarol was found in waters at a median concentration of 2 ng/L (Daehne et al., 2017). Another report (UK 2005) shows Irgarol concentrations of 2–12 ng/L at the lowest (Cresswell et al., 2006). Measurements taken in 2012 in Sydhavnen, Denmark, showed a concentration of 13 ng/L (Vorkamp et al., 2014). These concentrations were not reached in any of the marinas that were studied for this report, with the highest water concentration being 1.44 ± 0.34 ng/L in Sydhavnen. Irgarol has been commonly found in the water phase, in fact, Irgarol has been detected in many waters with maritime activities around the world (Ansanelli et al., 2017). Irgarol has a Kow of 4.07 and thus it can be

assumed that the equilibrium concentration between sediment and water is reached if there is 10.000 times more Irgarol/g sediment TOC than in the water phase. Sediments typically contain about 1% TOC (dry sediment), thus a concentration of 22 ng/g dry weight (Gilleleje) equals 2200 ng/g TOC or 2.200.000 ng/kg TOC. This would give an equilibrium concentration of 220 ng/L. As the measured concentration in the same location is just 0.6 ng/L, it can be concluded that Irgarol is deposited in the sediments and is leaching out of those. This was opposite to the findings in the older monitoring reports, where high concentrations in the water phase were reported (Biselli et al., 2000). These data, taken together, indicate that Irgarol concentrations have been decreasing in recent years, probably due to legislative measures. Additionally, Irgarol was classified as persistent in sediments in the EU assessment report (European Chemicals Agency, 2014a). A lack of Irgarol in the water phase but the presence in sediments points to past use and deposition in sediment.

TABLE 6: Concentrations of antifouling biocides in marinas on Sjælland (2019); n.d. represents not detected, while an – represents not analyzed.

Marina	DMSA		DMST		Irgarol	
	Water (ng/L)	Sediment (ng/g dry)	Water (ng/L)	Sediment (ng/g dry)	Water (ng/L)	Sediment (ng/g dry)
Roskilde (July)	2.62 ± 0.54	n.d.	0.29 ± 0.01	n.d.	n.d.	4.79 ± 1.63
Brøndby (July)	4.18 ± 1.90	n.d.	0.46 ± 0.03	n.d.	< 0.06	1.95 ± 0.19
Faxe ladeplads	6.73 ± 6.42	< 0.62.	< 0.05	n.d.	0.94 ± 0.59	< 0.1
Køge	2.01 ± 0.59	1.98 ± 1.77	0.41 ± 0.02	n.d.	n.d.	2.23 ± 2.38
Vordingborg	1.66 ± 1.45	n.d.	0.36 ± 0.31	n.d.	n.d.	2.65 ± 0.55
Holbæk	11.58 ± 0.58	n.d.	0.89 ± 0.02	n.d.	n.d.	4.53 ± 1.09
Kalundborg	n.d.	n.d.	0.27 ± 0.01	n.d.	n.d.	20.13 ± 9.11
Korsør	19.78 ± 1.57	n.d.	0.88 ± 0.47	n.d.	0.62 ± 0.57	6.51 ± 2.04
Frederikssund	3.14 ± 0.66	n.d.	0.34 ± 0.01	n.d.	n.d.	3.99 ± 2.85
Gilleleje	4.85 ± 1.25	n.d.	1.57 ± 0.20	n.d.	0.66 ± 0.42	21.95 ± 3.07
Rungsted	7.05 ± 6.43	n.d.	0.31 ± 0.06	n.d.	0.30 ± 0.38	10.44 ± 3.21
Langelinie	n.d.	-	n.d.	-	n.d.	-
Sydhavnen	0.83 ± 0.37	-		-	1.44 ± 0.34	-

6.2   Seasonal trend in two marinas

Water and sediment samples were collected over the course of a year in two selected marinas, Roskilde and Brøndby. These samples were analysed for the organic antifouling biocides (Figure 8 & Figure 9). The data indicate that antifouling biocide concentrations are higher during summer than during winter periods, which reflects the sailing season as the boats are removed from the water in winter.

6.2.1   Water samples

In Roskilde marina, two of the biocides were detected, DMSA and DMST (Figure 8A). DMSA was found in higher concentrations than DMST across all samples. The sample in March was taken before the onset of the sailing season and already showed the presence of DMSA at 2.15 ng/L. DMSA concentrations reached a peak in May and June (4.81 ± 1.35 ng/L and 4.82 ± 0.65 ng/L), early in the sailing season. Hereafter, concentrations dropped to 2.62 ± 0.54 ng/L in July and 2.90 ± 0.35 ng/L in September. DMSA remained within quantifiable limits during the winter period, November (1.53 ± 0.07 ng/ L) and January (0.99 ± 0.10 ng/L). DMST showed a similar trend, with concentrations of 0.73 ± 0.90 ng/L in March. A peak in May at 1.11 ± 0.11 ng/L was followed by a drop in concentration from June (0.59 ± 0.04 ng/L), July (0.29 ± 0.01 ng/L) and September (0.40 ± 0.03 ng/L) to non-detectable levels in November and January (< 0.02 ng/L).

In Brøndby, besides DMSA and DMST, Irgarol was detected (Figure 8B). Similar to Roskilde, DMSA was also found in the highest concentrations compared to the other biocides in this marina. DMSA was found in March at a concentration of 0.34 ± 0.09 ng/L. The concentration of DMSA gradually increased during the consecutive months: to 1.55 ± 0.90 ng/L in May, 2.67 ± 0.71 ng/L in June and reaches a peak at 4.18 ± 1.91 ng/L in July. DMSA concentrations dropped to 2.34 ± 0.36 ng/L in September and down to 0.61 ± 0.52 ng/L in November and 0.66 ± 0.03 ng/L in January. DMST was found at a concentration of 0.67 ± 0.35 ng/L in March, increasing to a peak at 1.20 ± 0.85 ng/L in May. Hereafter concentrations dropped to 0.74 ± 0.13 ng/L in June, 0.46 ± 0.03 ng/ L in July and 0.37 ± 0.03 ng/L in September. DMST was not detected during the winter months, November and January. Irgarol was only found during the late sailing season and in the winter period. In September, Irgarol was measured at a concentration of 0.37 ± 0.11 ng/L. A peak was reached in November at 0.73 ± 0.06 ng/L, which was at that moment higher than concentrations of DMSA or DMST. The Irgarol concentration in January was 0.48 ± 0.01 ng/L. For the other months Irgarol was below the detection limit (< 0.06 ng/L).
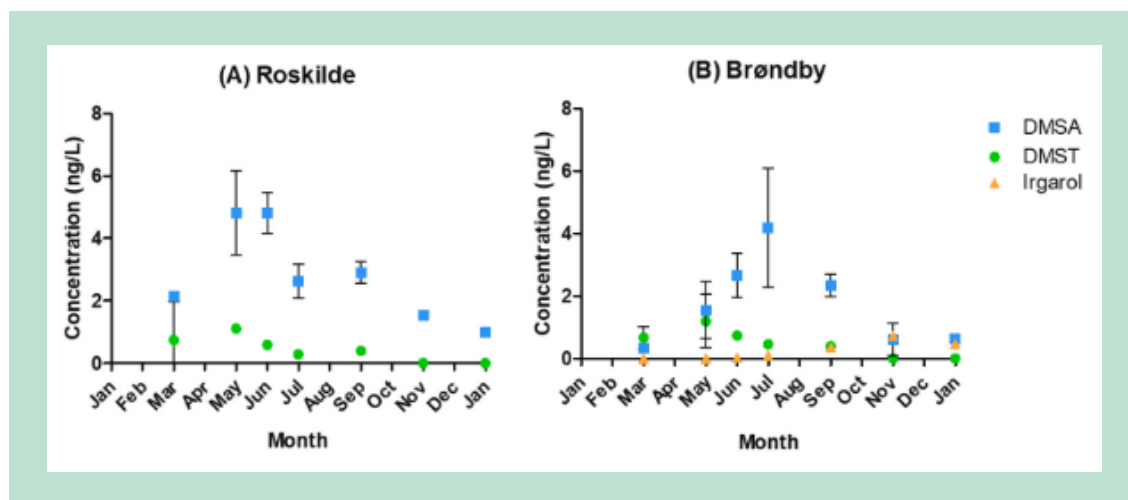
FIGURE 7: Seasonal changes of antifouling biocide concentrations in the water of Roskilde and Brøndby marinas. Seasonal variations were observed for DMSA and DMST, which from the start of the sailing season (May) are increasing in concentration. Irgarol was only detected in Brøndby marina during September, November, and December. Irgarol was not detected in Roskilde and was therefore not included in the figure. Concentrations are plotted as means ± standard deviation (n = 3).

6.2.2 Sediment samples

Only Irgarol was detected in the sediment samples in both Marinas. For Roskilde marina, Irgarol was found in all collected samples, with concentrations ranging from 1.47 ± 0.49 ng/g in September to 4.81 ± 1.63 ng/g in May (Figure 9A). For the others months, Irgarol concentrations were 2.06 ± 1.90 ng/g in March, 1.56 ± 1.30 ng/g in June, 4.79 ± 1.63 ng/g in July, 2.32 ± 0.32 ng/g in November and 3.38 ± 1.23 ng/g in January. For these samples, no clear seasonal trend could be established. In Brøndby, Irgarol concentrations were generally lower than those found in Roskilde marina. The lowest Irgarol concentration in Brøndby (0.90 ± 0.19 ng/g) was found in June and the highest occurred in November at 1.99 ± 0.24 ng/g (Figure 9B). Irgarol was otherwise found at the following concentrations: 1.91 ± 0.56 ng/g in March, 1.23 ± 0.44 ng/g in May, 1.95 ± 0.19 ng/g in July, 1.80 ± 0.54 ng/g in September and 1.46 ± 0.43 ng/g in January. For the Irgarol concentrations in Brøndby, no seasonal trends were observed. Whether this indicates that Irgarol is being sorbed to the deep layers of the sediments or whether the sediments contain old Irgarol containing paint particles is not known at the moment. If paint particles were involved, higher deviations in the samples would be expected, assuming an inhomogeneous distribution of rather big particles.

The seasonal variation in the samples was especially clear in the case of DMSA, which increased in concentration at the start of the sailing season (May). This corresponded with freshly painted boats being launched into the marina. However, the peak concentration of DMSA was reached in different periods in the two selected marinas: in May in Roskilde and in July in Brøndby. It is unclear, why the concentration in Roskilde peaked two months before they did in Brøndby. A variety of factors may influence biocide concentrations, such as tides, rainfall, freshwater input, wind direction and strength, the number of vessels, and the openness/ exchange to sea. We assume that the tides or rainfall would not have contributed (significantly) to the difference in peak timing, especially regarding DMSA, since i) The marinas at the Baltic Sea do not experience tides and ii) Each month the samples for Roskilde and Brøndby were taken on the same day suggesting similar rain pattern and there may have been only a minimal difference in rainfall as there is only 21 km between the two locations. Wind may have caused the difference in peak timing between the two marinas, as Roskilde marina lies open towards the north while Brøndy is closed by a seawall that is open only on the southwest. Therefore, the wind blowing from the north has the potential to accumulate water in Roskilde marina and to refresh the water in Brøndy marina. This was the case for the samples in May, while the wind came from the east in both June and July. The number of vessels in each marina may mostly affect the ultimate concentration of biocides. For most marinas the amount of indeginous vessels (boats) stays more or less the same during a year, and it can be assumed that changes in the number of vessels are mostly due to tourism. Fluctuations in concentrations of antifoulings could be due to the presence of tourist vessels painted with Dichlofluanid or Tolylfluanid during the time of sampling.

Seasonal variability of antifouling biocide concentrations is well established and the current findings are in line with previous results (Biselli et al., 2000; Bowman et al., 2003). Past studies made similar observations of peak concentrations for a particular biocide at different months during the summer (Lamoree et al., 2003; Yang and Maguire, 2000).

Irgarol was observed in the sediment year-round and the water concentration of Irgarol in November may have been caused by desorption or through perturbation of the sediment due to construction and/or dredging works that were taking place at that time and originating from former times. Alternatively, The presence of Irgarol in water samples from November in Brøndby may have been caused by maintenance activities that are performed during winter periods (Biselli et al., 2000; Bowman et al., 2003). This implies that Irgarol, despite being disapproved for use, may still be present on vessels from older applications.
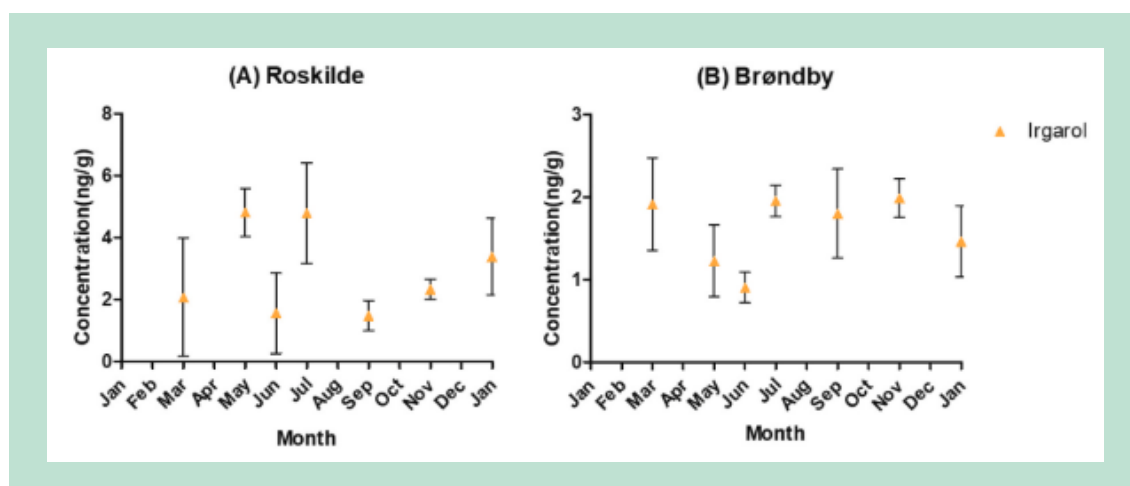

FIGURE 8: Seasonal variations of Irgarol in sediments of Roskilde and Brøndby marinas. Irgarol was the only biocide to be detected in the sediments of these marinas. No clear seasonal variations could be observed in the concentration of Irgarol. Concentrations are plotted as mean ± standard deviation (n = 3).

6.3   Transect from marina into open sea

Water samples were collected along a transect from the marina and to open water. The transect in Roskilde went up to 820 m and the transect in Brøndby up to 2210 m away from the marina. As shown in Figure 10, the antifouling biocides reached background concentrations after ~200 m from the marina. For these samples, DMSA, DMST, and Irgarol were detected in both marinas. In Roskilde (Figure 10A), DMSA was found inside the marina at a concentration of 5.12 ± 0.51 ng/L. This dropped to 3.95 ± 0.01 ng/L after 50 m. A concentration of 2.60 ± 0.11 ng/L was found at 120 m from the first sampling site. The samples taken at 230 m, 440 m, and 820 m all showed concentrations of DMSA between 2.25 ± 0.05 ng/L and 2.31 ± 0.17 ng/L. DMST and Irgarol were only found in the samples from the inner harbor DMST at a concentration of 0.97 ± 0.79 ng/L and Irgarol below 0.06 ng/L. The samples at 50 m and further did not have detectable levels of either antifouling biocide.

In Brøndby marina, similar to previous observations DMSA was found at the highest concentrations (Figure 10B). The first sample showed a DMSA concentration of 1.59 ± 0.12 ng/L. The concentration dropped to 1.19 ± 0.05 ng/L at 60 m and to 0.26 ± 0.03 ng/L at 230 m. In the remaining samples, DMSA was not detected. DMST was also found in the first sample at a concentration of 0.32 ± 0.03 ng/L, which decreased to 0.30 ± 0.01 ng/L at 60 m. From 230 m onward no DMST was detected (< 0.02 ng/L) in the samples. A similar trend evolved for Irgarol, which was initially found at a concentration of 0.77 ± 0.14 ng/L and dropped to 0.55 ± 0.01 ng/L at 60 m before dropping to below detection limits (< 0.06 ng/L) after 230 m. From these transect studies it became clear that the concentrations of the detected antifouling biocides rapidly drop from inside the marina to outside the marina, even in open marinas. In general, background or residuals levels were reached at a distance of 200 m. This means that antifouling biocides are, indeed, concentrated in and around marinas.

In the Roskilde transect, Irgarol was detected in the inner harbour near the slipway. This is in contrast to the seasonal trend study, where Irgarol was not detected in Roskilde marina. It is possible that high pressure cleaning in proximity to the slipway, or just the use of the slipway, releases antifouling paint particles (Turner, 2010). These antifouling paint particles may lead to elevated concentrations of the antifouling biocides, especially around the slipways. A previous transect study shows similarities in the results (Steen et al., 2004). In this study the authors took samples around a single ship and up to 128 m away and observed a clear reduction in concentration with distance to the vessel (Steen et al., 2004).
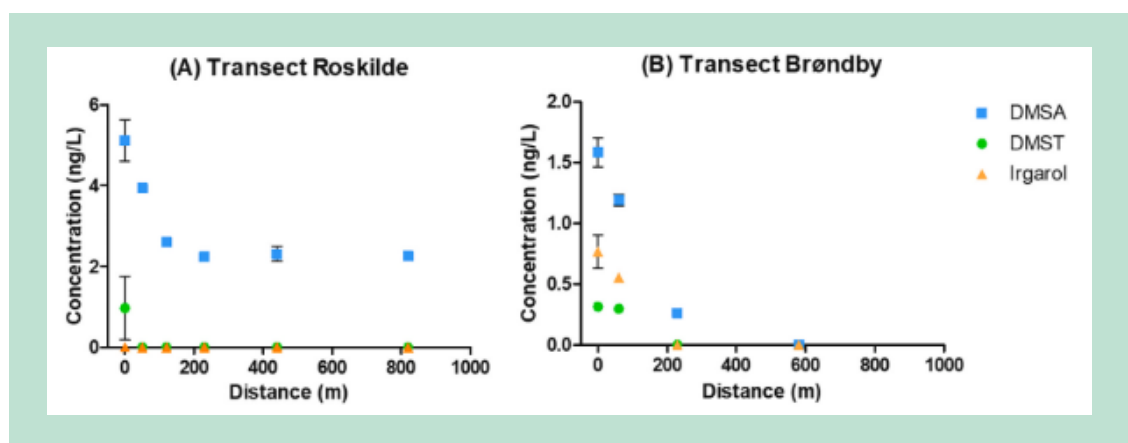

FIGURE 9: Antifouling biocides in water samples collected in a transect in the marinas of Roskilde and Brøndby. The transect studies were performed at different dates, Roskilde in late July 2019 and Brøndby in early October 2019. The graph for Brøndby does not include samples taken at 1480 m and 2210 m since all biocides were below detection limits at these distances. All samples are plotted as means± standard deviation (n = 2).

Key findings – Antifouling biocides in Danish marinas

DMST and DMSA (hydrolysis products of Tolylfluanid and Dichlofluanid) are present in the waters of Danish Marinas while Irgarol isstill present in the sediments.

The highest concentrations of **DMST / DMSA** are detected in summer. Though the concentrations of DMST/DMSA are relatively low (0.3-20 ng/L) it is expected that the concentrations of these transformation products will increase with growing market penetration of Tolylfluanid and Dichlofluanid.

Since **Irgarol** is not approved as an active substance in current antifouling paints and is appearing all-year round (independent from seasonal yachting activities), it is most probable that Irgarol is mobilized from the sediments and not leached from current boats.

7. Degradation and fate

Antifouling biocides are exposed to different degradation processes. Thus, both the abiotic processes hydrolysis (paragraph 7.1) and photodegradation (paragraph 7.2) as well as biodegradation (paragraph 7.3) were evaluated.

7.1 Hydrolysis

In this first experiment, all of the organic biocides were allowed to stand in water for up to two weeks at room temperature, in order to determine, which biocides are prone to hydrolyze. In these experiments it became very clear that Tralopyril, Tolylfluanid and Dichlofluanid hydrolyze within 24 hours under these conditions, see Figure 11a. These three compounds were not detected at all after 48 hours. The other compounds, Irgarol, Medetomidine and DCOIT, are more stable and barely degrade during the two-week time course, as seen in Figure 11b.
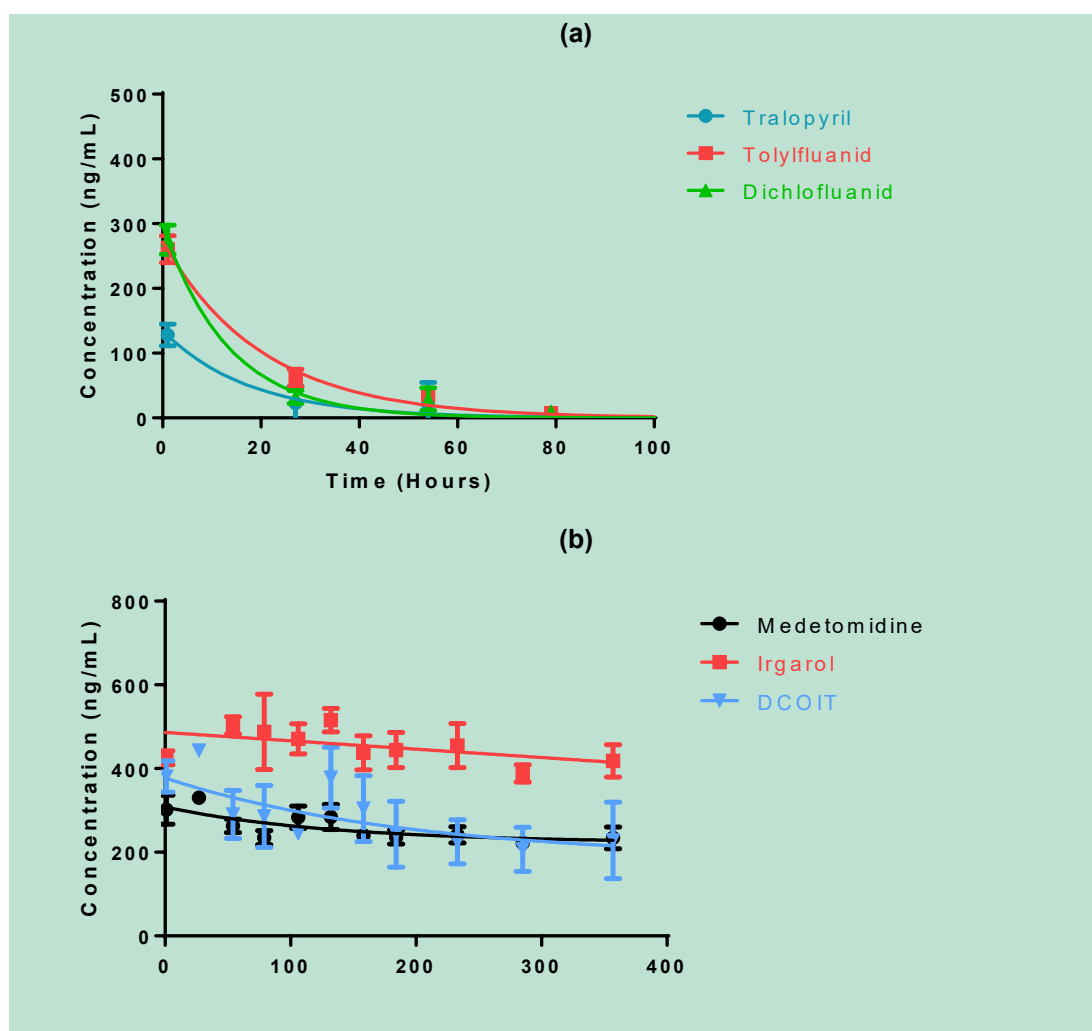
FIGURE 10: Initial decrease of concentration by hydrolysis of organic biocides in deionized water (data point= mean, error bar= SD).

Dichlofluanid & Tolylfluanid

These two compounds are structurally similar (Figure 12). Tolylfluanid contains an extra methyl group by which it can be distinguished. These two compounds are known to hydrolyse rapidly and have been shown to be more stable under acidic conditions. For each compound the main hydrolysis product is known (Daehne et al., 2017). These hydrolysis products, dimethylphenylsulfamide (DMSA) and dimethyltolylsulfamide (DMST) respectively, also only differ structurally by a methyl group.
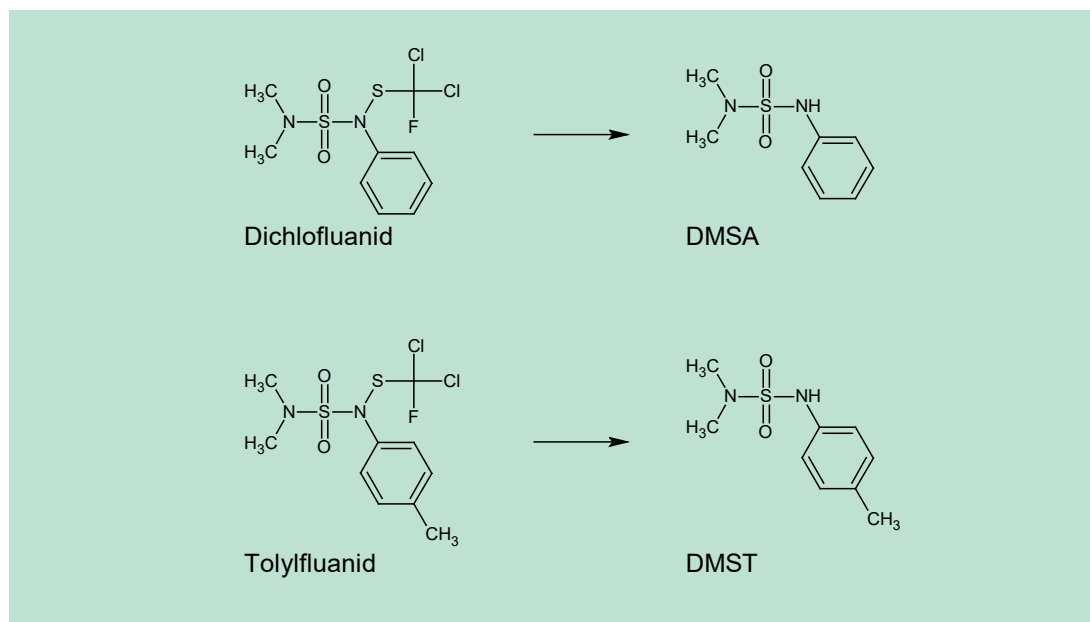
FIGURE 11: Hydrolysis of Dichlofluanid and Tolylfluanid leads to the formation of DMSA and DMST.

During the hydrolysis experiments, differences in the stability of Tolylfluanid and Dichlofluanid in deionized and coastal water were detected (Figure 13). The hydrolysis rate constants for Dichlofluanid are similar (0.4 h^{-1}) both in deionized (single first order with plateau) and coastal waters (singlefirst order). In contrast, Tolylfluanid has a slightly lower rate constant in coastal water (0.25 h^{-1}) than in deionized water (0.48 h^{-1}). However, while both compounds decreased below the limit of quantification (0.9 nM) within 20 hours in the coastal water, it seems that a hydrolysis-equilibrium was reached in deionized water as the concentration never gets close to zero as for the natural waters. About 86% (0.65 µM) Tolylfluanid was remaining after 24 hours in deionized water. Similarly, 67% of Dichlofluanid was still present after 24 hours in deionized water. Half-times of 1.6 h and 2.7 h were determined for Dichlofluanid and Tolylfluanid in coastal water, respectively. Faster removal of organic pesticides by hydrolysis in deionized water than in coastal water has also been observed by other authors (Greenhalgh et al., 1980).

During these experiments, DMST and DMSA were formed as Tolylfluanid and Dichlofluanid hydrolyzed. As expected, the formation of the hydrolysis products closely follows the degradation of the corresponding parent compound. Nevertheless, the hydrolysis product formation rates were slightly lower than the degradation rates of the respective parent compounds (0.1 h^{-1}-0.3 h^{-1}). The transformation products, DMSA and DMST, reached levels close to the originally applied molar concentrations. Calculations show that the mass balance can be closed (99% ± 5%) and that there were no other major transformation products. However, these results indicate that phototransformation not only of the parent compounds but also of the hydrolysis products might be relevant for natural waters.
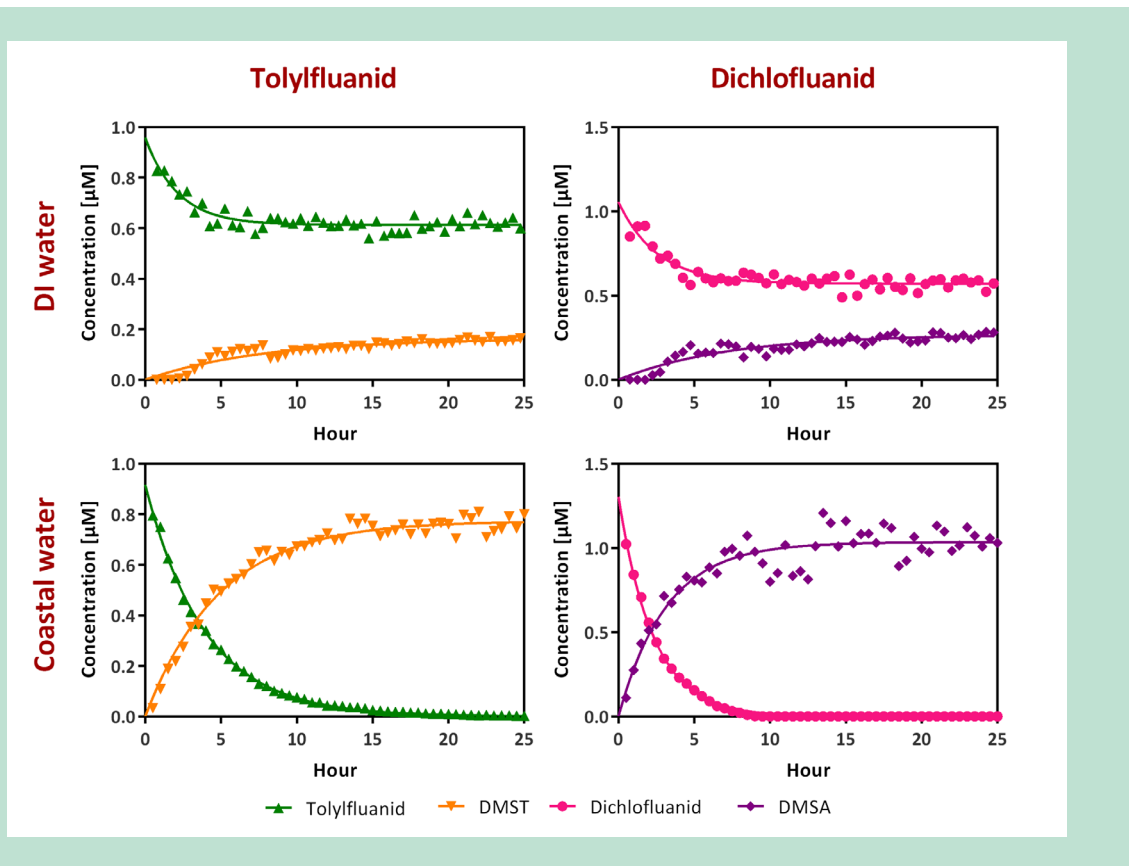
FIGURE 12: Hydrolysis of Tolylfluanid and Dichlofluanid and formation of their hydrolysis products (DMST and DMSA) in deionized and coastal water in comparison.

TABLE 7: Hydrolysis rate constants K (standard error in brackets), half-time and final plateau of Dichlofluanid and Tolylfluanid [C=(C$_0$-Plateau)*e^{-kx}+Plateau] and their hydrolysis products DMSA and DMST [C=C$_0$+(Plateau-C$_0$)*(1-e^{-kx})] in coastal and deionized water.

	DMSA		DMST		Dichlofluanid		Tolylfluanid	
	Coastal water	DI	Coastal water	DI	Coastal water	DI	Coastal water	DI
C$_0$ [μM]	= 0	= 0	= 0	= 0	1.304 (0.013)	1.056 (0.054)	0.917 (0.007)	0.959 (0.044)
Plateau [μM]	1.034 (0.017)	0.269 (0.011)	0.774 (0.007)	0.163 (0.007)	= 0	0.571 (0.007)	= 0	0.613 (0.005)
k [h^{-1}]	0.315 (0.026)	0.138 (0.017)	0.203 (0.007)	0.130 (0.015)	0.437 (0.005)	0.390 (0.056)	0.254 (0.003)	0.468 (0.072)
Half-time [h]	2.20	5.04	3.41	5.35	1.59	1.78	2.73	1.48

In general it can be concluded, that Tolylfluanid and Dichlofluanid hydrolyze so rapidly that it is most probable that their transfer from the paint into the water is slower than the hydrolysis - their presence in water is thus highly unlikely. Hence, for the analysis in environmental matrices, the hydrolysis products DMSA and DMST should be targeted. Nevertheless, it is even questionable whether Tolylfluanid and Dichlofluanid are actually stable in the respective (water-based) paint products.

Tralopyril

Tralopyril was also susceptible to hydrolysis (Figure 14). The reaction was, again, faster in fjord water compared to deionized water. However, transformation products for Tralopyril are relatively unknown and are rarely mentioned in open literature (Downs et al., 2017). Q1 scans of Tralopyril in deionised water indicated the presence of **3**-bromo-5-(4-chlorophenyl)-4-cyano-1H-pyrrole-2-carboxylic acid (BCCPCA).
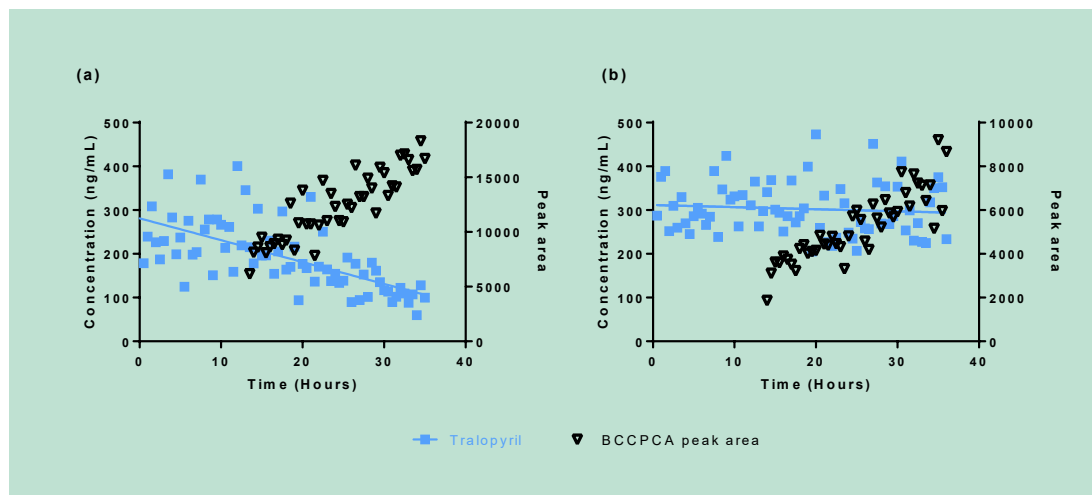

FIGURE 13: Hydrolysis of Tralopyril in (a) fjord and (b) deionized water. The peak area of the suspected hydrolysis product BCCPCA is shown, as the standard was not yet available at the time of analysis of this experiment.

Nevertheless, besides BCCPCA, another more intense peak was also present in the sample at the same retention time, meaning one of the two is most probably formed as rearrangement product by loss of CO_2 in the ion-source. Only for BCCPCA a standard was made available in the final phase of the project, while the other transformation products would need to be synthesized with considerable effort. Figure 15 shows the Q1 scans and Figure 16 shows the suspected transformation product structures.
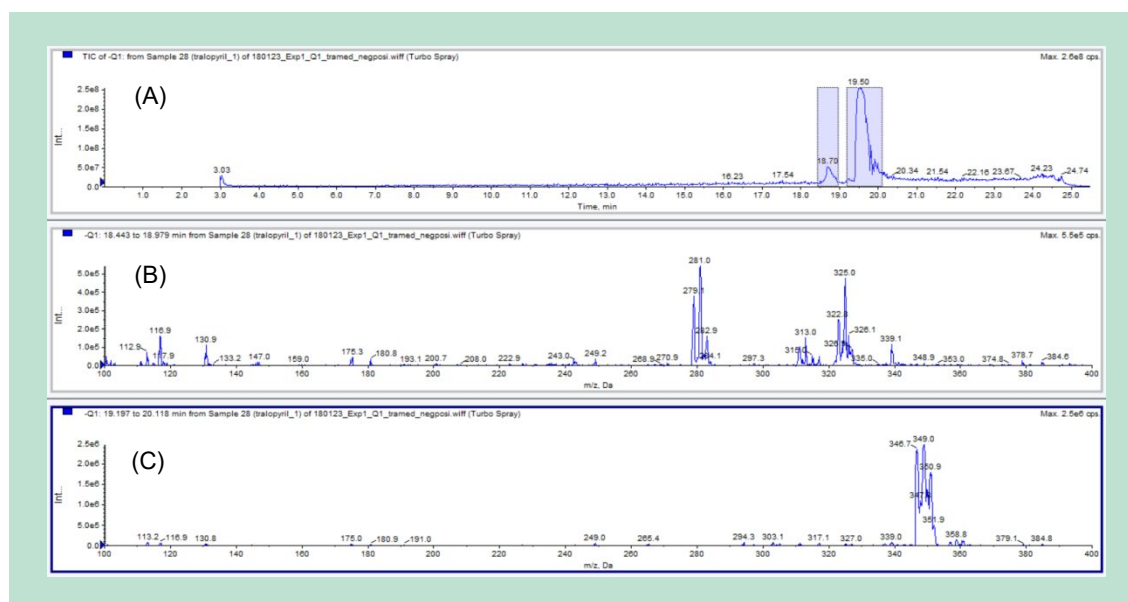

FIGURE 14: HPLC-MS data of hydrolysis of Tralopyril in deionized water. (A) The chromatogram of Tralopyril in water shows peaks for two retention times. The mass spectrum of the first of these peaks is shown in (B) and reveals two compounds: BCCPCA (m/z 323/325/327) and a product without a carboxylic group (m/z 279/281/283). (C) Shows the extracted spectrum from

the peak eluting at 19.80 mins in the top image and corresponds to Tralopyril, which was expected as the hydrolysis was not yet complete at the time of analysis.
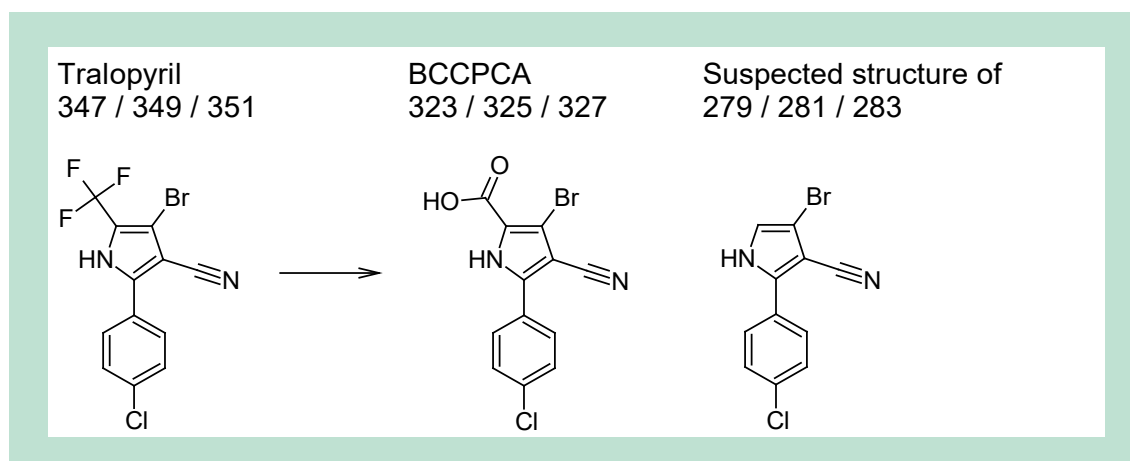

FIGURE 15: Tralopyril and its hydrolysis products. Two products have been found for tralopyril: BCCPCA and the BCCPCA rearrangement product (minus CO_2). The structures are suggested based on isotope patterns and product ion scans. BCCPCA is a known and confirmed hydrolysis product of Tralopyril. The other structure, with an [m-h}- of 279 / 281 / 283 is more likely a product formed in the ion source during this experiment, as it was not seen in other experiments (supporting information in appendix 2).

Medetomidine

Medetomidine was shown to be stable in deionized water and is not prone to hydrolysis, according to the assessment report. LC-MS/MS analysis for Medetomidine has to be performed under acidic conditions; otherwise, it will not be possible to ionize Medetomidine. Moreover, pH is also important when extracting this compound; a variable pH will lead to variable recoveries. Therefore, the water will have to be buffered to maintain a stable recovery of Medetomidine in solid phase extractions; Medetomidine remains in a net neutral charge in this range.

DCOIT & Irgarol

These two compounds are discussed together in this section, due to their similar results. DCOIT and Irgarol do not hydrolyse and are, therefore, rather stable in water. Both compounds can be extracted using the methods described in the materials and methods section. Moreover, for each compound a list of bio/photo degradation products is already available (Bollmann et al., 2017a,b).

Key findings – Hydrolysis

Modern antifouling biocides seem to hydrolyze quickly (within a few hours). However, the hydrolysis products can be described and were taken into account in the biodegradation and photolysis studies. It will make sense to include the hydrolysis products in future monitoring and assessment procedures.

7.2 Photodegradation
7.2.1 Indirect photolysis
DMST and DMSA

Photosensitized degradation rates of DMST and DMSA were studied under UVA in the presence of lumichrome (LC), a photosensitizer with high excited-state reduction potential ($E^{0*}(3S^*/S^{\bullet-})$ =1.91 V) (McNeill and Canonica, 2016), and zinc porphyrin (ZnP, ($E^{0*}(3S^*/S^{\bullet-})$= 0.78 V), a pure source of $^1O_2$ (Kalyanasundaram and Neumann-Spallart, 1982), respectively (Figure 17a). The reactions followed pseudo-first order kinetics, herein, the bimolecular reaction rate constants for DMST with $^3LC^*$ and $^1O_2$ were calculated at $1.165(\pm0.01)\times10^8$ M^{-1}S^{-1} and $4.5(\pm0.04)\times10^7$ M^{-1}S^{-1}, respectively. The phototransformation of DMSA with $^3LC^*$ and $^1O_2$ showed only slight decrease against FFA degradation. Faster photodegradation for DMSA with $^3LC^*$ ($k_{DMSA, {}^3LC^*}$ = $7.0(\pm0.1)\times10^6$ M^{-1}S^{-1}) was observed than with $^1O_2$ ($k_{DMSA, {}^1O_2}$= $2.4(\pm0.07)\times10^6$ M^{-1}S^{-1}). Additionally, the reaction rate constants for DMST and DMSA with hydroxyl radicals were $7.47(\pm0.07)\times10^9$ M^{-1}S^{-1} and $6.23(\pm0.09)\times10^9$ M^{-1}S^{-1} (Figure 17b).
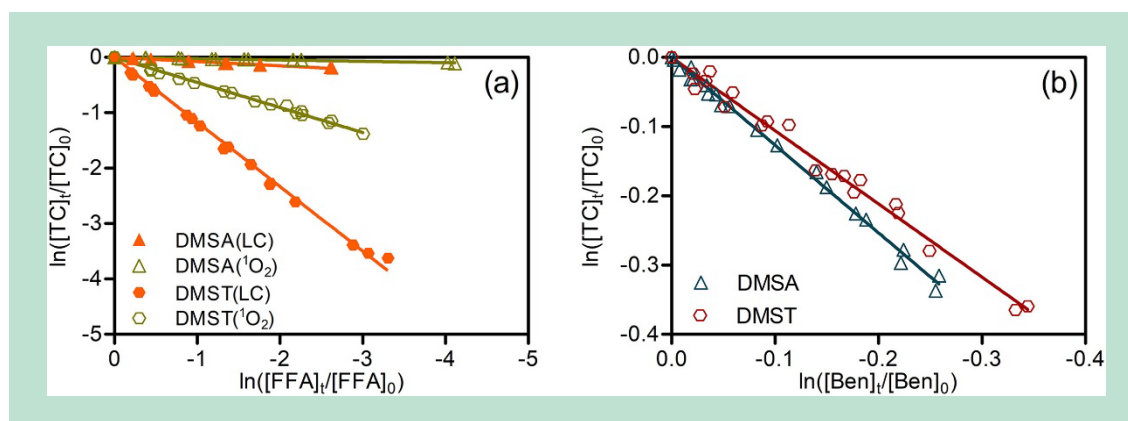

FIGURE 16: (a) Photodegradation kinetics of DMSA and DMST sensitized by singlet oxygen and lumichrome plotted against furfuryl alcohol (FFA) at pH 8.2; (b) Degradation kinetics of DMSA and DMST plotted against benzoate reacts with hydroxyl radical using H_2O_2 as a source at pH 8.2.

The overall observed reaction rate constant (Eq. 4) was calculated using steady-state concentrations of the reactive species in natural waters obtained from literature. Peterson et al. (2012) determined the steady-state concentration of singlet oxygen in natural water at 10^{-13} M, and McNeill and Canonica (2016) postulated that steady-state concentration of singlet dissolved organic matter $[^3CDOM^*]_{ss}$ is equal to $[^1O_2]_{ss}$. Accordingly, we assume the steady-state concentration of lumicrome $[^3LC^*]_{SS}$ being equal to $[^1O_2]_{ss}$. Mopper and Zhou (1990) determined the steady-state concentration of hydroxyl radical for coastal upwelled water (2.63×10^{-17} M). Hence, the $^3LC^*$-mediated and $^1O_2$-mediated phototransformation of DMST accounted for 71.3% and 27.5%, respectively. The $^3LC^*$-mediated and $^1O_2$-mediated phototransformation of DMSA accounted for 63.4% and 21.7%, respectively. The contribution of DMST and DMSA loss by hydroxyl radical were calculated at 1.2% and 14.9% (Eq. 4).

These results suggest that triplet excited lumichrome ($^3LC^*$) was the major contributor to the loss of DMST and DMSA. This is consistent with a recent study by Ossola et al. (2019), which proposed that $^3LC^*$ reactivity centered on the anilide moiety compounds, such as fenfuram, furcarbanil and methfuroxam. Additionally, Li et al. (2016) introduced that $^3NOM^*$ is mainly responsible for the phototransformation of the aniline-N compounds (sulfapyridine) and succeeded the degradation mechanisms.

Medetomidine

The steady-state phototransformation of Medetomidine with singlet oxygen followed pseudo-first-order kinetics. No phototransformation was observed at pH 5 (Figure 18a&b). Therefore, the bimolecular rate constant of deprotonated Medetomidine (pH > 9.1) with singlet oxygen was determined by multiplying the reaction rate constant of furfuryl alcohol at 1×10^8 M^{-1}S^{-1} (Appiani et al., 2017) and calculated to be 1.8×10^8 M^{-1} S^{-1}.

No obvious increase of degradation rate was observed compared to using ZnP as singlet oxygen sensitizer, which indicated no ^{3}LC*-mediated reaction attributed to the indirect phototransformation of Medetomidine (Figure 18b).

(a)

k = 1.767 ± 0.01581

○ pH9.24 Borate buffer
○ pH9.29 Borate buffer
◇ pH10.46 Carbonate buffer
◇ pH10.54 Carbonate buffer

ln([Med]$_t$/[Med]$_0$)

ln([FFA]$_t$/[FFA]$_0$)

(b)

○ pH5 ^{1}O$_2$
△ pH5 ^{3}LC*
◇ pH9 ^{1}O$_2$
□ pH9 ^{3}LC*

ln([Med]$_t$/[Med]$_0$)

ln([FFA]$_t$/[FFA]$_0$)
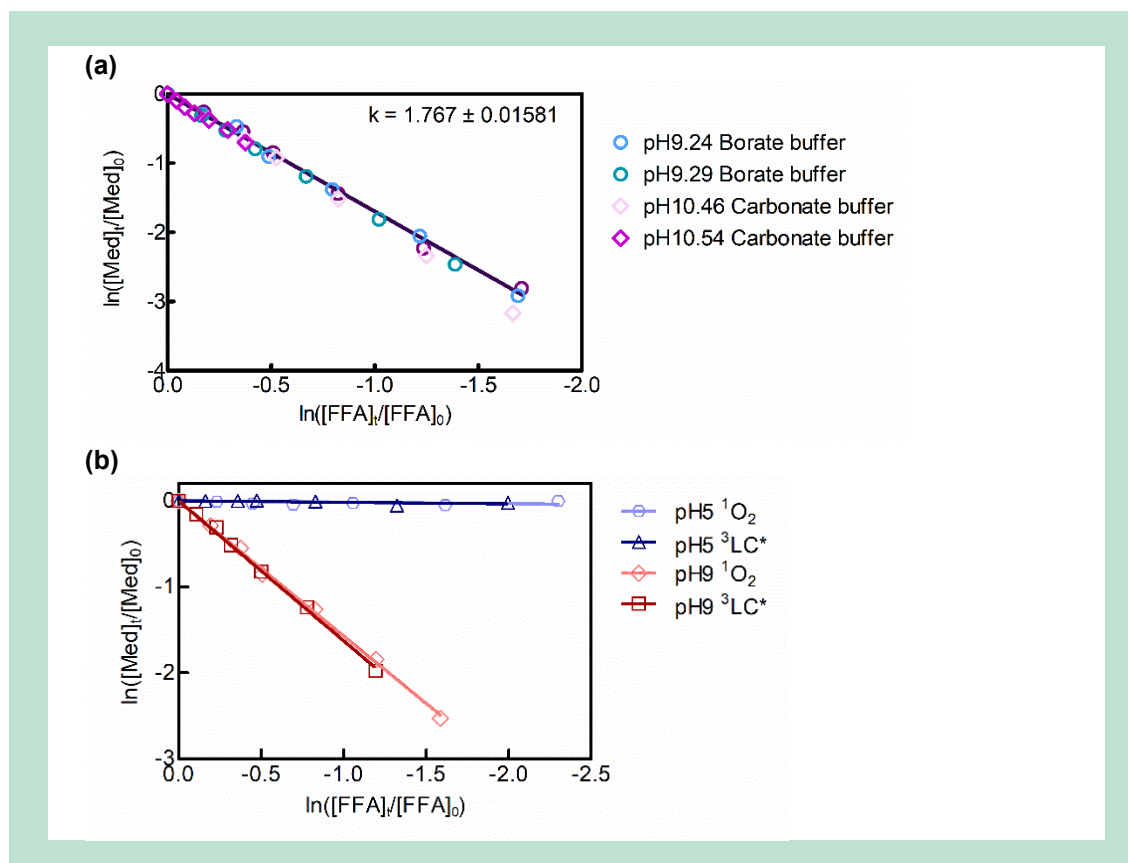
FIGURE 17: (a) ^{1}O$_2$-mediated phototransformation of Medetomidine sensitized by ZnP (1 µM) at pH 9.24 and pH 9.29 by using a borate buffer at pH1 0.46 and pH 10.54 by using carbonate buffer. Degradation of Medetomidine was plotted against the singlet oxygen probe furfuryl alcohol (FFA). (b) Comparison of ^{3}LC*-mediated and ^{1}O$_2$-mediated phototransformation of medetomidine sensitized by lumichrome and ZnP at pH5 and pH9.2, respectively.

The •OH-mediated reaction rate was conducted by using H_2O_2 and $NaNO_2$ as resources, respectively. The phototransformation rate constant of protonated Medetomidine was determined at pH5.6 (97.3% of protonated Medetomidine), where deprotonated benzoate (pKa =4.2) could be used as a probe, while the rate constant of deprotonated Medetomidine was determinated at pH9.2 (Figure 19). Bimolecular reaction rate constants were determined by multiplying the benzoate reaction rate constants with hydroxyl radical (5.9×10^9 M^{-1}S^{-1})(Samuni and Neta, 1973) .The bimolecular rate constants of deprotonated Medetomidine with hydroxyl radical was 1.0(±0.14) x10^{10} M^{-1}S^{-1}; protonated Medetomidine were 8.5(±0.12) x10^9 M^{-1}S^{-1} (H_2O_2 as source) and 7.6(±0.12) x10^9 M^{-1}S^{-1} ($NaNO_2$ as source), respectively.
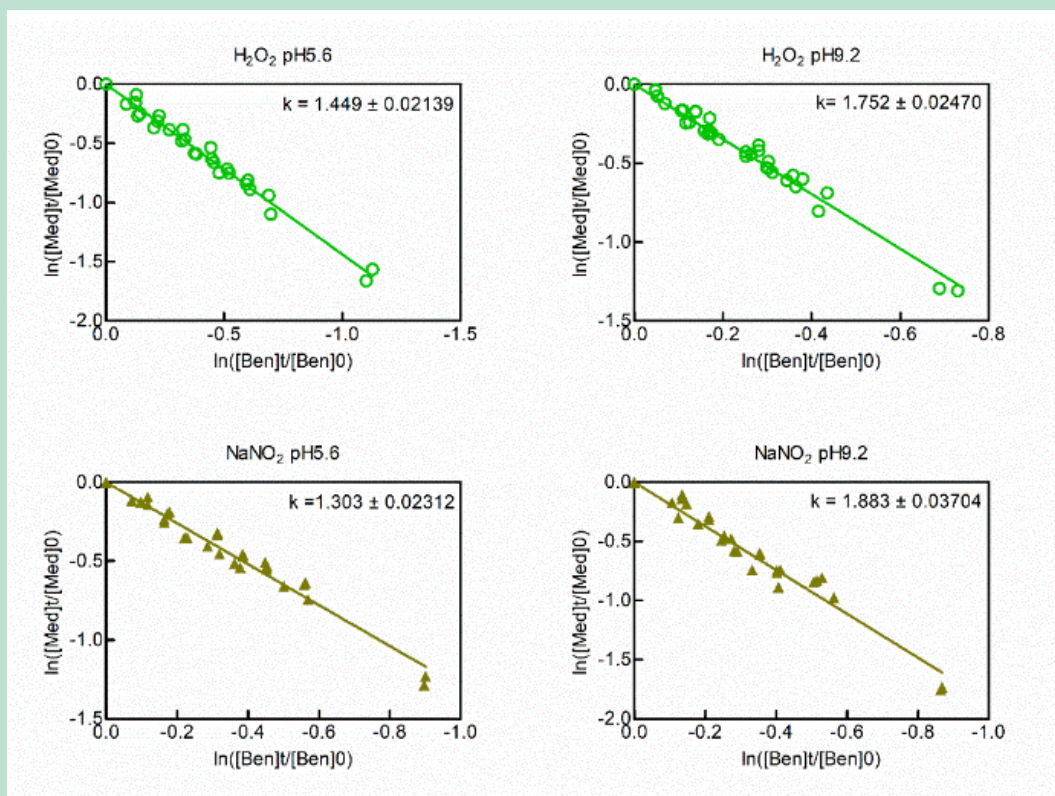
FIGURE 18: Bimolecular reaction rate constant of Medetomidine against degradation rate of sodiumn benzoate by using hydroperioxide and sodium nitrite as hydroxyl radical sources under UVA-light. Experiments at pH 5.6 and pH 9.2 were conducted by using phosphate buffer and borax/borate buffer, respectively.

In the previous sections, the phototransformation rate constants of protonated and deprotonated Medetomidine with individual reactive species were determined. The total rate constant for the loss of Medetomidine via indirect photodegradation will be the sum of the reaction with PPRIs multiplied by the steady-state concentration of PPRIs (eq. 4). The steady-state concentration of ·OH in sunlit waters was reported to be 2.63×10^{-17} M in coastal upwelled water by Mopper and Zhou (1990), and the steady-state concentration of $^1O_2$ was reported to be 10^{-13} M by Peterson et al. (2012). Accordingly, the degradation of protonated Medetomidine was fully attributed to the ·OH-mediated reaction, as the $^1O_2$-mediated reaction was negligible. By contrast, the $^1O_2$-mediated reaction exhibited the highest contribution for neutral Medetomidine, accounting for 98.5%, while ·OH-mediated reaction contributed the remainder.

7.2.2   Identification of phototransformation products
Tolylfluanid and Dichlofluanid

The formation of transformation products from Tolylfluanid and Dichlofluanid was studied under UVC-irradiation. Signals of suspected transformation products were detected using high-resolution mass spectrometry (MS- and MS^2-data). The detected mass-to-charge ratios are listed in Table 8 and Table 9, together with proposed formulas, names, nominal masses and structures. The mass error between detected and theoretical mass-to-charge ratio of the proposed structures were calculated. For those compounds for which true standards were available, these were injected and retention times and MS-fragmentation pattern were compared (see Figure Appendix 3.2-7). Confidence levels of validation are listed according to (Schymanski et al., 2015). In brief, Level 1: confirmation of retention time and MS^2-spectra with true chemical standard; level 2: the measured data of a probable structure is matching the information from a library; while

level 3: tentative candidates by interpretation of MS and MS^2-spectra; level 4 and level 5 were reached as unequivocal molecular formula and mass of interest.

Besides their hydrolysis products, five additional phototransformation products were identified for Dichlofluanid and six for Tolylfluanid. As expected, Dichlofluanid and Tolylfluanid are following similar phototransformation pathways. The structural analogy of the parent compounds and their hydrolysis products, just differing in one methyl group, is also visible in several transformation products.

The two structural analogs 2HBT (from Dichlofluanid, 1,3-benzothiazol-2(3H)-one, m/z 152.0163 Da) and MBZO (from Tolylfluanid, 6-methyl-1,3-benzothiazol-2(3H)-one, m/z 166.0321 Da) were validated with analytical standards in this study. Previously, benzothiazole has been identified as transformation product of dichlofluanid by GC-MS (Roberts and Hutson, 1999; Sakkas and Albanis, 2003). 2HBT (1,3-benzothiazol-2(3H)-one or 2-hydroxybenzothiazole) and benzothiazole differ solely in one hydroxyl-group. Due to the different analytical approaches, also the previous experiment might have led to 2HBT, which might have been detected as benzothiazole in GC-MS. The possible mechanism of the formation of MBZO could be that Tolylfluanid was phototransformed to 5-methyl-2,1-benzothiazol-3(1H)-one under UVC irradiation, followed by the photoisomerization of 5-methyl-2,1-benzothiazol-3(1H)-one to 6-methyl-1,3-benzothiazol-2(3H)-one (MBZO) due to a ring contraction ring expansion reaction (Figure Appendix 3.8). A similar photoisomerization of 2-substituted thiazol-3(2H)-one to 3-substituted thiazol-2(3H)-one has been described previously (Bollmann et al., 2017b). Likewise, the same reaction route might have yielded 2HBT. However, the intermediate 5-methyl-2,1-benzothiazol-3(1H)-one was not detected in the present study, thus, the full confirmation of the proposed pathway is pending.

In addition, DBZA (N,N-dimethyl-1,3-benzothiazol-2-amine) from Dichlofluanid was confirmed by an analytical standard based on matched retention time and fragmentation information. A corresponding transformation product of Tolylfluanid at 193.0794 Da is thus proposed to be the structural analog from DBZA, with a methyl group difference in all MS and MS^2-spectral data (see Figure Appendix 3.9). However, this identification still needs full validation by a true standard compound.

TDBS (N,N,6-trimethyl-2-oxo-2,3-dihydro-1,3-benzothiazole-3-sulfonamide), corresponding to the observed mass of 273.0365 Da, was validated as a transformation product from tolylfluanid by a chemical standard, which does not have a CAS registry number yet (synthesized on request). Additionally, CMSD (N'-(2-chloro-4-methylphenyl)-N,N-dimethylsulfuric diamide) was found as a phototransformation product of tolylfluanid, which was confirmed by a standard providing the same MS^2-fragment ions (140.0252 [C7H7NCl]$^+$, 113.0145 [C6H6Cl]$^+$, 104.0490 [C7H6N]$^+$, 77.0384 [C6H5]$^+$). However, analogous phototransformation products of dichlofluanid were not detected.

Furthermore, 5-amino-2-methylphenol (5A2MP) and 4-methylbenzenamine (p-toluidine) were formed by the phototransformation of both, tolylfluanid and its hydrolysis product DMST. The chemical formulas and structures of two additional transformation products of dichlofluanid (m/z 288.0475 Da and m/z 302.0633 Da) were not elucidated. A suspect screening revealed that none of the previously identified transformation products (see Table Appendix 3.1) was detected in the present experiments.

TABLE 8: Tolylfluanid and detected phototransformation products: detected m/z in Q-ToF with deviation of measured versus theoretical mass (m/z), compound name, structure, abbreviation and validation level (Schymanski et al., 2015).
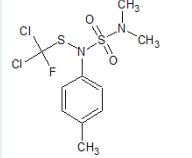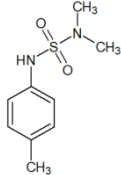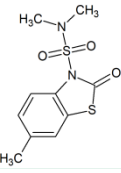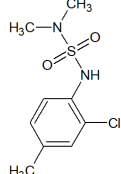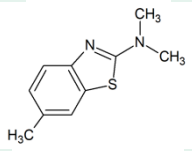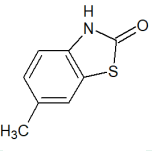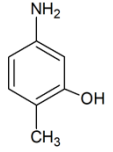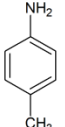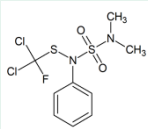
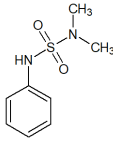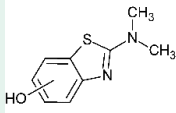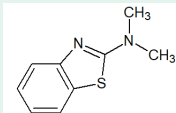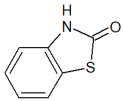| Transformation product and formula	Detected m/z [Da] Theoretical m/z [Da] Δm/z [mDa]	(Proposed) Compound (Abbreviation)	(Proposed) Structure	Main product ions	Validation level
Tolylfluanid (C$_{10}$H$_{13}$Cl$_2$FN$_2$O$_2$S$_2$)		Tolylfluanid			Level 1
DMST (C$_9$H$_{14}$N$_2$O$_2$S)	215.0851 215.0854 -0.3	*N,N*-Dimethyl-*N'*-P-tolylsulphamide		106.0644 [C7H8N]$^+$ 77.0380 [C6H5]$^+$ 44.0484 [C2H6N]$^+$	Level 1
TP273 (C$_{10}$H$_{12}$N$_2$O$_3$S$_2$)	273.0365 273.0362 0.3	*N,N*,6-Trimethyl-2-oxo-2,3-dihydro-1,3-benzothiazole-3-sulfonamide (TDBS)		164.0170 [C8H7NOS]$^+$ 108.0108 [C2H6NO2S]$^+$ 44.0492 [C2H6N]$^+$	Level 1
TP249 (C$_9$H$_{13}$ClN$_2$O$_2$S)	249.0462 249.0459 0.3	*N'*-(2-Chloro-4-methylphenyl)-*N,N*-dimethylsulfuric diamide (CMSD)		140.0252 [C7H7NCl]$^+$ 113.0145 [C6H6Cl]$^+$ 104.0490 [C7H6N]$^+$ 77.0384 [C6H5]$^+$	Level 1
TP193 (C$_{10}$H$_{12}$N$_2$S)	193.0792 193.0794 -0.2	*N,N*,6-Trimethylbenzo[d]thiazol-2-amine		178.0556 [C9H10N2S]$^+$ 150.0372 [C8H8NS]$^+$ 122.0181 [C6H4NS]$^+$ 91.0539 [C7H7]$^+$ 77.0380 [C6H5]$^+$	Level 3
TP166 (C$_8$H$_7$NOS)	166.0321 166.0324 -0.3	6-Methyl-1,3-benzothiazol-2(3*H*)-one (MBZO)		151.0073 [C7H8NS]$^+$ 106.0633 [C7H8N]$^+$ 94.0656 [C6H8N]$^+$	Level 1
TP124 (C$_7$H$_9$NO)	124.0753 124.0756 -0.3	5-Amino-2-methylphenol (5A2MP)		106.0652 [C7H8N]$^+$ 94.0644 [C6H8N]$^+$ 89.0379 [C7H5]$^+$ 44.0491 [C2H6N]$^+$	Level 1
TP108 (C$_7$H$_9$N)	108.0805 108.0807 -0.2	4-Methylbenzenamine (*p*-toluidine)		91.0539 [C7H7]$^+$ 65.0382 [C5H5]$^+$ 39.0226 [C3H3]$^+$	Level 1

TABLE 9: Dichlofluanid and detected phototransformation products: detected m/z in Q-ToF with deviation of measured versus theoretical mass (Δm/z), compound name, structure, abbreviation and validation level (Schymanski et al., 2015).

Transformation product and formula	Detected m/z [Da] Theoretical m/z [Da] Δm/z [mDa]	(Proposed) Compound (Abbreviation)	(Proposed) Structure	Main product ions	Validation level
Dichlofluanid ($C_9H_{11}Cl_2FN_2O_2S_2$)		Dichlofluanid			Level 1
DMSA ($C_8H_{12}N_2O_2S$)	201.0693 201.0692 0.1	*N,N*-Dimethyl-*N´*-phenylsulfamide		92.0495 [C6H6N]⁺ 65.0386 [C5H5]⁺ 39.0226 [C3H3]⁺	Level 1
TP195 ($C_9H_{10}N_2OS$)	195.0585 195.0586 -0.1	2-(Dimethylamino) benzothiazolol		180.0343 [C8H7N2OS]⁺ 152.0415 [C7H6NOS]⁺ 125.0286 [C6H5OS]⁺ 93.0552 [C6H5O]⁺	Level 4
TP302 ($C_5H_{19}FN_2O_7S_2$)	302.0633			193.0433 150.0021 122.0071 66.0342	Level 5
TP288	288.0475			242.9874 179.0260 90.0333	Level 5
TP179 ($C_9H_{10}N_2S$)	179.0647 179.0637 1.0	*N,N*-Dimethyl-1,3-benzothiazol-2-amine (DBZA)		164.0396 [C8H8N2S]⁺ 136.0215 [C7H6NS]⁺ 108.0019 [C6H4S]⁺ 65.0390 [C5H5]⁺	Level 1
TP152 (C_7H_5NOS)	152.0163 152.0164 -0.1	1,3-Benzothiazol-2(3*H*)-one (2HBT)		124.0206 [C6H6NS]⁺ 92.0497 [C6H6N]⁺ 80.0492 [CH6NOS]⁺ 65.0382 [C5H5]⁺	Level 1

Additionally, DMS (*N,N*-dimethylsulfamide) was described as a metabolite of both tolylfluanid and dichlofluanid in an earlier study by (Schmidt and Brauch, 2008). However, it has not been mentioned as a photoproduct before. In this study, DMS has not been detected in the transformation product identification process due to its extreme polarity, and therefore not retained on the used analytic column. In the indirect photolysis of DMST and DMSA with reactive species under UVA irradiation, the concentration of DMS was determined (Figure 20). An increasing accumulation of DMS was found with time during 24 hours exposure. To examine DMS's contribution to the mass balance of initial concentration, results at three selected time points (0, 6 and 24h) are presented in Figure 20. In these reactive species ($^3LC^*$, $^1O_2$ and ·OH) induced phototransformation of DMST, DMS eventually reached a final concentration of 13.3, 11.9 and 8.3 µM, respectively. The sum of DMST and DMS closed the mass balance of these reactions at 93%, 91% and 73%. Similarly, the sum of DMSA and DMS accounted for 95%, 98% and 48% of the mass balance in these respective processes. These outcomes imply that DMS was the major photoproduct of DMST and DMSA of PPRI-induced reactions.

For ·OH-sensitized experiments, a possible explanation for the mass balance gaps could be the formation of other hydroxylation photoproducts through particular pathways. Several studies (Ge et al., 2015; Page et al., 2010) investigated the hydroxylation of aromatic compounds, such as terephthalate and fluoroquinolones, with hydroxyl radicals. Therefore, it is likely that phenolic products are formed during the OH-adduct processes of DMST and DMSA and likewise, 3-OH-DMST, OH-methyl-DMST, and 2-OH-DMST were reported upon ozonation (Schmidt and Brauch, 2008).
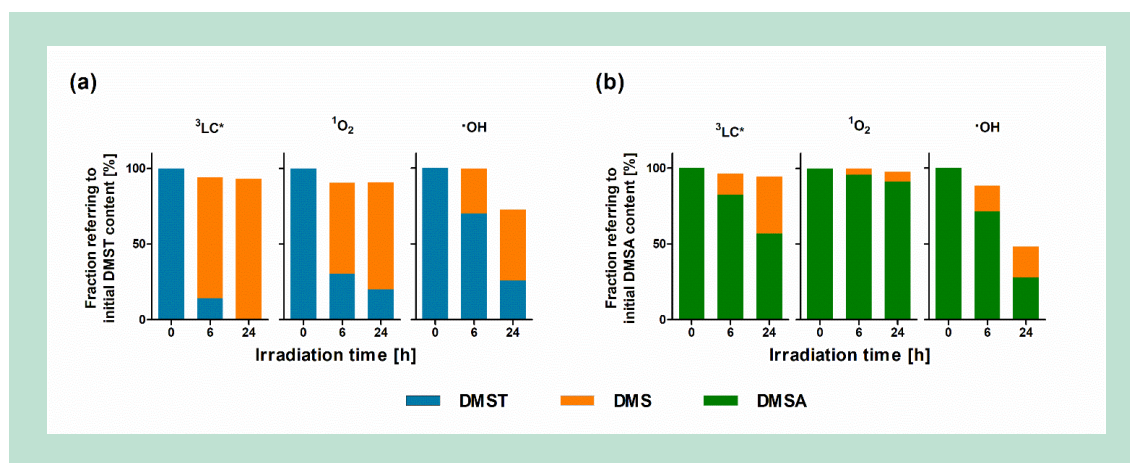
FIGURE 19: Photosensitized reaction of (a) DMST and (b) DMSA under UVA irradiation with lumichrome ($^3LC^*$), singlet oxygen ($^1O_2$), and hydroxyl radical ($\cdot OH$) and formation of their phototransformation product DMS.

Medetomidine

Only little transformation of Medetomidine dissolved in deionized water was determined when exposed to UVC-light (Figure 21). Thus, no direct phototransformation was observed for Medetomidine.
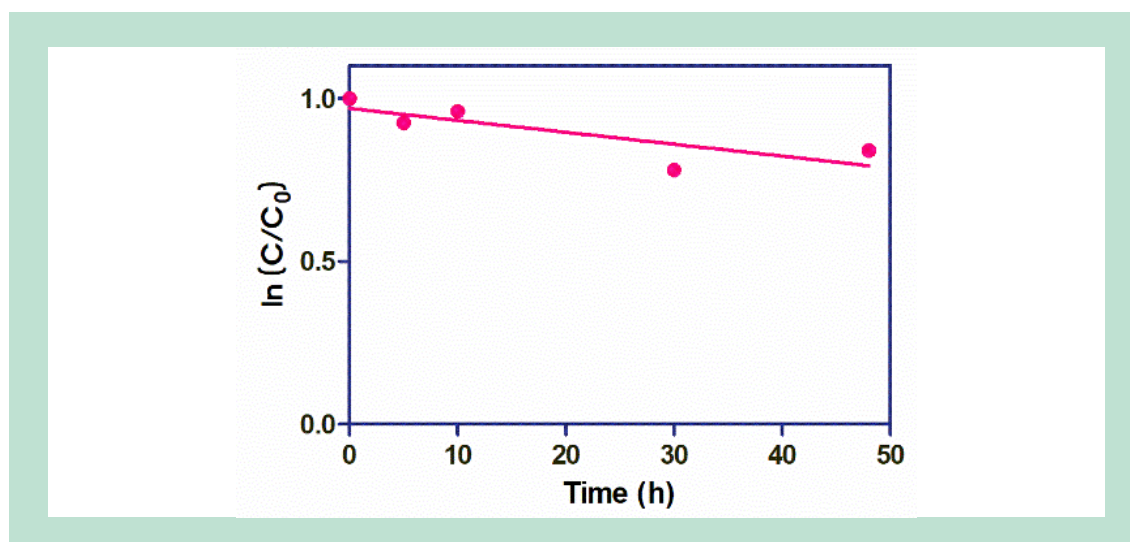

FIGURE 20: Degradation of Medetomidine in deionized water irradiated with UVC-light.

The additional phototransformation study of photosensitized degradation of Medetomidine under UVA-light revealed degradation. Three phototransformation products (TP 5, 6, and 10) were formed in $^1O_2$-mediated phototransformation process (Figure 22). Their structures were elucidated by using NMR and further validated by using q-TOF. However, TP2 was only proposed based on HRMS information. TP10 shows the highest intensity during the isolation processes. TP5 and TP6 had the similar peak areas in the whole procedures.

TP10 had an m/z of 178.1227 (M+H)$^+$. It has major fragmentations 133.1020, 105.0703, 91.0546 and 77.0390, corresponding to C10H13+, C8H9+, C7H7+ and C6H5+. They show that the elimination of imidazole ring along with the addition of oxygen. TP% and TP6 are diastereomers. They had m/z of 233.1318 and 233.1276 (M+H) $^+$, respectively. It shows an addition of two oxygen. TP2 is an intermediate of the first reaction pathway. It had m/z of 251.1403. It has a fragments of 145.1015, which suggests the elimination of 1,2-dimethyl-benzene. Fragment of

105.0695 indicates the rest part of the structure. Although TP2 and TP9 have the same monoisotopic mass, the specific m/z 173.097 indicates that the structure should be TP2 than TP9.

The indirect photolysis of Medetomidine with singlet oxygen proceeds via two main pathways (Figure 22). The singlet oxygen was proposed to react with imidazole (Latch et al., 2003; Tomita et al., 1969) by 2,5 or 4,5-cycloaddition to form *endo*-peroxide or dioxetane (photoproduct 1 and 7). The endo-peroxide was ruptured by water molecular attack to yield 2. The following formation of 3 is proposed by the subsequent dehydration of hydroperoxide by a loss of water. Photoproduct 4, 5 and 6 were proposed due to the subsequent tautomerizations of 3. The formation of photoproduct 5 and 6 were proposed due to the parent compound Medetomidine was a racemic mixture.

We proposed a similar pathway of reaction with singlet oxygen, and a dioxetane intermediate was formed. Subsequent ring-opening process is proposed to yield TP8. By hydration process, TP9 was yielded. Afterwards, TP10 was formed due to the retro aldol reaction by a loss of $C_2H_3NO_2$. In $^1O_2$-mediated reaction, TP10 was the major photoproduct, while TP5 and TP6 are the second major photoproducts.
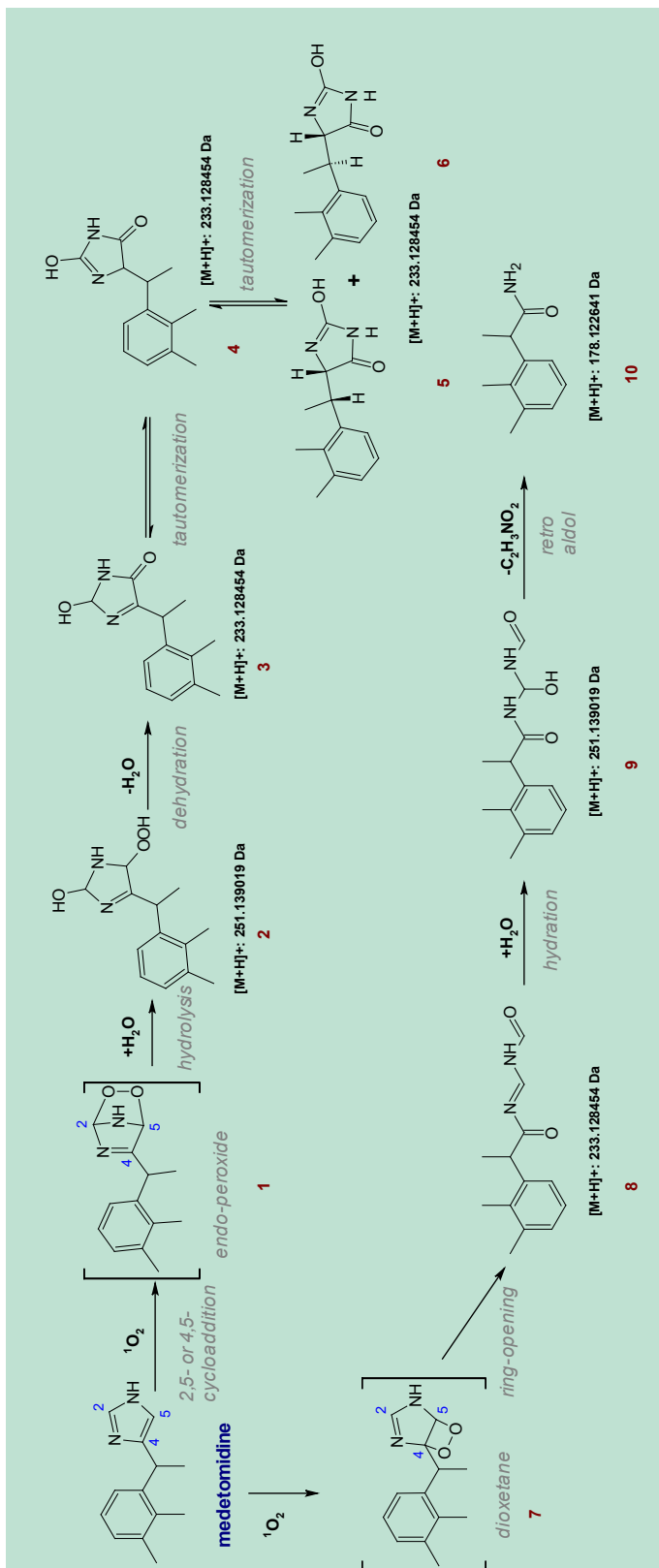
FIGURE 21: Proposed pathway of Medetomidine reaction with singlet oxygen.

7.2.3 Phototransformation kinetics of antifouling biocides under natural sunlight and formation of transformation products

7.2.3.1 Tolylfluanid and Dichlofluanid

In this experiment, a two-step process was observed: first the hydrolysis of antifouling biocides, followed by the phototransformation of the hydrolysis products (Figure 23). Relatively high concentrations of 15 µM were used for this experiment, in order to have higher signals to quantify transformation products. The applied concentrations exceeded the solubility limit for Tolylfluanid and Dichlofluanid in deionized water; however, the solubility limit was not reached due to rapid hydrolysis in coastal and sea water. These observations are consistent with the previous results (see paragraph 4.4.1), showing that the hydrolysis process is complete in coastal water, while a remaining fraction is observed in deionized water. In deionized water (Figure 23a, and b), Tolylfluanid and Dichlofluanid kept relatively high concentrations in the system, equaling their water solubility, while DMST and DMSA where constantly formed. Data in Figure 23c and d shows that Tolylfluanid and Dichlofluanid hydrolyzed rapidly to DMST and DMSA in coastal water – already 88% and 94% of the initial concentration was transformed into DMST and DMSA after stirring in dark for 6h, respectively. After one day, most of Tolylfluanid and Dichlofluanid were transferred to their hydrolysis products. For sea water, hydrolysis was observed to occur at a slower rate: 71% of Dichlofluanid was transferred to its hydrolysis product at the first measurement after 6h dark-incubation and 93% after three days (Figure 23). This rapid hydrolysis and formation of DMSA is in agreement with earlier studies (Hamwijk et al., 2005). The same trend was observed for tolylfluanid with a slower reaction rate (Figure 23). Therefore, the expected increase in concentration of DMST was slightly slower than DMSA. These findings, together with the properties of the waters (Table 10), suggest that Tolylfluanid and Dichlofluanid hydrolyze rapidly in alkaline conditions, which is in agreement with the EU assessment reports (European Chemicals Agency, 2016, 2014b). Furthermore, the hydrolysis rates of these compounds could be influenced in the presence of humic substances (Perdue and Wolfe, 1982; Prosen and Zupančič-Kralj, 2005). Due to the rapid hydrolysis of Tolylfluanid and Dichlofluanid in coastal and sea water, not only the phototransformation of the parent compounds but also of the hydrolysis products is expected to be relevant for the environment.
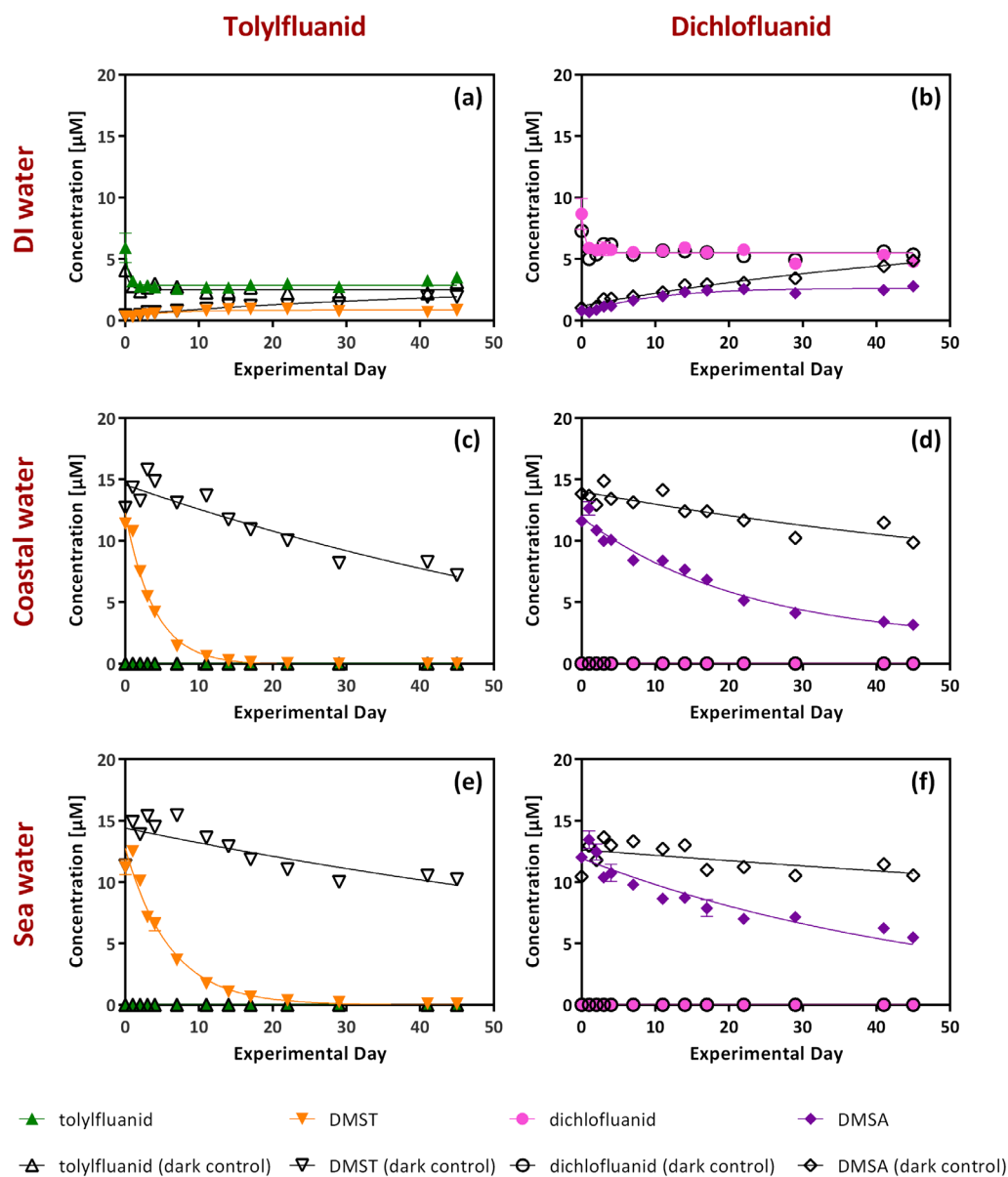
FIGURE 22: Concentration of Tolylfluanid, Dichlofluanid, DMST and DMSA in DI water, coastal water and sea water over time; Initial concentrations of Tolylfluanid and Dichlofluanid are 14.5 µM and 14.7 µM, respectively. Plotted functions are pseudo-first-order kinetics.

Rapid photodegradation of DMSA and DMST was observed in sunlit waters compared to the dark control, indicating that phototransformation was their major dissipation pathway in natural waters (Figure 23). As mentioned earlier, DMST and DMSA were constantly formed in deionized water during the course of the experiment. Nevertheless, while their concentrations were constantly increasing in the dark control, their concentrations reach a plateau during sunlight irradiation. This is leading to the conclusion that their photodegradation rates are somewhat similar to the formation rate through hydrolysis of Tolylfluanid and Dichlofluanid in deionized water. As illustrated in Figure 20, photodegradation of DMSA and DMST followed pseudo-first-order kinetics in natural waters. The measured DMSA half-lives were 15.6 days in coastal water and 23 days in sea water, while half-lives of DMST were 2.7 days in coastal water and 4.2 days in sea water (Table 7). The phototransformation rates of DMST and DMSA were contributed by indirect photolysis in the presence of photo-sensitizers (Figure 24). Although the reaction pathways for

the two compounds are very similar, DMST is reacting considerably faster than DMSA. This is leading to the conclusion that the electron-donating methyl-group on the benzene ring of DMST could enhance the photodegradation rates of DMST compared to DMSA (structures shown in Figure 12). Moreover, the dark controls showed one-third concentration loss of DMST and DMSA, considerably more noticeable in coastal than in sea water over 45 days in the absence of light. This effect could be attributed to biodegradation by suspended organisms.

TABLE 10: Degradation rate constants k (standard error in brackets), half-time and final plateau of DMSA and DMST in coastal and sea water with and without sunlight irradiation.

	DMSA		DMST		Dichlofluanid		Tolylfluanid	
	Coastal water	DI	Coastal water	DI	Coastal water	DI	DI	Coastal water
C_0 [µM]	= 0	= 0	= 0	= 0	1.304 (0.013)	1.056 (0.054)	= 0	= 0
Plateau [µM]	1.034 (0.017)	0.269 (0.011)	0.774 (0.007)	0.163 (0.007)	= 0	0.571 (0.007)	0.269 (0.011)	0.774 (0.007)
k [h^{-1}]	0.315 (0.026)	0.138 (0.017)	0.203 (0.007)	0.130 (0.015)	0.437 (0.005)	0.390 (0.056)	0.138 (0.017)	0.203 (0.007)
Half-time [h]	2.20	5.04	3.41	5.35	1.59	1.78	5.04	3.41

Formation of transformation products of Tolylfluanid and Dichlofluanid

During the phototransformation experiment of tolylfluanid, N'-(2-chloro-4-methylphenyl)-N,N-di-methylsulfuric diamide (CMSD) was continuously formed in DI water under sunlight due to the lasting presence of parent compound. In coastal and sea water, the concentrations of CMSD increased rapidly from first to fourth sampling point (0.005 µM) and showed decrease in the remaining experimental days (Figure 24a). It indicates that CMSD was formed directly from tol-ylfluanid. Through the parallel-irradiation of DMST and Tolylfluanid under UVC-light, it was con-firmed that CMSD was directly formed from Tolylfluanid. Nevertheless, it also underwent photo-transformation. However, it has to be mentioned that CMSD was also formed to some extent in the dark controls in coastal and sea water (0.002 to 0.004 µM), which might be due to organisms in the natural water, while nothing was detected in the DI water dark control.

In coastal and sea water (Figure 24b), 6-methyl-1,3-benzothiazol-2(3H)-one (MBZO) exceeded the detection limit starting from the second day of the experiment. However, MBZO did not ex-ceed the quantitation limit during the experiment and remained steadily detected. On the other hand, there was a constant increase of MBZO in the experimental period in deionized water (Figure 24b). It was hypothesized that MBZO was formed directly from Tolylfluanid. While Tol-ylfluanid is constantly present in deionized water (Figure 24a) and thus can be transformed to MBZO, the fast hydrolysis leads rapidly to a lack of the parent in coastal and sea water. This hypothesis was confirmed by an additional pathway validation experiment, in which MBZO was only formed during irradiation of Tolylfluanid, while it was absent in the incubations of DMST. Additionally, the data showed that MBZO is photostable.

As no analytical standard was available at the time of analysis, TDBS (N,N,6-trimethyl-2-oxo-2,3-dihydro-1,3-benzothiazole-3-sulfonamide) is presented by the recorded peak areas (Figure 24c). Verification with an analytical standard has been performed in a later stage. It is noticeable that it was formed in both dark control and irradiated samples with constant, high signals in coastal and sea water, starting from the second time point. The signal of TDBS in sunlit coastal water (Peak area = 6e^4 counts ≈ 40xLOQ) was slightly higher than in the dark control, while in sea water, the signal in samples exposed to sunlight (Peak area = 1.5e^5 counts) was three times higher than in the dark control. Nevertheless, a gradual increase was observed in deionized water exposure to sunlight (Peak area = 6e^6 counts at 45 days), compared to a very slow gradual increase in the dark control (Peak area = 8e^4 counts at 45 days). Hence, a conclusion could be

drawn that TDBS is both a biodegradation product and a photodegradation product. Furthermore, it showed rather constant peak areas in natural waters during experimental days; therefore, it was assumed being photolytically stable.

The formation of 5A2MP (5-amino-2-methylphenol) and p-toluidine (4-methylbenzenamine), both validated as phototransformation products with analytical standards in the laboratory experiments, could not be confirmed in the present experiment under natural sunlight.
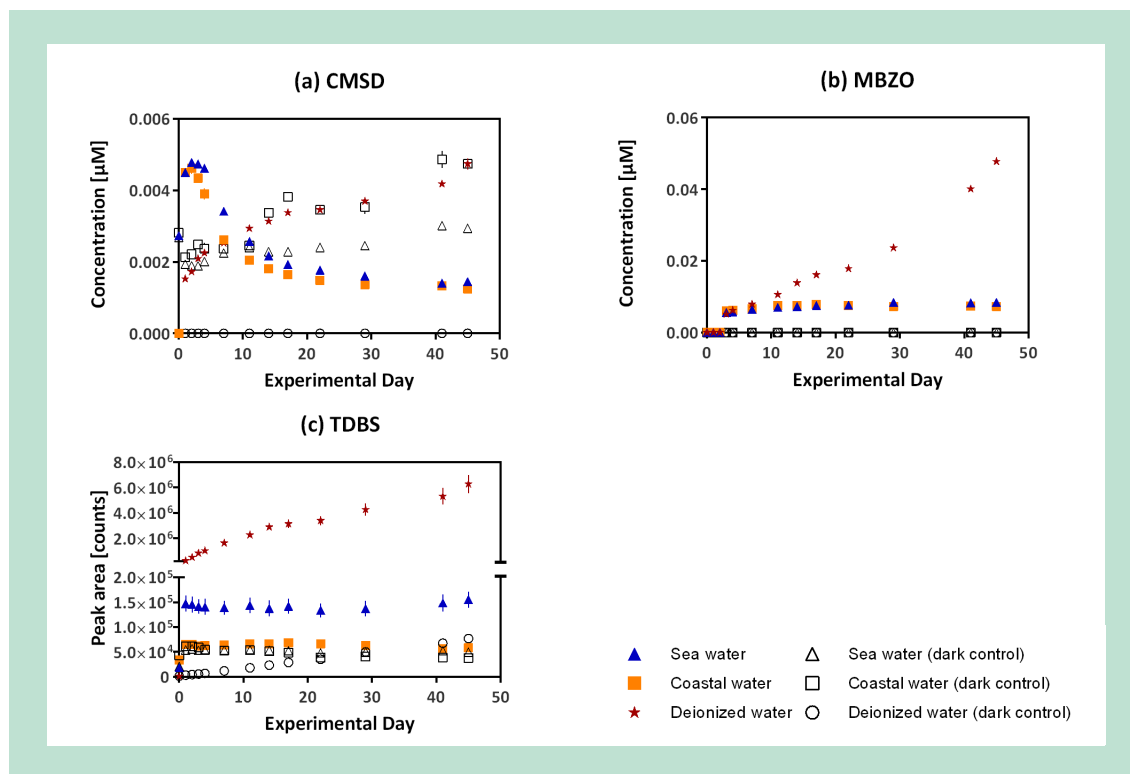

FIGURE 23: Formation of (a) CMSD (*N'*-(2-chloro-4-methylphenyl)-*N,N*-dimethylsulfuric diamide), (b) MBZO (6-methyl-1,3-benzothiazol-2(3*H*)-one) and (c) TDBS (*N,N*,6-trimethyl-2-oxo-2,3-dihydro-1,3-benzothiazole-3-sulfonamide) from tolylfluanid both in dark control and under natural sunlight in DI water, coastal water and sea water. Peak area of TDBS is shown as no standard was available during quantification.

Regarding the phototransformation of Dichlofluanid, it was demonstrated that 1,3-benzothiazol-2(3*H*)-one (2HBT) was gradually formed to reach maximum concentrations of 0.03 µM over 45 experimental days (Figure 25a) in deionized water exposed to sunlight. Similarly as the formation of MBZO from Tolylfluanid, the formation of 2HBT can be attributed to the direct formation from Dichlofluanid, which was constantly present in the DI water incubations. This phototransformation product was not quantified in other sunlit waters, most probably due to its low concentration and high limit of quantitation (LOQ = 0.019 µM).

DBZA (*N,N*-dimethyl-1,3-benzothiazol-2-amine), was found in both dark control and sunlit samples (Figure 25b). Its concentrations in natural waters were detected at 0.0016 µM (LOQ = 0.0016 µM) starting from the second and to the last time point both in dark control and sunlit samples, while it increased during the course of the experiment in deionized water, reaching a final concentration of 0.06 µM. A significant signal of DBZA (signal = 6 × LOD) was detected in the samples with Dichlofluanid under UVC irradiation, without any signals measured in DMSA samples. Thus, it can be concluded that DBZA could be a direct photodegradation product from Dichlofluanid, and at the same time formed in biodegradation processes.
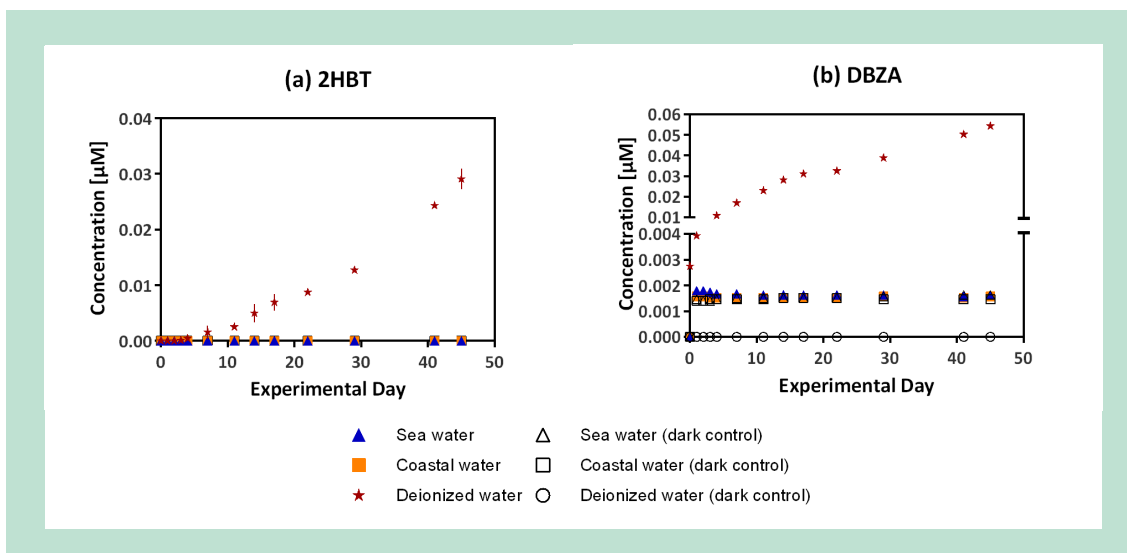
FIGURE 24: Formation of 2HBT (1,3-benzothiazol-2(*3H*)-one) and DBZA (*N,N*-dimethyl-1,3-benzothiazol-2-amine) from Dichlofluanid during the exposure to natural sunlight and in dark control in DI water, coastal water and sea water.

To confirm the photolytic formation of DMS in natural aquatic conditions, the concentration of DMS in coastal water was determined (Figure 26). Since DMS originated from both DMST and DMSA, the sum concentration of DMST and DMSA was considered as an integration to display the transformation rates. The total of DMST and DMSA showed a steep decrease, following pseudo-first order during the phototransformation process, while linear degradation was observed in the dark control as a consequence of biodegradation. The concentration of DMS in sunlit samples showed a sharp increase over 45 days and reached 13.5 µM ultimately. Moreover, a gradual increase of DMS could also be observed in the dark control (reaching 3.1 µM), which suggests that DMS is both a photodegradation and biodegradation product of DMST and DMSA. The latter is in agreement with previous research (Schmidt and Brauch, 2008), while DMS as photodegradation product has not been described before.
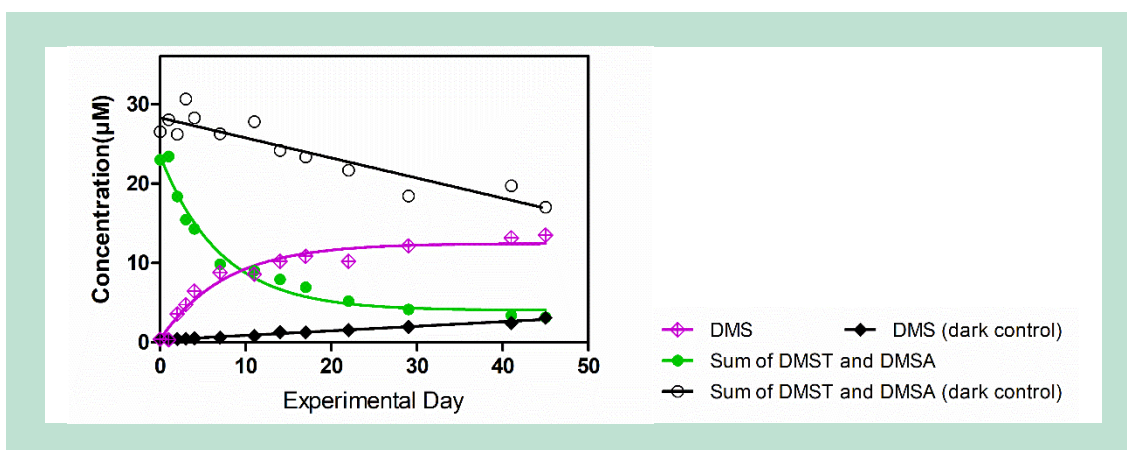
FIGURE 25: Degradation of the sum of DMST and DMSA (round circle) and the formation of DMS (diamond) under sunlight and in dark control in coastal water over time.

Mass balance of Tolylfluanid and Dichlofluanid

Two processes contribute to the overall mass balance of Tolylfluanid and Dichlofluanid: a) the hydrolysis of the parent compounds; b) the phototransformation of the parent compounds and their respective hydrolysis products. Due to the rapid hydrolysis in coastal water and sea water,

DMST and DMSA accounted for nearly 100% of the mass balances of tolylfluanid and di-chlofluanid at the starting phase of the natural sunlight irradiation experiments (see Figure Appendix 3.11 & 12). After 45 days irradiation of tolylfluanid, CMSD accounted for 0.3% and 0.4% of the initial amount of tolylfluanid in coastal water and sea water, respectively, while MBZO was formed about 1.2% and 1.4% in total. With regard to Dichlofluanid, *N,N*-dimethyl-1,3-benzothia-zol-2-amine (DBZA) was gradually accumulated to 0.4% in deionized water samples under sunlight, and it accounted for 0.01% in both, coastal water and sea water. 1,3-benzothiazol-2(*3H*)-one (2HBT) was only detected in sunlight-irradiated deionized water; it finally contributed with 0.2% to the total mass balance of Dichlofluanid. As this was obviously not adding up to a full mass balance, it was tested whether the well-known metabolite DMS did contribute to the mass balance of the two antifouling compounds.

As Tolylfluanid and Dichlofluanid were irradiated together, a combined mass balance needs to be considered regarding the formation of DMS. The combined mass balances in sunlit and dark environment are shown in Figure 27. In sunlit samples, approximately 47% of the initial Tol-ylfluanid and Dichlofluanid was transformed to DMS. While Tolylfluanid has been completely degraded, remaining DMSA from Dichlofluanid accounted for 11% of the total mass balance (Figure 27a). In contrary, the total of Tolylfluanid and Dichlofluanid was transformed to DMST (25%), DMSA (34%) and DMS (11%) in the dark control (Figure 27b). Eventually, the combined mass balance of Tolylfluanid and Dichlofluanid has been closed at 58% and 69% in sunlit and dark conditions, respectively. Additionally, other photoproducts accounted for 1.51% and 0.05% in total, respectively. The unclosed mass balance by transformation may result from ·OH-medi-ated pathways and halogen radicals reaction in salinity condition (Parker and Mitch, 2016), which requires further studies.
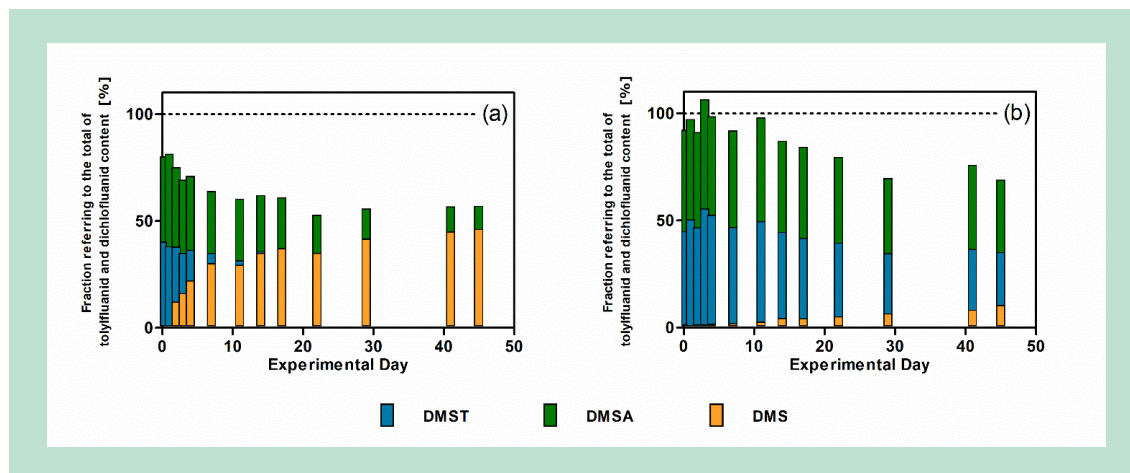

FIGURE 26: Combined mass balance of Tolylfluanid and Dichlofluanid, including their hydrolysis and degradation products DMST, DMSA and DMS under natural sunlight (a) and dark control (b) in coastal water. Other determined phototransformation products account for less than 2% and are thus not shown in this graph. The dashed line represents the expected total transfor-mation of the combined Tolylfluanid and Dichlofluanid content.

7.2.3.2 Medetomidine

The following section describes the degradation of 22 µM Medetomidine in deionized water, coastal and sea water under natural sunlight and in dark control (Figure 28) There was no sig-nificant decay of concentration over time in deionized water as expected, suggesting that the direct photolysis was very slow. This result matches with the low absorption in visible light from absorption spectrum (Figure Appendix 3.13). The concentration of Medetomidine in coastal and sea waters showed decay exponentially as a function of irradiation time in sunlit condition and dark control, which implies that both photodegradation and biodegradation were followed first-order kinetics. Within the scope of this paper, we want to focus on the photodegradation aspect. In coastal water, the rate constant of decay in sunlit system (half-life = 0.78 d) was 12 times

faster than in dark control (half-life = 9.3 d), while 9 times faster in seawater ($T1/2_{light}$= 1.24 d, $T1/2_{dark}$ = 11.3 d). The significant rapid decay in sunlit system than dark control observed was contributed by the indirect photodegradation. Furthermore, shorter half-live in coastal water than sea water was expected to be impacted by the elevated dissolved organic matter concentration (8.08 mg C/L and 4.09 mg C/L in coastal and sea water, respectively). The indirect phototransformation of Medetomidine could be contributed by reaction with reactive species, such as triplet organic matter, singlet oxygen and hydroxyl radicals. Kinetics, pathways and photoproducts of different reactive species under UVA condition in lab scale were investigated in the subsequent sections.
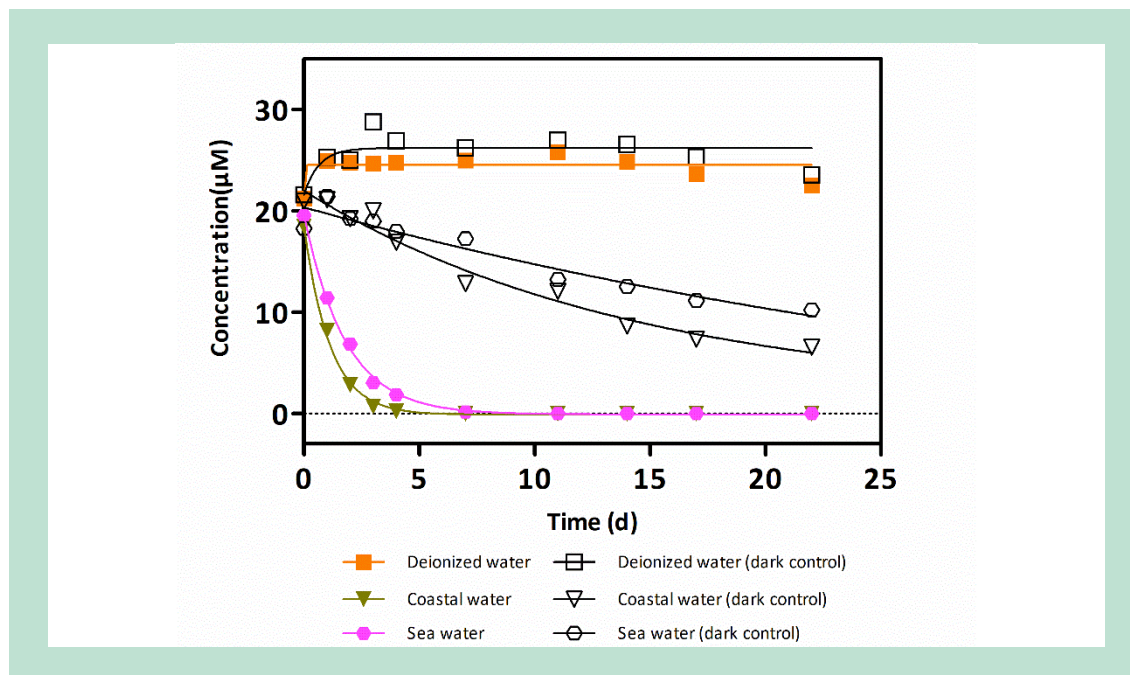
FIGURE 27: Concentration of Medetomidine in deionized, coastal and sea water under natural sunlight over time. The starting concentration was 22 µM.

Transformation products of Medetomidine

As shown in Figure 29, highest concentrations where observed for TP178 in the coastal water samples exposed to natural sunlight. TP178 showed a significant accumulation over time and peaked at day 7 (peak area = 1.22×10^5) and showed a decrease later on. TP251 reached a maximum peak area of 1.5×10^4. The TP233 isomers were likely to reach peak areas of 3.8×10^4. Its TPs are slightly more hydrophobic than the original Medetomidine and are expected to appear in sediment than in water phase.

FIGURE 28: Formation of phototransformation products of Medetomidine in coastal waterover time.

Key findings – Photolysis

The photolysis reactions are complex but lead to defined photodegradation products. Photolysis rates and to some extent -products depend on whether the reactions are conducted in pure water, tap water or marine water.
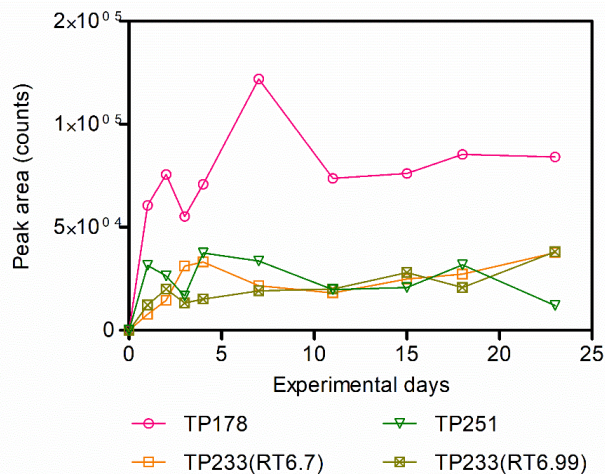
Concerning **Tolylfluanid/Dichlofluanid**, DMS is the dominant/prevalent end product, but several other transformation products are formed as well. At this moment, little can be outlined on toxicity of these photoproducts, thus the respective risk cannot be evaluated. This was also not within the scope of this project.

Interestingly, **Medetomidine** that was stated as "photostable" in the assessment report is degrading in natural waters due to indirect photodegradation. Both, reaction rate constants and photodegradation products were determined in this project. As for the assessment report only a comparison of the UV-spectrum of the compound with the spectrum of natural sunlight was performed, while full photolysis experiments were conducted within this project, this difference can easily be explained. It seems advisable that assessment reports in the future conduct more than a spectral comparison.

7.3   Biodegradation
7.3.1   Dichlofluanid and Tolylfluanid

In sediments, the first timepoint showed a DMSA concentration of 0.29 ± 0.01 µM (µmol/L), which is equivalent to 62% of the spiked concentration (Figure 30b). The DMST concentration at the first time point was 0.21 ± 0.003 µM, which corresponds to 44% of the spiked concentration (Figure 30b). To check to which extent DMSA and DMST sorb to the sediment, an assessment of sorption based on partitioning to the TOC of the sediment was conducted. The K_{ow} of DMSA is 1.59, and the K_{ow} of DMST is 1.99 (European Chemicals Agency, 2016, and 2014).

For DMSA this means that a K_{oc} of 1.63 was calculated, while the K_{oc} for DMST was 1.92. For DMSA this means that 0.14 ± 0.01 µM was expected in sediment, equivalent to 30% of the theoretically spiked concentration, which agrees well with only 58% being found in the water after one day, leaving only a gap of 12% in the initial mass balance, which is almost covered by the standard deviation in mass balance percentage (±3% in water and ±8% in sediment). For DMST the expected sediment concentration was 0.20 ± 0.02 µM or 42% of its spiked concentration with 38% found in the water after the first day. The mass balance for DMST evens out with 80% explained and 20% missing – with ±4% in sediment and ±1% in the water this leaves 15% uncovered with the uncertainty of the original data.

DMSA is removed from the system and follows a zero-order removal in both the control and the treatment (Table 11). Moreover, the reaction rate between the control and the treatment was significantly different (p-value = 0.03). Here, the control has a higher reaction rate, which points to abiotic removal.

For **DMST**, clear biodegradation in sediments was observed, following first-order kinetics (Table 11). These first-order kinetics were used to calculate a half-life for DMST at 5.78 ± 0.97 days in sediment-water systems. The control remained stable throughout the experiment.

The degradation of DMST in sediments resulted in the formation of **DMST-acid.** DMST-acid was formed up to the estimated half-life of DMST, after which degradation of DMST-acid occurred (Figure 30b). The maximum of DMST-acid was likely to be reached between day 2 and day 7. Day 2 marks the last observation where DMST-acid concentrations were increasing. Day 7 marks the first observation where the DMST-acid was decreasing in concentration, and the concentration of DMST-acid dropped below detection limits after 24 days (Figure 30b). The expected maximum was calculated to be around 5.4 days.

N,N-DMS was formed in sediment during this experiment (Figure 30b). It can in principle be derived from both Tolylfluanid and Dichlofluanid since the biocides were applied as a mixture and are structurally similar. *N,N*-DMS formation could be fitted to zero-order kinetics. The reaction rate constant of the incubation and the control were both significantly different from zero (Table 11). Since the control showed formation, that means that the abiotic transformation of DMSA and DMST will lead to *N,N*-DMS formation (Fig 30a). Nonetheless, the biodegradation of DMST led to an increased formation of *N,N*-DMS, which was especially apparent from day 7 onwards (Figure 30b).

In the literature, **Dichlofluanid** and the hydrolysis product DMSA are described as non-readily biodegradable in the assessment report (European Chemicals Agency, 2016), which agrees to the presented data as DMSA did not undergo significant biodegradation. However, DMSA did show some abiotic degradation in the sediments (Figure 30a and b). The result of this abiotic degradation is *N,N*-DMS, which fills the mass balance. In contrast, **Tolylfluanid** showed a distinctly different pathway to form *N,N*-DMS. The first step, hydrolysis, is similar to dichlofluanid (Figure 31). The hydrolysis product of Tolylfluanid is DMST (European Chemicals Agency, 2014b). The second step, however, from DMST to *N,N*-DMS can be facilitated both biotically and abiotically as shown in Figure 31. The biodegradation of DMST must therefore be facilitated by the methyl group on the *para* position, which is lacking in DMSA (Figure 30). Nonetheless, DMST is described as non-readily biodegradable with the report showing a half-life of 48 days in water/sediment systems (European Chemicals Agency, 2014b). In the presented experiment DMST had a half-life of only 6 days in the water/sediment system, this is significantly faster than the assessment reports. The assessment report described detecting *N,N*-DMS, and DMST-acid as > 10% each of the mass balance in the water/sediment system, with the DMST-acid a likely intermediate (European Chemicals Agency, 2014b). From the currently presented data, it becomes clear that DMST-acid is a biodegradation intermediate from DMST to *N,N*-DMS (Figure 31). Moreover, the data showed that *N,N*-DMS constitutes nearly 100% of the DMST mass balance and the majority of the DMSA mass balance. *N,N*-DMS is the apparent stable product resulting from transformation of both, DMST and DMSA.

7.3.2 Medetomidine

The measured initial Medetomidine concentration was 0.14 ± 0.01 µM, which corresponds to only 29% of the spiked concentration (Figure 30d). The sediment incubation started at a lower concentration than the control, as the control started at 0.21 ± 0.01 µM (44% of spiked) (Figure 30c). The initial concentration difference might be caused by a difference in partitioning, e.g., by inhomogeneities in TOC distribution in the sediment.

For Medetomidine, using its K_{ow} (2.6 at pH 7, 20°C (European Chemicals Agency, 2015)), a K_{oc} of 2.36 was calculated. Using this K_{oc}, a concentration of 0.32 ± 0.03 µM in sediments was calculated for the controls, corresponding to 67% of the mass balance. For the sediment incubation itself, a concentration of 0.13 ± 0.02 µM was calculated on the first day, which fits 27% of the mass balance. These values add up to 94% of the mass balance for the control, which with the uncertainty (±6% and 2%) fits well within expectations.

Over time, the concentration of Medetomidine in the sediment incubation drops, following a first-order degradation model (Table 11). A first-order degradation was also applied to the control sediments (Figure 30c). No significant difference in reaction rate constant between the sediment incubation and the control was established (p-value = 0.15).

Medetomidine-acid was also formed in the sediments, but could not be detected in the controls (Figure 30c, chromatograms in Supplementary Figure 1.2). The formation of medetomidine-acid in the sediment incubation was fitted to a zero-order kinetic model (Table 11). In sediments, medetomidine-acid accounts for 6% of the mass balance, when compared to spiked medetomidine values (Figure 30d). When the remaining medetomidine fraction in the water at day 27 is added then only 8% of the mass balance can be explained at that timepoint with 67% still assumed to be present in the sediment (Figure 30d). Hydroxymedetomidine, previously identified as a metabolite in the rat (Salonen and Eloranta, 1990), was not detected during this experiment. The formation of medetomidine-acid can be taken as an indicator of biotransformation in the sediment incubations. Medetomidine-acid is formed at a rate of 0.001 ± 0.002 µM per day, therefore it would reach half the initial concentration after 71.6 days or half of the theoretically spiked concentration (0.48 µM) after 246 days. This is a rough estimate, as it is currently unclear which other transformation products are formed and whether medetomidine-acid itself undergoes further transformation or degradation.

Medetomidine is described as breaching the trigger to be labeled as very persistent in water/sediment systems by the assessment report (European Chemicals Agency, 2015). In the present experiment, some removal of Medetomidine was observed; this, however, goes for both the control and the incubation and as such is likely a result of abiotic transformation. Moreover, the transformation products hydroxymedetomidine and medetomidine-acid have not been included in the assessment report. In fact, these transformation products were first described as metabolites in the rat (Salonen and Eloranta, 1990). To the authors' knowledge, these transformation products have not before been included in environmental studies. Currently, it seems that hydroxymedetomidine is not an environmentally relevant transformation product since it was not detected in the study, while medetomidine-acid was formed albeit at a low percentage of the mass balance (reactions in Figure 31).

7.3.3 Tralopyril

The hydrolysis product from Tralopyril called BCCPCA was used for the biodegradation experiment. BCCPCA in the water had an initial concentration of 0.21 ± 0.03 µM, which represents 45% of the spiked BCCPCA (Figure 30f). Sorption might explain the remaining mass fraction. With EpiSuite™ predicting a K_{ow} of 3.3 for BCCPCA the compound seemingly has a considerable potential to partition into the sediment. However, the assessment report for tralopyril describes a log K_{ow} of 0.54 for the transformation product (called CL322,250 in the report) that assumingly is BCCPCA (European Chemicals Agency, 2019). These values would lead to a sediment concentration of 1.45 ± 0.007 µM or 0.015 ± 0.001 µM, respectively.

The calculations lead to either 302% or 3% of the BCCPA partitioning to the sediment, which indicates that these K_{ow} values are not valid. Considering the structure of BCCPCA both K_{ow}-values seem unlikely for this hydrolysis product. The first value would end up at a concentration

far higher than was spiked (section 4.4.3.1), while the second value is three orders of magnitude lower than the K_{ow} of the parent compound. On the contrary, the assessment report also states that CL322,250 has a strong potential to sorb to soil/sediments, with a calculated K_{oc} of 3.32 in marine sediments (European Chemicals Agency, 2019). As such the assessment report describes two disagreeing values, the mentioned K_{oc} of 3.32 fits better to the EPIsuite prediction which predicts a K_{oc} of 2.87. Nonetheless, the K_{ow} of 0.54 was used throughout the report (European Chemicals Agency, 2019). With the currently presented data, the K_{ow} for BCCPCA was back-calculated using the averages of the control and the sediment incubations after 1 day, as they were not significantly different. This yielded a K_{ow} of 2.47 for BCCPCA and a K_{oc} of 2.27 for BCCPCA.

Considering the period day one (i.e., after partition equilibrium) to day 27, a zero-order kinetic model showed a reaction rate constant that was significantly different from zero (Table 11) for BCCPCA. Using the model parameters a half-life of 87 days was calculated. However, this result was not significantly different from the controls (p-value = 0.73), meaning the decrease was likely the result of abiotic degradation (Figure 30e and f). To the authors' knowledge, the assessment report is the only available source on the biodegradation of tralopyril. The report described the hydrolysis product of tralopyril as CL322,250 (Figure 31) (European Chemicals Agency, 2019). The hydrolysis product was only identified as BCCPCA in scientific literature (Downs et al., 2017). The assessment report also describes a half-life of 30 days for CL322,250 in water/sediment systems. BCCPCA was stable to biodegradation in the currently presented experiment, which disagrees with the assessment report (European Chemicals Agency, 2019). It is not entirely clear whether CL322,250 from the assessment report corresponds to BCCPCA, due to the difference in K_{ow} and degradation half-life. However, CL322,250 is described as the only hydrolysis product and it can therefore be assumed that it is, in fact, BCCPCA.
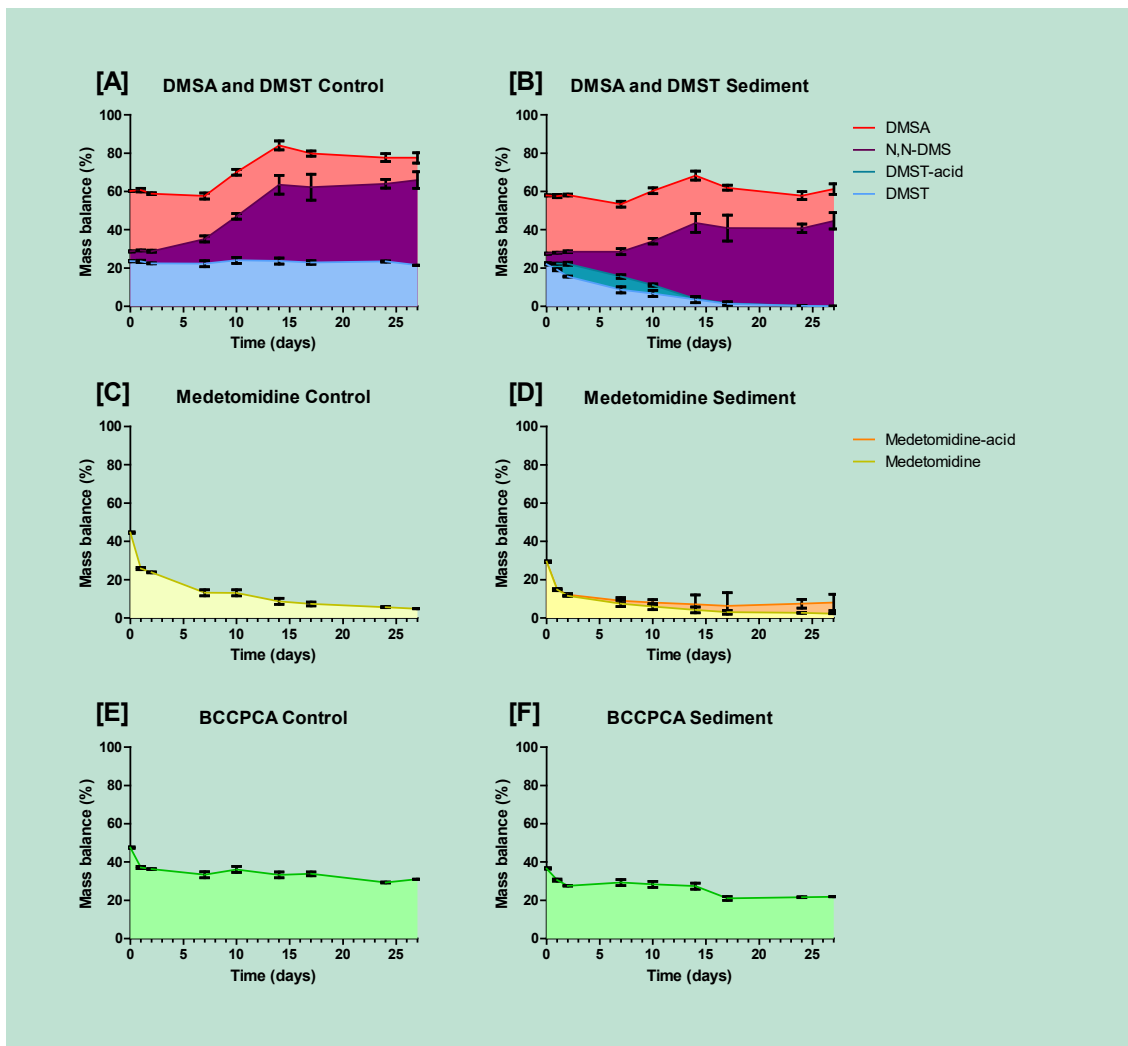
FIGURE 29: Biodegradation of the antifouling biocides in sediments. The filled areas represent the fraction of the mass balance (y-axis) that the compound encompasses. The x-axis represents the time of incubation in days. All data points were plotted as average ± standard deviation (n = 3).

FIGURE 30: Observed reactions during the biodegradation experiments. Blue arrows represent hydrolysis, and in the experiment, the hydrolysis products were tested for biodegradation. Green arrows represent biodegradation, while black arrows represent abiotic transformations.

TABLE 11: Kinetic model parameters for sediment incubations.

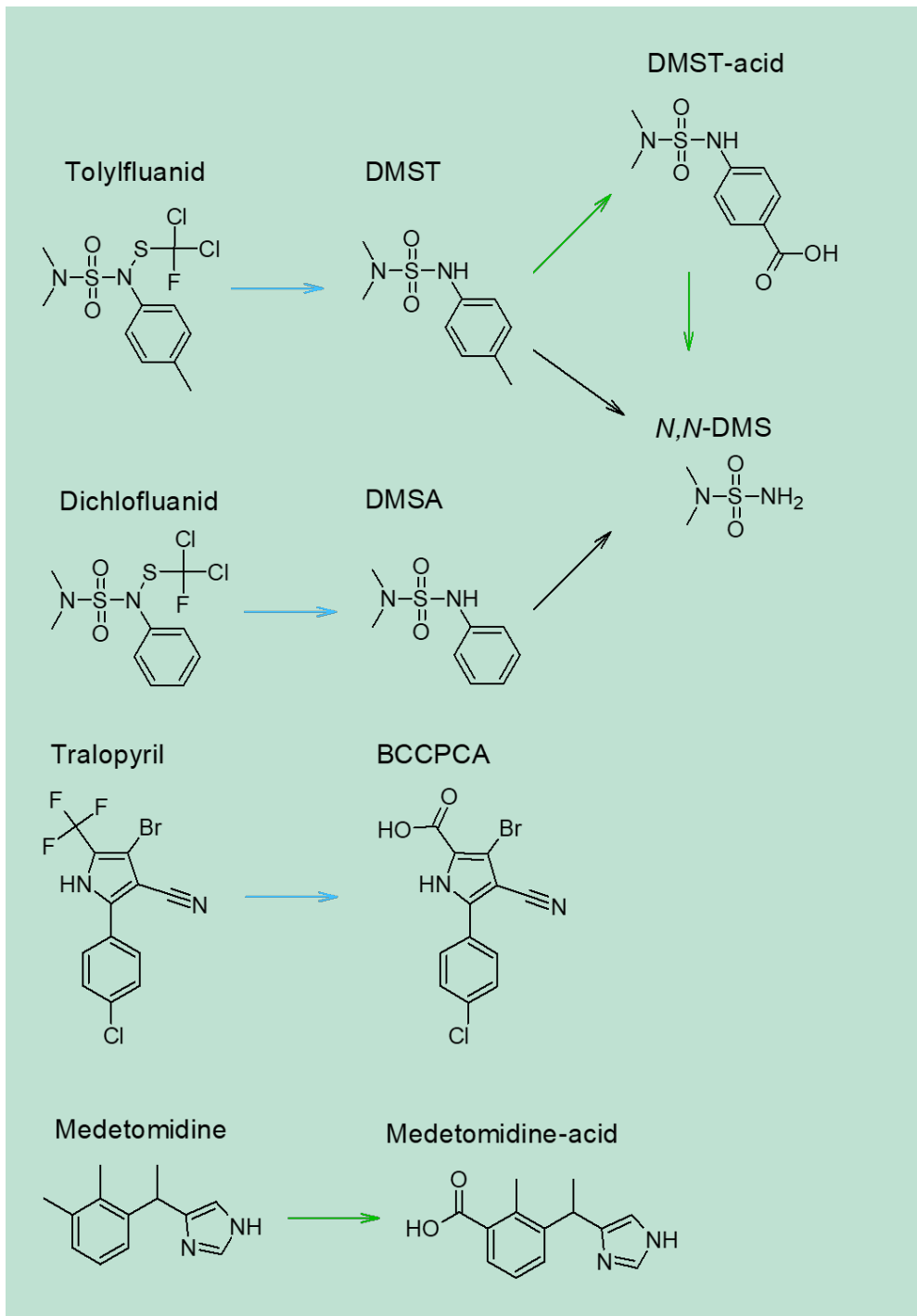| Compound	Kinetic model	Initial concentration (µM)	K (µM)	*P*-value reaction rate	R^2
Dichlofluanid					
DMSA	Zero order	0.29 ± 0.004	-0.005 ± 0.0004	≤ 0.001	0.90
DMSA Control	Zero order	0.29 ± 0.01	-0.007 ± 0.0008	≤ 0.001	0.73
Tolylfluanid					
DMST	First order	0.20 ± 0.004	0.12 ± 0.01		0.98
DMST-acid					
N,N-DMS	Zero order	0.05 ± 0.02	0.02 ± 0.001	≤ 0.001	0.87
DMST Control	Zero order	0.22 ± 0.005	-0.0002 ± 0.0003	0.40	0.03
N,N-DMS control	Zero order	0.04 ± 0.005	0.008 ± 0.0004	≤ 0.001	0.95
Medetomidine	First order	0.14 ± 0.01	0.71 ± 0.08		0.94
Medetomidine-acid	Zero order	0.0001 ± 0.0007	0.001 ± 0.0001	≤ 0.001	0.94
Medetomidine Control	First order	0.21 ± 0.01	0.46 ± 0.09		0.90
Tralopyril					
BCCPCA	Zero order	0.16 ± 0.005	-0.002 ± 0.0003	≤ 0.001	0.61
BCCPCA Control	Zero order	0.20 ± 0.006	-0.002 ± 0.0004	≤ 0.001	0.46

Key findings – Biodegradation

Tolylfluanid and Dichlofluanid hydrolyze to DMST and DMSA. These hydrolysis products themselves were biodegraded and formed quantitatively DMS (and little fractions of DMST-acid). No gap in the mass balance was detected within one-month incubation, thus there is no indication for rapid mineralization (or mineralization at all). Medetomidine seems rapidly removed from the sediment system, however a larger fraction of this is sorption while the biodegraded fraction leads to quantitative formation of Medetomidine acid.

Tralopyril is only hydrolysed to BCCPCA, which is no further degraded in the sediment incubations.

8. Leaching

8.1 Dichlofluanid as case study

DMSA, the hydrolysis product of Dichlofluanid, was found at all sampled timepoints, while no Dichlofluanid signals were detected (Figure 32). This was expected due to the rapid hydrolysis rate of Dichlofluanid (Cai et al., 2021). The hydrolysis product, DMSA, was found at the highest concentrations in the façade paint (Fig 35a). Starting concentrations of DMSA in the façade paint were 131.42 ± 8.41 ng/mL for the two layers and 161.42 ± 19.01 ng/mL for the five layers of paint (Fig 35a).

These starting concentrations were a factor 100 higher than those of the antifouling paints (Figure 32b & c). For the insoluble matrix antifouling paint, the starting concentrations were 1.20 ± 0.36 ng/mL for two layers and 1.00 ± 0.22 ng/mL for five layers (Figure 32b). Similar starting concentrations were observed for the soluble matrix antifouling paint at 1.53 ± 0.34 ng/mL for two layers and 1.67 ± 0.35 ng/mL for five layers (Figure 32c).

The ratio of the starting concentrations to the concentrations after one hour was between 2 and 3 for all paints, whereas, concentrations from one hour to two hours did not drop as significantly. This is due to the high initial dissolution of the readily accessible biocides at the surface (Uhlig et al., 2019). This initial dissolution process is rapid and, afterward, leaching continues according to water-filled pore dissolution and diffusion mechanisms.

After the initial time point, another clear difference between the façade and the antifouling paints can be observed. Since the water concentrations in the façade paint drop over time (Figure 32a), while the biocide release in the antifouling paints remained rather constant (Figure 32b & c).

The data was transformed to M_t/M_0 (presented as $F_{released}$) in order to determine whether the leaching process is dominated by dissolution or diffusion. The façade paint was plotted both against time in hours (Figure 33a) and against the square root of time (Figure 33b), in order to determine linearity. The antifouling plots were plotted against time in hours (Figure 33c & d), as linearity was already observed in the water concentrations (Figure 32).

The façade paint plotted against the time in hours showed data that would not fit to a linear model (Fig 35a). For two layers of façade paint, the data started with an $F_{released}$ of 0.49 ± 0.023, which increased to reach the plateau at $F_{released}$ of 1 after seven hours (Figure 32a). For the five layers of antifouling paint, the starting $F_{released}$ was 0.23 ± 0.02. The $F_{released}$ for the five layers façade paint increases to 0.60 ± 0.04 (60% leached) after 10 hours, the increase here does not fit to a straight line (Fig 35a). The increase, however, does increase in a linear fashion after 10 hours to reach an $F_{released}$ of 0.86 ± 0.04 at 30 hours (Figure 32a).

The façade data does become more linear when plotted against the square root of time (Figure 32b). Here, from the initial $F_{released}$ to an $F_{released}$ of 0.6 a linear model was fitted resulting in a slope of 0.0028 ± 0.00013 $s^{-0.5}$ (Figure 32b). This slope was then used to calculate the diffusion coefficient for DMSA in the façade paint, yielding a D of 37.39 ± 1.76 · 10-15 m^2 s^{-1}.

For the antifouling paints results were plotted against the time in hours, which already showed a linear tendency (Figure 32c & d). For the insoluble matrix paint the two layers starting $F_{released}$ was 0.0045 ± 0.001, which then increased to reach 0.044 ± 0.018 after 30 hours (Figure 32c). Five layers of insoluble paint showed an $F_{released}$ of 0.0014 ± 0.00024, which increased to 0.013 ± 0.003 after 30 hours (Figure 32c). Linear models were plotted through the data leading to slopes of 0.0013 ± 0.00011 for two layers of paint, and a slope of 0.00036 ± 0.00002 for five layers of insoluble matrix paint.

Two layers of soluble antifouling matrix initially showed an $F_{released}$ of 0.0051 ± 0.0013 that increased to 0.052 ± 0.012 after 30 hours (Figure 33d). The five-layer soluble matrix was found at an initial $F_{released}$ of 0.0027 ± 0.0005, which increased to 0.028 ± 0.0061 after 30 days (Figure 33d). A straight line was also fitted to these data, yielding slopes of 0.0015 ± 0.00007 for two-layer and 0.0008 ± 0.00004 for five layers of the soluble matrix paint.

A comparison of the slopes reveals that for each type of paint the two-layer and five-layer treatments were significantly different (P-value < 0.001), which was expected. However, comparisons between the insoluble and soluble matrix did reveal a significant difference between the five-layer treatments (P-value < 0.001), but not for the two-layer treatments. In this case, leaching was faster from the soluble matrix, which might be explained by the self-polishing properties. It seems that water enters the paints up to at least two layers deep, giving similar leaching rates for the two-layer treatment. However, water might not be able to penetrate all five layers. But, since the soluble matrix is dissolving the layers grow thinner (or pores grow wider) resulting in increased leaching from the deeper layers (Yebra et al., 2005).

It does remain unclear whether dissolution or diffusion is the driving mechanism behind leaching in the antifouling paints. This is despite the apparent linearity when the $F_{released}$ was plotted against time, which would point towards dissolution controlled leaching (Erich and Baukh, 2016). Yet, it cannot be excluded that a non-linear function would be visible if the timing of the experiment was extended, since only a fraction (< 0.05%) was leached. Previous leaching experiments with antifouling biocides show nonlinearity that is visible after ~20 days (Thouvenin et al., 2002). What is clear is that leaching from antifouling paints is much more limited than from the façade paints, probably due to both dissolution and diffusion being more limited in antifouling paints by design.

It should be noted that the biocides were spiked into the paint from a methanol standard, while the biocides would probably be added in a micro-crystalline form in commercial paints (Urbanczyk et al., 2019). Nonetheless, leaching and diffusion would only occur for dissolved biocides, therefore, both paints contained petroleum solvent (>10-<25%), which likely would dissolve the micro-crystalline biocides.
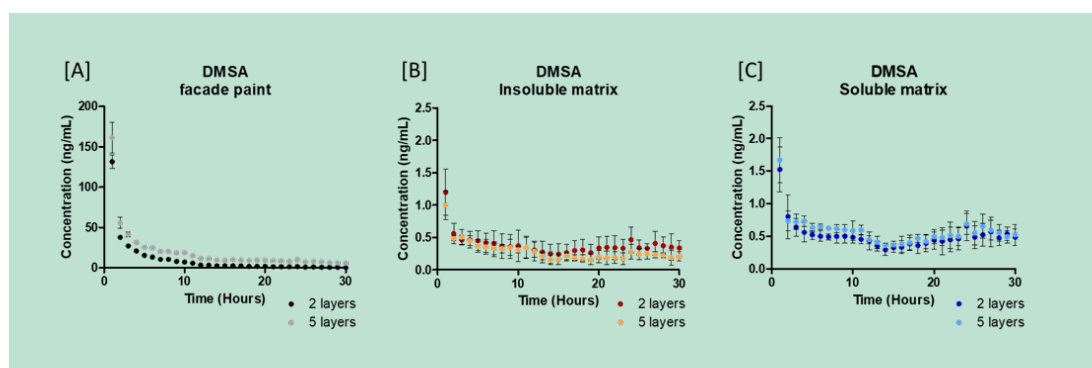

FIGURE 31: Leaching of DMSA from a façade paint (A), and insoluble matrix antifouling paint (B), and a soluble matrix antifouling paint (C). As expected, leaching from the façade paint is more rapid than the antifouling paints. Moreover, high starting concentrations of all paints are an indicator of fast dissolution of biocides at the paint surface. In the graphs, the y-axis represents the water concentration in ng/mL, while the x-axis represents the time in hours. All points were plotted as means ± standard deviation (n = 3).
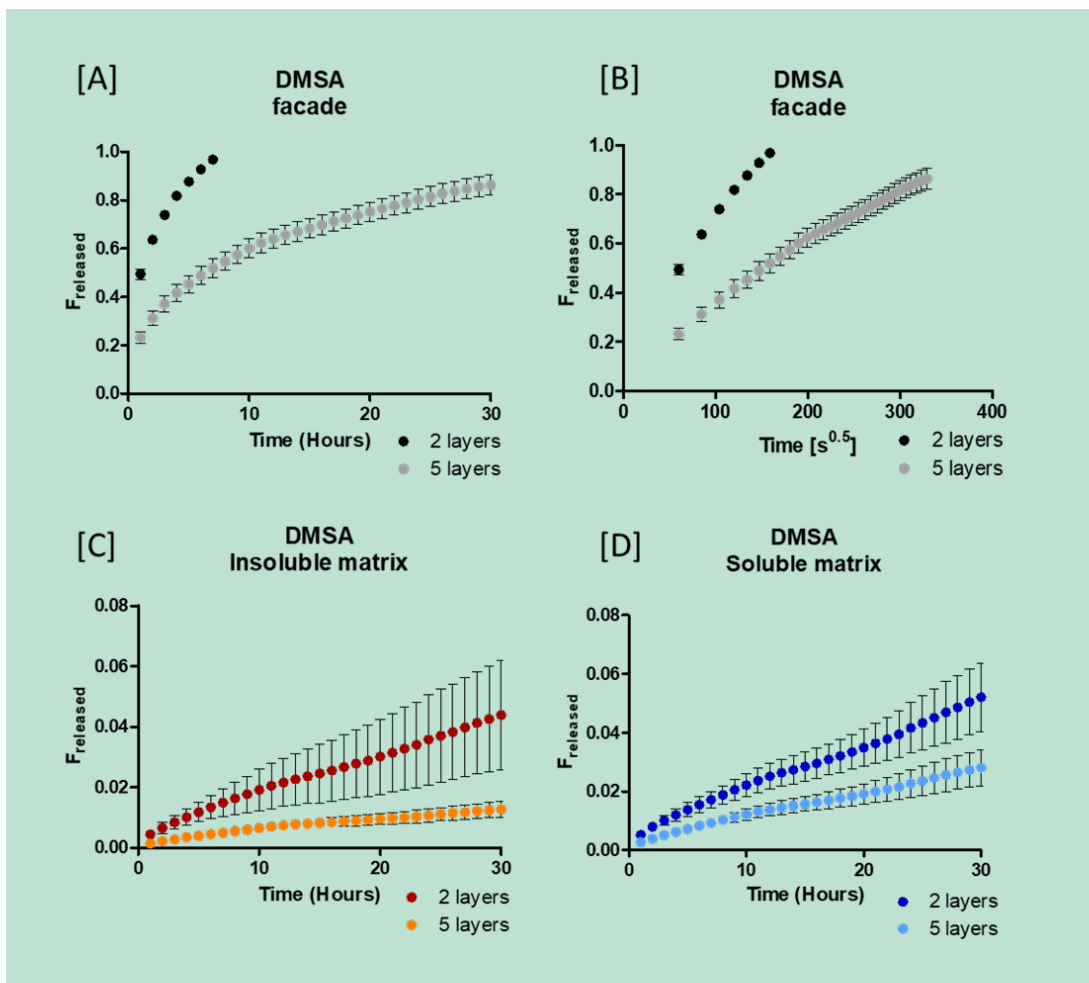
FIGURE 32: $F_{released}$ (M_t/M_0) of DMSA in facade and antifouling paints. The façade paint shows a nonlinear increase when plotted with the time in hours (a) while showing a linear increase when plotted against the square root of time (b). This is a clear indicator of diffusion-controlled leaching. Leaching from antifouling paints appears linear (c & d), but this is likely due to the low overall leaching. All data are plotted as means ± standard deviation (n = 3).

Key findings – Leaching

The leaching of antifouling biocides is seriously decreased in comparison to paints such as used on the facades, even though the backbone of the polymer might be the same. How far just the diffusion is reduced, or really blocked and whether other release mechanisms are relevant, needs a more sophisticated data analysis than possible in the framework of this project.

9. Conclusion

The project succeeded in **establishing methods** for the organic antifouling compounds. The project succeeded in making suggestion on using markers for the Pyrithione compounds, but a standardisation could not yet be accomplished. However, a standardized analytical method is highly needed in future, as paint manufacturers are waiting for the approval of Zinc-pyrithione. There will be products on the market for leisure boats based on Zinc-pyrithione and Tralopyril or another organic booster biocide to avoid the use of copper. In the professional area, the use of Copper-pyrithione will also increase due to its use in modern SPCs and biocidal foul release coatings.

The **monitoring** conducted by this project showed that contemporary organic antifouling compounds themselves can hardly be detected in marinas or fjords. However, their hydrolysis products can often be found, even if the concentration are still considerably lower (ng/L-range) than the antifouling compounds of previous generations such as Tributyltin, Diuron and Irgarol (μg/L-range). This is due to the fact that most applications have changed to copper oxide or copper, in combination with organic booster biocides. Neither of the copper compounds are degradable. Copper formulations of the Pyrithione family hydrolyse under application, and need to be monitored with respect to copper and the Pyrithiones.

We were also able to demonstrate hydrolysis and biodegradation, identify the hydrolysis products and metabolites. Biodegradation mass balances and kinetics and the photodegradation resulted in identification of photolysis products, mass balances and kinetics. In detail: Rapid hydrolysis is a feature that is common of nearly all contemporary organic antifouling compounds. Nonetheless, these hydrolysis products are semi stable as they are photo- or biodegraded further to their final metabolites and photo-oxidation products:

Parent compound	→	Hydrolysis product	→	Metabolite/ phototransformation product
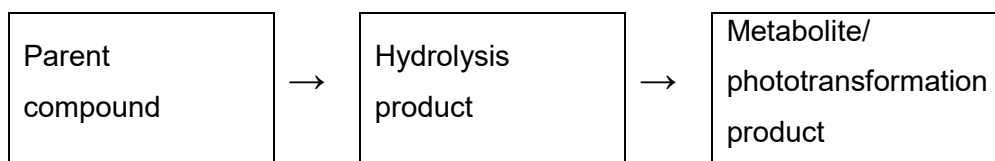
There are very little data on the toxicity of these transformation products and it cannot be excluded that some of them also have biocidal effects. Data are still missing but highly needed for a scientific sound risk assessment. Even in recent reviews on the toxicity of antifouling biocides, data on the biocidal action of their metabolites is lacking (NZ- Environmental Protection Agency, 2012; Amara et al., 2018)). Daehne et al. (2017) reported on concentrations of DMST far below the effect level, which is set by the ECHA at 140μg/l. Nevertheless, it can be expected that the use of organic biocides will increase, thus increasing the input in brackish and marine waters, as the use of Dichlofluanid and Tolylfluanid is not approved for the use in freshwater.

Also in future monitoring, efforts should be directed more on the hydrolysis products and final transformation products than the parents.

The leaching of antifouling compounds from two antifouling paints (one insoluble and one soluble matrix antifouling paint in comparison to an façade paint for quality assurance) were determined both antifouling paints have considerably decreased leaching in comparison to the façade paint. In both paints, it is the hydrolysis products that are leached while no significant fractions of the parent compounds were determined in the water.

The data from the monitoring is compliant to the market survey, the hydrolysis and transformation rates, except for Irgarol, which is probably deposited in the marina sediments.

10. Perspectives

Risk assessments for biocides, especially antifouling biocides, in future should include transformation products especially if compounds are rapidly hydrolysing as most of the current antifouling compounds are.

More toxicological data would be needed for metabolites and transformation products to fuel the risk assessment.

Considering photolysis, a risk assessment should not only be based on direct photolysis (or spectral comparison) but need to include indirect photolysis, which is important for natural waters.

A larger effort is needed to further develop and standardize an analytical procedure to analyse Zinc- and Copper-Pyrithione as sum of hydrolysed Pyrithiones to be able to produce quantitative data on release and emissions of Pyrithiones.

11. References

Albanis, T.A., Lambropoulou, D.A., Sakkas V.A., Konstantinou, I.K., 2002. Antifouling paint booster biocide contamination in Greek marine sediments. Chemosphere 48, 475-85. 10.1016/S0045-6535(02)00134-0

Almeida, E., Diamantino, T.C., de Sousa, O., 2007. Marine paints: The particular case of antifouling paints. Prog. Org. Coatings 59, 2–20. https://doi.org/10.1016/j.porgcoat.2007.01.017

Amara, I., Miled, W., Ben Slama, R., Ladhari, N., 2018. Antifouling processes and toxicity effects of antifouling paints on marine environment. Environ. Toxicol. Pharmacol 115–130.

Ansanelli, G., Manzo, S., Parrella, L., Massanisso, P., Chiavarini, S., Di Landa, G., Ubaldi, C., Cannarsa, S., Cremisini, C., 2017. Antifouling biocides (Irgarol, Diuron and dichlofluanid) along the Italian Tyrrhenian coast: Temporal, seasonal and spatial threats. Reg. Stud. Mar. Sci. 16, 254–266. https://doi.org/10.1016/j.rsma.2017.09.011

Appiani, E., Ossola, R., Latch, D.E., Erickson, P.R., McNeill, K., 2017. Aqueous singlet oxygen reaction kinetics of furfuryl alcohol: Effect of temperature, pH, and salt content. Environ. Sci. Process. Impacts 19, 507–516. https://doi.org/10.1039/c6em00646a

Biselli, S., Bester, K., Hühnerfuss, H., Fent, K., 2000. Concentrations of the antifouling compound Irgarol 1051 and of organotins in water and sediments of German North and Baltic Sea marinas. Mar. Pollut. Bull. 40, 233–243. https://doi.org/10.1016/S0025-326X(99)00177-0

Bollmann, U.E., Badawi, N., 2020. A fast and simple SPE-LC-MS/MS procedure for extraction and quantitative analysis of 1,2,4-triazole, N,N-dimethylsulfamide, and other small polar organic compounds in groundwater. Anal. Bioanal. Chem. 5683–5693.

Bollmann,U.E., Fernández-Calviño, D., K. Brandt, K.K., Storgaard, M.S., Sanderson, H.,and Bester, K. 2017a. Biocide Runofffrom Building Facades: Degradation Kinetics in Soil, Environ. Sci. Technol. 51, 3694−3702. https://doi.org/10.1021/acs.est.6b05512

Bollmann, U.E., Minelgaite, G., Schlüsener, M., Ternes, T.A., Vollertsen, J., Bester, K., 2017b. Photodegradation of octylisothiazolinone and semi-field emissions from facade coatings. Nat. Publ. Gr. 1–9. https://doi.org/10.1038/srep41501

Bollmann, U. E., Vollertsen, J., Carmeliet, J., Bester, K., 2014. Dynamics of biocide emissions from buildings in a suburban stormwater catchment - Concentrations, mass loads and emission processes, *Water Research*, 56, 66-76. https://doi.org/10.1016/j.watres.2014.02.033

Bones, J., Thomas, K. V., Paull, B., 2006. Improved method for the determination of Zinc-Pyrithione in environmental water samples incorporating on-line extraction and preconcentration coupled with liquid chromatography atmospheric pressure chemical ionisation mass spectrometry. J. Chromatogr. A 1132, 157–164. https://doi.org/10.1016/j.chroma.2006.07.068

Bowman J.C., Readman J.W., Zhou, J. (2003) Seasonal variability in the concentrations of Irgarol 1051 in Brighton Marina, UK; Including the impact of dredging, Marine Pollution Bulletin 46, 444-51 DOI: 10.1016/S0025-326X(02)00464-2

Buxton, G. V., Greenstock, C.L., Helman, W.P., Ross, A.B., 1988. Critical Review of rate constants for reactions of hydrated electrons, hydrogen atoms and hydroxyl radicals (·OH/·O− in Aqueous Solution. J. Phys. Chem. Ref. Data 17, 513–886. https://doi.org/10.1063/1.555805

Cai, Y., Koning, J.T., Bester, K., Bollmann, U.E., 2021. Abiotic fate of tolylfluanid and dichlofluanid in natural waters. Sci. Total Environ. 752. https://doi.org/10.1016/j.scitotenv.2020.142160

Chambers, L.D., Stokes, K.R., Walsh, F.C., Wood, R.J.K., 2006. Modern approaches to marine antifouling coatings. Surf. Coatings Technol. 201, 3642–3652. https://doi.org/10.1016/j.surfcoat.2006.08.129

Cresswell, T., Richards, J.P., Glegg, G.A., Readman, J.W., 2006. The impact of legislation on the usage and environmental concentrations of Irgarol 1051 in UK coastal waters 52,

1169–1175. https://doi.org/10.1016/j.marpolbul.2006.01.014

Daehne, D., Fürle, C., Thomsen, A., Watermann, B., Feibicke, M., 2017. Antifouling biocides in German marinas: Exposure assessment and calculation of national consumption and emission. Integr. Environ. Assess. Manag. 13, 892–905. https://doi.org/10.1002/ieam.1896

Doose, C. A., Ranke, J., Stock, F., Bottin-Weber, U., Jastorff, B., 2004. Structure-activity relationships of pyrithiones - IPC-81 toxicity tests with the antifouling biocide Zinc-Pyrithione and structural analogs. Green Chem. 6, 259–266. https://doi.org/10.1039/b314753c

Doose, C. A., Szaleniec, M., Behrend, P., Müller, A., Jastorff, B., 2004. Chromatographic behavior of pyrithiones. J. Chromatogr. A 1052, 103–110. https://doi.org/10.1016/j.chroma.2004.08.028

Downs, R., Dean, J., Downer, A., Perry, J., 2017. Determination of the Biocide Econea® in Artificial Seawater by Solid Phase Extraction and High Performance Liquid Chromatography Mass Spectrometry. Separations 34. https://doi.org/10.3390/separations4040034

Eklund, B., Eklund, D., 2014. Pleasure boatyard soils are often highly contaminated. Environ. Manage. 53, 930–946. https://doi.org/10.1007/s00267-014-0249-3

Erich, S.J.F., Baukh, V., 2016. Modelling biocide release based on coating properties. Prog. Org. Coatings 90, 171–177. https://doi.org/10.1016/j.porgcoat.2015.10.009

European Chemicals Agency, 2019. Regulation (EU) No 528/2012 concerning the making available on the market and use of biocidal products - Tralopyril (PT21).

European Chemicals Agency, 2016. Regulation (EU) No 528/2012 concerning the making available on the market and use of biocidal products - Dichlofluanid (PT21).

European Chemicals Agency, 2015. Regulation (EU) No 528 / 2012 concerning the making available on the market and use of biocidal products. Assessment Report for Medetomidine.

European Chemicals Agency, 2014a. Regulation (EU) n°528/2012 concerning the making available on the market and use of biocidal products - Cybutryne Product type PT 21 (Antifouling).

European Chemicals Agency, 2014b. Regulation (EU) No 528/2012 concerning the making available on the market and use of biocidal products - Tolylfluanid (PT21).

European Comission, 2016. COMMISSION IMPLEMENTING DECISION (EU) 2016/107 of 27 January 2016 not approving cybutryne as an existing active substance for use in biocidal products for product- type 21. Off. J. Eur. Union.

Falaye, B.J., Oyewumi, K.J., 2011. Solutions of the Dirac equation with spin and pseudospin symmetry for the trigonometric scarf potential in D-dimensions. African Rev. Phys. 6, 211–220. https://doi.org/10.1016/j.marpolbul.2011.01.012

Francisco, S., Goka, K., 2005. Unexpected effects of Zinc-Pyrithione and imidacloprid on Japanese medaka fish (Oryzias latipes). Aquat. Toxicol. 74, 285–293. https://doi.org/10.1016/j.aquatox.2005.06.003

Ge, L., Na, G., Zhang, S., Li, K., Zhang, P., Ren, H., Yao, Z., 2015. New insights into the aquatic photochemistry of fluoroquinolone antibiotics: Direct photodegradation, hydroxyl-radical oxidation, and antibacterial activity changes. Sci. Total Environ. 527–528, 12–17. https://doi.org/10.1016/j.scitotenv.2015.04.099

Greenhalgh, R., Dhawan, K.L., Pearl, W., 1980. Hydrolysis of Fenitrothion in Model and Natural Aquatic Systems. J. Agric. Food Chem. 28, 102–105. https://doi.org/10.1021/jf60227a016

Grunnet, K.S., Dahllöf, I., 2005. Environmental Fate of the Antifouling Compound Zinc-Pyrithione in Seawater. Environ. Toxicol. Chem. 24, 3001. https://doi.org/10.1897/04-627R.1

Guthery, E., Seal, L.A., Anderson, E.L., 2005. Zinc-Pyrithione in alcohol-based products for skin antisepsis : Persistence of antimicrobial effects. Am J Infect Control 15–22. https://doi.org/10.1016/j.ajic.2004.07.012

Haag, W.R., Hoignr, J., Gassman, E. and Braun, A.M., 1984. Singlet oxygen in surface waters- Part 1. Chemosphere, 13, 631-640

Hamwijk, C., Schouten, A., Foekema, E.M., Ravensberg, J.C., Collombon, M.T., Schmidt, K., Kugler, M., 2005. Monitoring of the booster biocide dichlofluanid in water and marine

sediment of Greek marinas. Chemosphere 60, 1316–1324.
https://doi.org/10.1016/j.chemosphere.2005.01.072

Hellio, C., Diego Meseguer, Y., 2009. Advances in Marine Antifouling Coatings and
Technologies. Woodhead Publishing Limited, UK, Cambridge.

Hirotogu Akaike, 1973. Information Theory and an Extension of the Maximum Likelihood
Principle. Break. Stat.

Højenvang, J., 2003. Afvaskning og afslibning af biocidholdig bundmaling i forbindelse med
vedligeholdelse af lystbåde på land. Danish Environ. Prot. Agency, Copenhagen.

Kalyanasundaram, K., Neumann-Spallart, M., 1982. Photophysical and redox properties of
water-soluble porphyrins in aqueous media. J. Phys. Chem. 86, 5163–5169.
https://doi.org/10.1021/j100223a022

Kiil, S., Dam-Johansen, K., Weinell, C.E., Pedersen, M.S., Codolar, S.A., 2003. Estimation of
polishing and leaching behaviour of antifouling paints using mathematical modelling: A
literature review. Biofouling 19, 37–43. https://doi.org/10.1080/0892701021000060851

Koning, J.T., Bollmann, U.E., Bester, K., 2020. The occurrence of modern organic antifouling
biocides in Danish marinas. Mar. Pollut. Bull. 158.
https://doi.org/10.1016/j.marpolbul.2020.111402

Konstantinou, I.K., Albanis, T.A., 2004. Worldwide occurrence and effects of antifouling paint
booster biocides in the aquatic environment: A review. Environ. Int. 30, 235–248.
https://doi.org/10.1016/S0160-4120(03)00176-4

Latch, D.E., Stender, B.L., Packer, J.L., Arnold, W.A., McNeill, K., 2003. Photochemical fate of
pharmaceuticals in the environment: Cimetidine and ranitidine. Environ. Sci. Technol. 37,
3342–3350. https://doi.org/10.1021/es0340782

McNeill, K., Canonica, S., 2016. Triplet state dissolved organic matter in aquatic
photochemistry: Reaction mechanisms, substrate scope, and photophysical properties.
Environ. Sci. Process. Impacts 18, 1381–1399. https://doi.org/10.1039/c6em00408c

Minelgaite, G., Nielsen, A.H., Pedersen, M.L., Vollertsen, J., 2017. Photodegradation of three
stormwater biocides. Urban Water J. 14, 53–60.

Mopper, K., Zhou, X., 1990. Hydroxyl Radical Photoproduction in the Sea and Its Potential
Impact on Marine Processes. Science (80-.).

Page, S.E., Arnold, W.A., McNeill, K., 2010. Terephthalate as a probe for photochemically
generated hydroxyl radical. J. Environ. Monit. 12, 1658–1665.
https://doi.org/10.1039/c0em00160k

Parker, K.M., Mitch, W.A., 2016. Halogen radicals contribute to photooxidation in coastal and
estuarine waters. Proc. Natl. Acad. Sci. 113, 5868–5873.
https://doi.org/10.1073/pnas.1602595113

Perdue, E.M., Wolfe, N.L., 1982. Modification of Pollutant Hydrolysis Kinetics in the Presence
of Humic Substances. Environ. Sci. Technol. 16, 847–852.
https://doi.org/10.1021/es00106a005

Peterson, B.M., McNally, A.M., Cory, R.M., Thoemke, J.D., Cotner, J.B., McNeill, K., 2012.
Spatial and temporal distribution of singlet oxygen in Lake Superior. Environ. Sci.
Technol. 46, 7222–7229. https://doi.org/10.1021/es301105e

Prosen, H., Zupančič-Kralj, L., 2005. Evaluation of photolysis and hydrolysis of atrazine and its
first degradation products in the presence of humic acids. Environ. Pollut. 133, 517–529.
https://doi.org/10.1016/j.envpol.2004.06.015

Riedel, N., Thorseth, A., Santamaria Lancia, A.A., Thorsteinsson, S., Poulsen, P., Iandolo, B.,
Davidsen, R.S., Benatto, G., 2018. Direct Beam and Diffuse Spectral Irradiance
Measurements in a Nordic Country Analyzed with the Average Photon Energy
Parameter. 2018 IEEE 7th World Conf. Photovolt. Energy Conversion, WCPEC 2018 - A
Jt. Conf. 45th IEEE PVSC, 28th PVSEC 34th EU PVSEC 2575–2580.
https://doi.org/10.1109/PVSC.2018.8548240

Roberts, T.R., Hutson, D.., 1999. Metabolic Pathways of Agrochemicals: Part 2: Insecticides
and Fungicides.

Ryuji Kojima, Toshiaki Shibata, Koichi Ueda, 2016. Leaching Phenomena of Antifouling
Agents from Ships' Hull Paints. J. Shipp. Ocean Eng. 6. https://doi.org/10.17265/2159-
5879/2016.05.002

Sakkas, V.A., Albanis, T.A., 2003. Photocatalyzed degradation of the biocides chlorothalonil
and dichlofluanid over aqueous TiO2 suspensions. Appl. Catal. B Environ. 46, 175–188.

https://doi.org/10.1016/S0926-3373(03)00198-X

Sakkas, V.A., Shibata, K., Yamaguchi, Y., Sugasawa, S., Albanis, T., 2007. Aqueous phototransformation of Zinc-Pyrithione. Degradation kinetics and byproduct identification by liquid chromatography-atmospheric pressure chemical ionisation mass spectrometry. J. Chromatogr. A 1144, 175–182. https://doi.org/10.1016/j.chroma.2007.01.049

Salonen, J.S., Eloranta, M., 1990. Biotransformation of medetomidine in the rat. Xenobiotica. 20, 471–80. https://doi.org/10.3109/00498259009046862

Saltzman, W.M., 2001. Drug Delivery: Engineering Principles for Drug Therapy. Oxford University Press.

Samuni, A., Neta, P., 1973. Hydroxyl radical reaction with phosphate esters and the mechanism of phosphate cleavage. J. Phys. Chem. 77, 2425–2429. https://doi.org/10.1021/j100639a012

Schlüsener, M.P., Kunkel, U., Ternes, T.A., 2015. Quaternary Triphenylphosphonium Compounds: A New Class of Environmental Pollutants. Environ. Sci. Technol. 49, 14282–14291. https://doi.org/10.1021/acs.est.5b03926

Schmidt, C.K., Brauch, H.-J., 2008. N,N -Dimethylsulfamide as Precursor for N - Nitrosodimethylamine (NDMA) Formation upon Ozonation and its Fate During Drinking Water Treatment. Environ. Sci. Technol. 42, 6340–6346. https://doi.org/10.1021/es7030467

Schoknecht, U., Sommerfeld, T., Borho, N., Bagda, E., 2013. Progress in Organic Coatings Interlaboratory comparison for a laboratory leaching test procedure with facade coatings. Prog. Org. Coatings 76, 351–359. https://doi.org/10.1016/j.porgcoat.2012.10.001

Schwarzenbach, R.., Gschwend, P.M., Imboden, D.M., 2002. Environmental Organic Chemistry.

Schwarzenbach, R.., Westall, J., 1981. Transport of Nonpolar Organic Compounds from Surface Water to Groundwater. Laboratory Sorption Studies. Environ. Sci. Technol. 1360–1367. https://doi.org/10.1021/es00093a009

Schymanski, E.L., Singer, H.P., Slobodnik, J., Ipolyi, I.M., Oswald, P., Krauss, M., Schulze, T., Haglund, P., Letzel, T., Grosse, S., Thomaidis, N.S., Bletsou, A., Zwiener, C., Ibáñez, M., Portolés, T., De Boer, R., Reid, M.J., Onghena, M., Kunkel, U., Schulz, W., Guillon, A., Noyon, N., Leroy, G., Bados, P., Bogialli, S., Stipaničev, D., Rostkowski, P., Hollender, J., 2015. Non-target screening with high-resolution mass spectrometry: Critical review using a collaborative trial on water analysis. Anal. Bioanal. Chem. 407, 6237–6255. https://doi.org/10.1007/s00216-015-8681-7

Steen, R.J.C.A., Ariese, F., Hattum, B. Van, Jacobsen, J., Jacobson, A., 2004. Monitoring and evaluation of the environmental dissipation of the marine antifoulant 4,5-dichloro-2-n-octyl-4-isothiazolin-3-one (DCOIT) in a Danish Harbor. Chemosphere 57, 513–521. https://doi.org/10.1016/j.chemosphere.2004.06.043

Styszko, K., Kupiec, K., 2016. Determination of diffusion coefficients of biocides on their passage through organic resin-based renders. Chemosphere 160, 273–279. https://doi.org/10.1016/j.chemosphere.2016.06.077

The European Parlament and the Council of the European Union, 2012. REGULATION (EU) No 528/2012 OF THE EUROPEAN PARLIAMENT AND OF THE COUNCIL of 22 May 2012 concerning the making available on the market and use of biocidal products. Off. J. Eur. Union.

Thomas, K. V., McHugh, M. and Waldock, M. 2002. Antifouling paint booster biocides in UK coastal waters: inputs, occurrence and environmental fate. *Sci Total Environ*, 293: 117–127. https://doi.org/10.1016/S0048-9697(01)01153-6

Thomas, K. V., Blake, S. J. and Waldock, M. J. 2000. Antifouling paint booster biocide contamination in UK marine sediments. *Mar Pollut Bull*, 40: 739–745 https://doi.org/10.1016/S0025-326X(00)00010-2

Thomas, K. V., 1999. Determination of the antifouling agent Zinc-Pyrithione in water samples by copper chelate formation and high-performance liquid chromatography-atmospheric pressure chemical ionisation mass spectrometry. J. Chromatogr. A 833, 105–109. https://doi.org/10.1016/S0021-9673(98)01009-7

Thomas, K. V., 1998. Determination of selected antifouling booster biocides by high-performance liquid chromatography-atmospheric pressure chemical ionisation mass spectrometry. J. Chromatogr. A 825, 29–35. https://doi.org/10.1016/S0021-

9673(98)00717-1

Thomas, K. V., Brooks, S., 2010. The environmental fate and effects of antifouling paint biocides. Biofouling 26, 73–88. https://doi.org/10.1080/08927010903216564

Thouvenin, M., Peron, J.J., Charreteur, C., Guerin, P., Langlois, J.Y., Vallee-Rehel, K., 2002. A study of the biocide release from antifouling paints. Prog. Org. Coatings 44, 75–83. https://doi.org/10.1016/S0300-9440(01)00246-6

Tomita, M., Irie, M., Ukita, T., 1969. Sensitized Photooxidation of Histidine and Its Derivatives. Products and Mechanism of the Reaction. Biochemistry 8, 5149–5160. https://doi.org/10.1021/bi00840a069

Turner, A., 2010. Marine pollution from antifouling paint particles. Mar. Pollut. Bull. 60, 159–171. https://doi.org/10.1016/j.marpolbul.2009.12.004

Uhlig, S., Colson, B., Schoknecht, U., 2019. A mathematical approach for the analysis of data obtained from the monitoring of biocides leached from treated materials exposed to outdoor conditions. Chemosphere 228, 271–277. https://doi.org/10.1016/j.chemosphere.2019.04.102

Urbanczyk, M.M., Bester, K., Bollmann, U.E., 2019. Multi-layered approach to determine diffusion coefficients through polymer films : Estimating the biocide release from paints. Build. Environ. 148, 294–298. https://doi.org/10.1016/j.buildenv.2018.11.011

Vergnaud, J.-M., 1993. Controlled Drug Release of Oral Dosage Forms. Ellis Horwood Limited.

Vorkamp, K., Bossi, R., Bester, K., 2014. Screening for miljøfarlige forurenende stoffer.

Voulvoulis, N., Scrimshaw, M.D., Lester J.N. 2000. Occurrence of Four Biocides Utilized in Antifouling Paints, as Alternatives to Organotin Compounds, in Waters and Sediments of a Commercial Estuary in the UK. Marine Pollution Bulletin 40, 938-946 DOI: 10.1016/S0025-326X(00)00034-5

Yamaguchi, Y., Kumakura, A., Sugasawa, S., Harino, H., Yamada, Y., Shibata, K., Senda, T., 2006. Direct analysis of Zinc-Pyrithione using LC-MS. Int. J. Environ. Anal. Chem. 86, 83–89. https://doi.org/10.1080/03067310500249930

Yebra, D.M., Kiil, S., Dam-Johansen, K., 2006. Mathematical Modeling of Tin-Free Chemically-Active Antifouling Paint Behavior. AIChE J. 52, 1926–1940. https://doi.org/10.1002/aic

Yebra, D.M., Kiil, S., Dam-Johansen, K., 2004. Antifouling technology - Past, present and future steps towards efficient and environmentally friendly antifouling coatings. Prog. Org. Coatings 50, 75–104. https://doi.org/10.1016/j.porgcoat.2003.06.001

Yebra, D.M., Kiil, S., Dam-Johansen, K., Weinell, C., 2005. Reaction rate estimation of controlled-release antifouling paint binders: Rosin-based systems. Prog. Org. Coatings 53, 256–275. https://doi.org/10.1016/j.porgcoat.2005.03.008

Appendix 1.   Analytical information

Appendix 1.1   MS/MS parameters and table
Supplementary Table 1. MS/MS parameters

Name	IUPAC Name	CAS	Formula	Molar Mass (g/mol)	K_{ow}	Mass spec Ionization mode Quantifier (I_{Quant}) and qualifier ion (I_{Qual})	LOD (µg/L)	LOQ (µg/L)	Internal Standard for Quantification
Dichlofluanid	*N*-[dichloro(fluoro)methyl]sulfa-nyl-*N*-(dimethylsulfamoyl)aniline	1085-98-9	C9H11Cl2FN2O2S2	333.2	3.50	ESI (+) I_{Quant}: 333 → 224 I_{Qual}: 333 → 123			
DMSA	*N,N*-dimethyl-*N*-phenylsulpha-mide	4710-17-2	C8H12N2O2S	200.26	1.59	ESI (+) I_{Quant}: 201 → 92 I_{Qual}: 201 → 137	0.03	0.08	DMST-D7
Tolylfluanid	*N*-[dichloro(fluoro)methyl]sulfa-nyl-*N*-(dimethylsulfamoyl)-4-methylaniline	731-27-1	C10H13Cl2FN2O2S2	347.3	3.90	ESI (+) I_{Quant}: 347 → 238			

|						I$_{Qual}$: 347 → 137			
DMST	1-(dimethylsulfamoylamino)-4-methylbenzene	66840-71-9	C9H14N2O2S	214.29	1.99	ESI (+) I$_{Quant}$: 215 → 106 I$_{Qual}$: 215 → 151	0.006	0.02	DMST-D7
DMST-acid	4-([(dimethylamino)sul-fonyl]amino)benzoic acid	90250-68-3	C9H12N2O4S	244.26	1.03*	ESI (+) I$_{Quant}$: 245 → 136 I$_{Qual}$: 245 → 120	0.02	0.08	DMST-D7
N,N-DMS	*N,N*-Dimethylsulfamide	3984-14-3	C2H8N2O2S	124.17	-1.11*	ESI (+) I$_{Quant}$: 125 → 125 I$_{Qual}$: 125 → 108	10.6	35.4	Pyridine-D5
Tralopyril	4-bromo-2-(4-chlorophenyl)-5-(trifluoromethyl)-1*H*-pyrrole-3-carbonitrile	122454-29-9	C12H5BrClF3N2	349.53	3.47	ESI (-) I$_{Quant}$: 347 → 131 I$_{Qual}$: 347 → 79			
BCCPCA	3-bromo-5-(4-chlorophenyl)-4-cy-ano-1*H*-pyrrole-2-carboxylic acid	890044-32-3	C12H6BrClN2O2	325.54	0.54	ESI (-) I$_{Quant}$: 325 → 81 I$_{Qual}$: 325 → 281	0.18	0.61	Propicona-zole-D5

|								
Medetomidine	5-[1-(2,3-dimethylphenyl)ethyl]-1*H*-imidazole	86347-14-0	C13H16N2	200.28	2.60**	ESI (+) I_{Quant}: 201 → 68 I_{Qual}: 201 → 95	0.04	0.12	Medetomidine-D3
hydroxymedetomidine	[3-[1-(1*H*-imidazol-5-yl)ethyl]-2-methylphenyl]methanol	128366-50-7	C13H16N2O	216.28	2.36*	ESI (+) I_{Quant}: 217 → 199 I_{Qual}: 217 → 95	0.008	0.03	Medetomidine-D3
Medetomidine-acid	3-(1-(1H-imidazol-5-yl)ethyl)-2-methylbenzoic acid	128366-51-8	C13H14N2O2	230.26	2.82*	ESI (+) I_{Quant}: 231 → 68 I_{Qual}: 231 → 170	0.03	0.08	Medetomidine-D3

* Derived from US EPA EPISuite

** pH-sensitive, recorded at pH 7, 20 °C

Appendix 1.2   Synthesis of BCCPCA

BCCPCA (the hydrolysis product of tralopyril) was synthesized using the methods described under 4.1 in-house synthesis of BCCPCA. It was clear that BCCPCA was synthesized successfully since its expected peaks at 323/325/327 where readily apparent (Appendix figure 1.1). Additional peaks at 337/339/341 correspond the addition of a methyl group on the carboxyl group of BCCPCA, this is caused by the use of methanol during the synthesis procedure. Tralopyril was also found at 347/349/351 indicating that Tralopyril was not hydrolysed completely during the procedure, in the future, a longer incubation would be required (now 48 hours was used). Products from 279/281/283 correspond to BCCPCA without the carboxylic group, and might be a secondary hydrolysis product. However, relatively little was formed and the retention time of 279/281/283 coincides exactly with that of BCCPCA and it was therefore considered an in source product. The peaks at 383/385/387 are also likely in source products or by-products of the synthesis procedure (structure remains unclear).
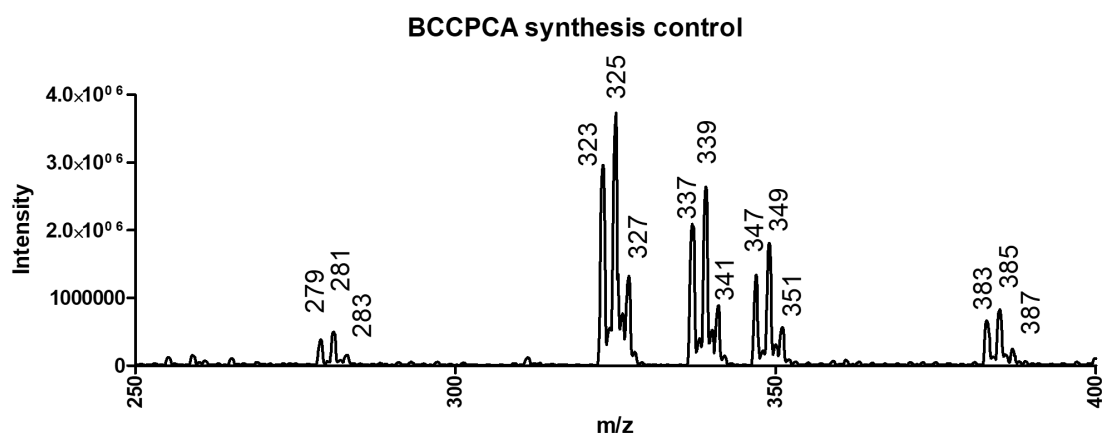
Appendix figure 1.1: Q1 scan of BCCPCA after synthesis, but before purification.
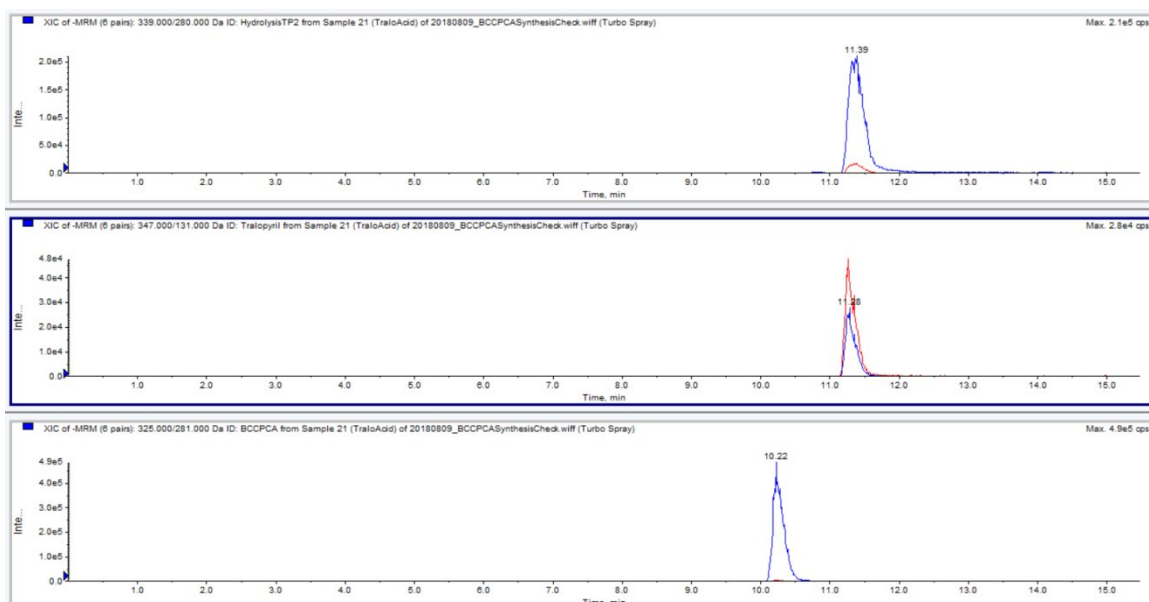
Appendix figure 1.2: Chromatographic separation of BCCPCA from tralopyril and byproduct (337/339/341). BCCPCA (bottom) shows a clearly different retention time from tralopyril (top) and the synthesis byproduct (middle). Chromatographic separation was important for collecting the BCCPCA fraction, yielding a pure BCCPCA standard for working with.

Appendix 2.   Monitoring

Appendix 2.1   Precise monitoring locations

Supplementary Table 2.1: Marinas, sampling sites and the water/sediment properties

Sample	Collection date	Latitude	Longitude	Salinity (PSU)	Temperature (°C)	Wind (m s^{-1})	WindDir (°)	NPOS (mg/L)	Nitrogen (mg/L)	TOC (g/kg sediment)
Roskilde 1	21-03-2019	55.652459	12.074277							29.43
Roskilde 2	21-03-2019	55.652168	12.074899							26.81
Roskilde 3	21-03-2019	55.652132	12.075275							29.85
Roskilde 4	16-05-2019	55.652459	12.074277							26.95
Roskilde 5	16-05-2019	55.652168	12.074899							
Roskilde 6	16-05-2019	55.652132	12.075275							
Roskilde 7	12-06-2019	55.652459	12.074277							
Roskilde 8	12-06-2019	55.652168	12.074899							
Roskilde 9	12-06-2019	55.652132	12.075275							
Roskilde 10	19-07-2019	55.652459	12.074277	12.39	20	4.2	315	4.751	1.572	
Roskilde 11	19-07-2019	55.652168	12.074899	12.39	20	4.2	315	4.751	1.572	
Roskilde 12	19-07-2019	55.652132	12.075275	12.39	20	4.2	315	4.751	1.572	
Roskilde 13	13-09-2019	55.652459	12.074277	13.64	14.8	7.7	315	7.309	0.685	
Roskilde 14	13-09-2019	55.652168	12.074899	13.64	14.8	7.7	315	7.309	0.685	
Roskilde 15	13-09-2019	55.652132	12.075275	13.64	14.8	7.7	315	7.309	0.685	
Roskilde 16	14-11-2019	55.652459	12.074277	13.14	5.9	3.0	225	6.427	0.7598	
Roskilde 17	14-11-2019	55.652168	12.074899	13.14	5.9	3.0	225	6.427	0.7598	
Roskilde 18	14-11-2019	55.652132	12.075275	13.14	5.9	3.0	225	6.427	0.7598	
Roskilde 19	15-01-2020	55.652132	12.075275							
Roskilde 20	15-01-2020	55.652132	12.075275							
Roskilde 21	15-01-2020	55.652132	12.075275							

Supplementary Table 2.1: Marinas, sampling sites and the water/sediment properties (continued)

Brøndby 1	21-03-2019	55.608633	12.441397							17.34
Brøndby 2	21-03-2019	55.608784	12.442212							22.41
Brøndby 3	21-03-2019	55.608833	12.443038							19.71
Brøndby 4	16-05-2019	55.608633	12.441397							21.86
Brøndby 5	16-05-2019	55.608784	12.442212							
Brøndby 6	16-05-2019	55.608833	12.443038							
Brøndby 7	12-06-2019	55.608633	12.441397							
Brøndby 8	12-06-2019	55.608784	12.442212							
Brøndby 9	12-06-2019	55.608833	12.443038							
Brøndby 10	19-07-2019	55.608633	12.441397	10.44	21.5	4.2	315	5.886	0.9525	
Brøndby 11	19-07-2019	55.608784	12.442212	10.44	21.5	4.2	315	5.886	0.9525	
Brøndby 12	19-07-2019	55.608833	12.443038	10.44	21.5	4.2	315	5.886	0.9525	
Brøndby 13	13-09-2019	55.608633	12.441397	6.94	15.7	8.1	315	3.688	0.3967	
Brøndby 14	13-09-2019	55.608784	12.442212	6.94	15.7	8.1	315	3.688	0.3967	
Brøndby 15	13-09-2019	55.608833	12.443038	6.94	15.7	8.1	315	3.688	0.3967	
Brøndby 16	14-11-2019	55.652459	12.074277	8.135	7.1	3.0	225	4.337	0.3864	
Brøndby 17	14-11-2019	55.652168	12.074899	8.135	7.1	3.0	225	4.337	0.3864	
Brøndby 18	14-11-2019	55.652132	12.075275	8.135	7.1	3.0	225	4.337	0.3864	
Brøndby 19	15-01-2020	55.652132	12.075275							
Brøndby 20	15-01-2020	55.652132	12.075275							
Brøndby 21	15-01-2020	55.652132	12.075275							
Køge 1	02-07-2019	55.468900	12.197140	4.879	14.3	9.4	180	5.637	1.817	
Køge 2	02-07-2019	55.469460	12.195100	4.879	14.3	9.4	180	5.637	1.817	
Køge 3	02-07-2019	55.469070	12.196880	4.879	14.3	9.4	180	5.637	1.817	
Faxe 1	02-07-2019	55.213280	12.159800	8.919	14.7	8.8	180	4.688	3.185	
Faxe 2	02-07-2019	55.213680	12.159840	8.919	14.7	8.8	180	4.688	3.185	
Faxe 3	02-07-2019	55.213490	12.160250	8.919	14.7	8.8	180	4.688	3.185	
Vordingborg 1	02-07-2019	55.003300	11.917920	6.283	15.8	8.6	180	4.562	4.099	
Vordingborg 2	02-07-2019	55.003390	11.918780	6.283	15.8	8.6	180	4.562	4.099	
Vordingborg 3	02-07-2019	55.003780	11.916890	6.283	15.8	8.6	180	4.562	4.099	

Supplementary Table 2.1: Marinas, sampling sites and the water/sediment properties (continued 2)

Holbæk 1	10-07-2019	55.723790	11.760240	19.89	16.1	5.9	180	5.841	1.062	
Holbæk 2	10-07-2019	55.723420	11.760220	19.89	16.1	5.9	180	5.841	1.062	
Holbæk 3	10-07-2019	55.723060	11.760140	19.89	16.1	5.9	180	5.841	1.062	
Kalundborg 1	10-07-2019	55.677990	11.072570	13.73	17.2	5.0	180	5.614	2.055	
Kalundborg 2	10-07-2019	55.677540	11.072730	13.73	17.2	5.0	180	5.614	2.055	
Kalundborg 3	10-07-2019	55.677390	11.073960	13.73	17.2	5.0	180	5.614	2.055	
Korsør 1	10-07-2019	55.326850	11.130240	16.14	19.5	5.5	135	5.529	2.663	
Korsør 2	10-07-2019	55.327530	11.129840	16.14	19.5	5.5	135	5.529	2.663	
Korsør 3	10-07-2019	55.327620	11.130810	16.14	19.5	5.5	135	5.529	2.663	
Frederikssund 1	16-07-2019	55.828450	12.061210	16.51	13.5	3.3	180	5.342	1.758	
Frederikssund 2	16-07-2019	55.827710	12.060940	16.51	13.5	3.3	180	5.342	1.758	
Frederikssund 3	16-07-2019	55.827390	12.060660	16.51	13.5	3.3	180	5.342	1.758	
Gilleleje 1	16-07-2019	56.127000	12.311980	17.07	14.2	3.2	225	4.68	4.228	
Gilleleje 2	16-07-2019	56.126280	12.311800	17.07	14.2	3.2	225	4.68	4.228	
Gilleleje 3	16-07-2019	56.126000	12.312310	17.07	14.2	3.2	225	4.68	4.228	
Rungsted 1	16-07-2019	55.886370	12.546590	8.894	16.0	2.5	225	6.096	0.6118	
Rungsted 2	16-07-2019	55.886690	12.545900	8.894	16.0	2.5	225	6.096	0.6118	
Rungsted 3	16-07-2019	55.886690	12.545000	8.894	16.0	2.5	225	6.096	0.6118	
Langelinie 1	16-07-2019	55.695840	12.600330	10.49	18.0	4.5	225	6.219	0.7436	
Langelinie 2	16-07-2019	55.703010	12.601050	10.49	18.0	4.5	225	6.219	0.7436	
Langelinie 3	16-07-2019	55.703490	12.601250	10.49	18.0	4.5	225	6.219	0.7436	
Sydhavnen 1	13-09-2019	55.641446	12.543267	15.37	17.3	8.0	315	3.644	0.2935	
Sydhavnen 2	13-09-2019	55.642167	12.543194	15.37	17.3	8.0	315	3.644	0.2935	
Sydhavnen 3	13-09-2019	55.642561	12.541776	15.37	17.3	8.0	315	3.644	0.2935	

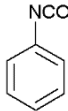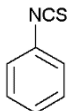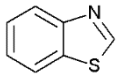Supplementary Table 2.1: Marinas, sampling sites and the water/sediment properties (continued 3)
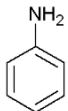
Transect Roskilde 1	31-07-2019	55.60806	12.44139	14.03				8.597	0.8065	
Transect Roskilde 2	31-07-2019	55.60806	12.44139	14.03				8.597	0.8065	
Transect Roskilde 3	31-07-2019	55.6075	12.44139	14.15				9.186	0.8484	
Transect Roskilde 4	31-07-2019	55.6075	12.44139	14.15				9.186	0.8484	
Transect Roskilde 5	31-07-2019	55.60667	12.43861	14.09				7.475	0.9757	
Transect Roskilde 6	31-07-2019	55.60667	12.43861	14.09				7.475	0.9757	
Transect Roskilde 7	31-07-2019	55.60389	12.43611	5.96				3.900	0.5121	
Transect Roskilde 8	31-07-2019	55.60389	12.43611	5.96				3.900	0.5121	
Transect Roskilde 9	31-07-2019	55.59667	12.42972	13.33				7.792	0.8963	
Transect Roskilde 10	31-07-2019	55.59667	12.42972	13.33				7.792	0.8963	
Transect Roskilde 11	31-07-2019	55.59083	12.42444	60				7.613	0.7959	
Transect Roskilde 12	31-07-2019	55.59083	12.42444	13.09				7.613	0.7959	

Supplementary Table 2.1: Marinas, sampling sites and the water/sediment properties (continued 4)

Transect Brøndby 1	03-10-2019	55.65194	12.075	10.1				3.842	0.3447	
Transect Brøndby 2	03-10-2019	55.65194	12.075	10.1				3.842	0.3447	
Transect Brøndby 3	03-10-2019	55.65222	12.07611	12.47				4.262	0.2834	
Transect Brøndby 4	03-10-2019	55.65222	12.07611	12.47				4.262	0.2834	
Transect Brøndby 5	03-10-2019	55.65306	12.07639	12.6				4.153	0.2821	
Transect Brøndby 6	03-10-2019	55.65306	12.07639	12.6				4.153	0.2821	
Transect Brøndby 7	03-10-2019	55.65389	12.07639	11.55				3.298	0.2131	
Transect Brøndby 8	03-10-2019	55.65389	12.07639	11.55				3.298	0.2131	
Transect Brøndby 9	03-10-2019	55.65583	12.07639	10.58				4.132	0.3358	
Transect Brøndby 10	03-10-2019	55.65583	12.07639	10.58				4.132	0.3358	
Transect Brøndby 11	03-10-2019	55.6575	12.07694	9.033				5.059	0.738	
Transect Brøndby 12	03-10-2019	55.6575	12.07694	9.033				5.059	0.738	

Appendix 3. Photo degradation

Table Appendix 3.1. Previously identified compounds.

Compound	Structure	Confidence	Reaction	Reference
Phenyl isocyanate		Level 1	UV-light, acetone	Clark and Watkins, 1978
Dimethylamidosulphonyl chloride		Level 1	UV-light, acetone	Clark and Watkins, 1978
Phenyl isothiocyanate		Level 1	UV-light, acetone	Clark and Watkins, 1978
Benzothiazole		Level 1	Simulated solar irradation, water, TiO_2	Sakkas and Albanis, 2003
Aniline		Level 1	Simulated solar irradation, water, TiO_2	Sakkas and Albanis, 2003
Dichlorofluoromethane		Level 2	Simulated solar irradation, water, TiO_2	Sakkas and Albanis, 2003

References

Clark, T., Watkins, D.A.M., 1978. Photolysis of Dichlofluanid. Pestic. Sci. 9, 225–228.

Sakkas, V.A., Albanis, T.A., 2003. Photocatalyzed degradation of the biocides chlorothalonil and dichlofluanid over aqueous TiO2 suspensions. Appl. Catal. B Environ. 46, 175–188.
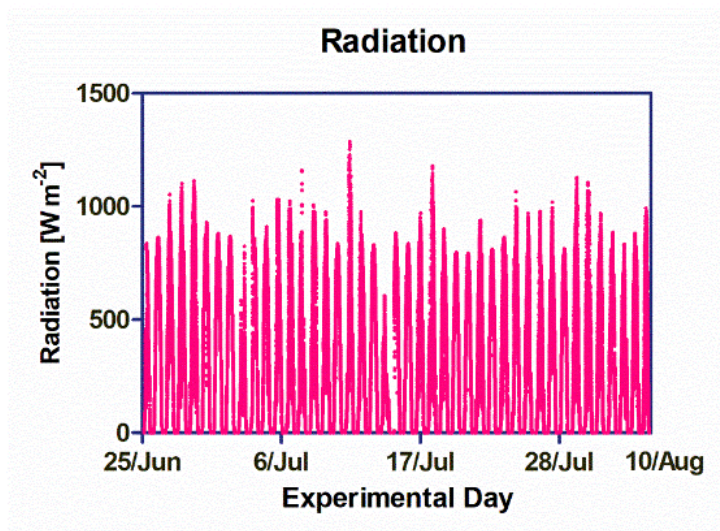
Figure Appendix 3.1. Radiation of natural sunlight during experimental days.

Table Appendix 3.2. LOQ and LOD of transformation products.

Compound	LOD [µg/L]	LOQ [µg/L]
Dichlofluanid	0.9	2.7
Tolylfluanid	0.9	2.7
DMSA	0.5	0.9
DMST	0.5	1.0
N,N-Dimethyl-1,3-benzothiazol-2-amine (DBZA)	0.3	0.3
N,N-Dimethyl-2-benzothiazolamine (2HBT)	1.1	3.2
[(2-Chloro-4-methylphenyl)sulfamoyl] dimethylamine (CMSD)	1.0	3.0
6-Methyl-3H-1,3-benzothiazol-2-one (MBZO)	1.0	3.0
5-Amino-2-methylphenol	0.9	2.7
p-Toluidine	0.9	2.8
Medetomidine-d3	0.2	0.6
Carbendazim-d4	0.6	1.8

Table Appendix 3.3. MS details for tolylfluanid, dichlofuanid and their transformation products by API4000 triple quadrupole MS (DP: declustering potential, EP: entrance potential, CE: collision energy, CXP: collision cell exit potential).

Compound	Precursor Ion	Product Ions	DP [V]	EP [V]	CE [V]	CXP [V]
Dichlofluanid	333	224	32	8	16	14
		123	31	7	37	21
Tolylfluanid	347	238	25	8	15	16
		137	35	3	33	15
DMSA	201	137	37	8	14	8
		92	39	6	25	8
DMST	215	151	30	10	10	18
		106	20	11	20	12
DMS	125	125	71	10	8	12
		108	50	10	15	12
		80	45	5	35	12
N,N-Dimethyl-1,3-benzothiazol-2-amine (DBZA)	179	164	50	10	30	12
		136	50	10	30	12
1,3-benzothiazol-2(*3H*)-one (2HBT)	152	124	69	13	28	10
		119	54	10	33	20
[(2-Chloro-4-methylphenyl)sulfamoyl] dimethylamine (CMSD)	249	140	50	10	30	12
		113	50	10	30	12
6-Methyl-3H-1,3-benzothiazol-2-one (MBZO)	166	138	50	10	30	12
		106	50	10	30	12
N,N,6-trimethyl-2-oxo-2,3-dihydro-1,3-benzothiazole-3-sulfonamide (TDBS)	273	164	50	10	30	12
		108	50	10	30	12
5-Amino-2-methylphenol	124	109	35	8	27	20
		77	31	9	34	14
p-Toluidine	108	93	32	10	25	12
		65	44	11	36	5
Medetomidine-d3	204	98	44	8	25	18
		71	44	7	25	13
Carbendazim-d4	196	164	78	10	28	11
		136	81	10	45	13
Pyridine-d5	101	84	45	4	28	16
		56	56	10	44	10
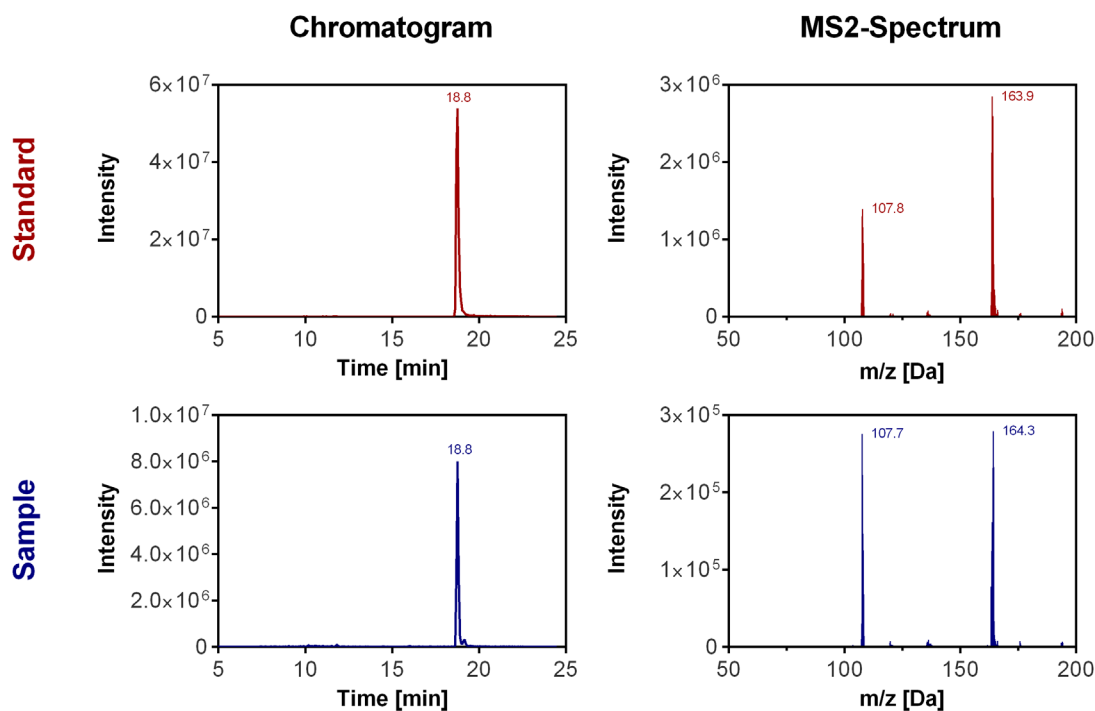
Figure Appendix 3.2. Comparison of chromatogram and MS2 fragmentation of N,N,6-trimethyl-2-oxo-2,3benzothiazole-3-sulfonamide (TDBS) in standard (top) and samples (bottom).
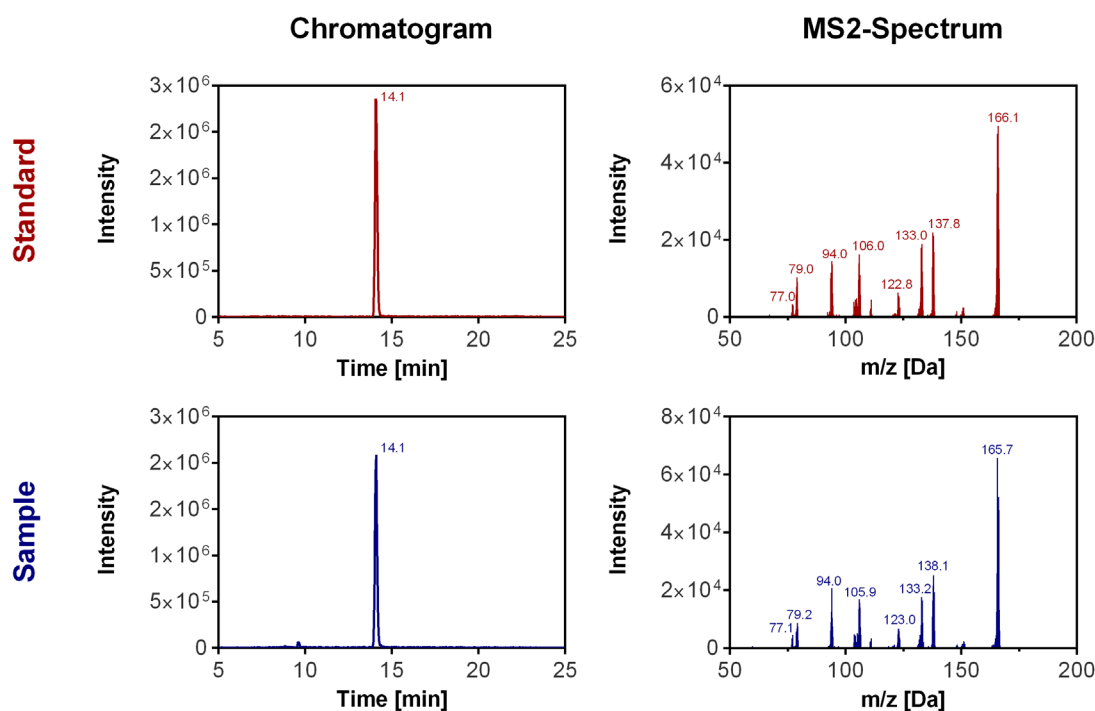
Figure Appendix 3.3. Comparison of chromatogram and MS2 fragmentation of 6-methyl-1,3-benzothiazol-2(3H)-one (MBZO) in standard (top) and samples (bottom).
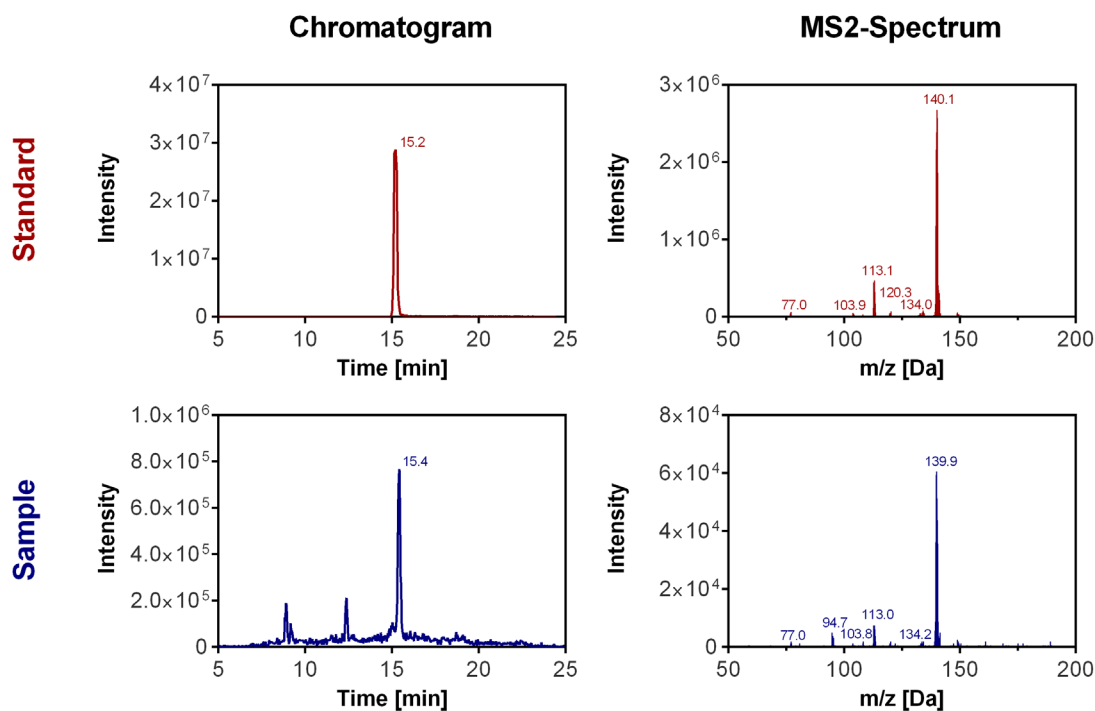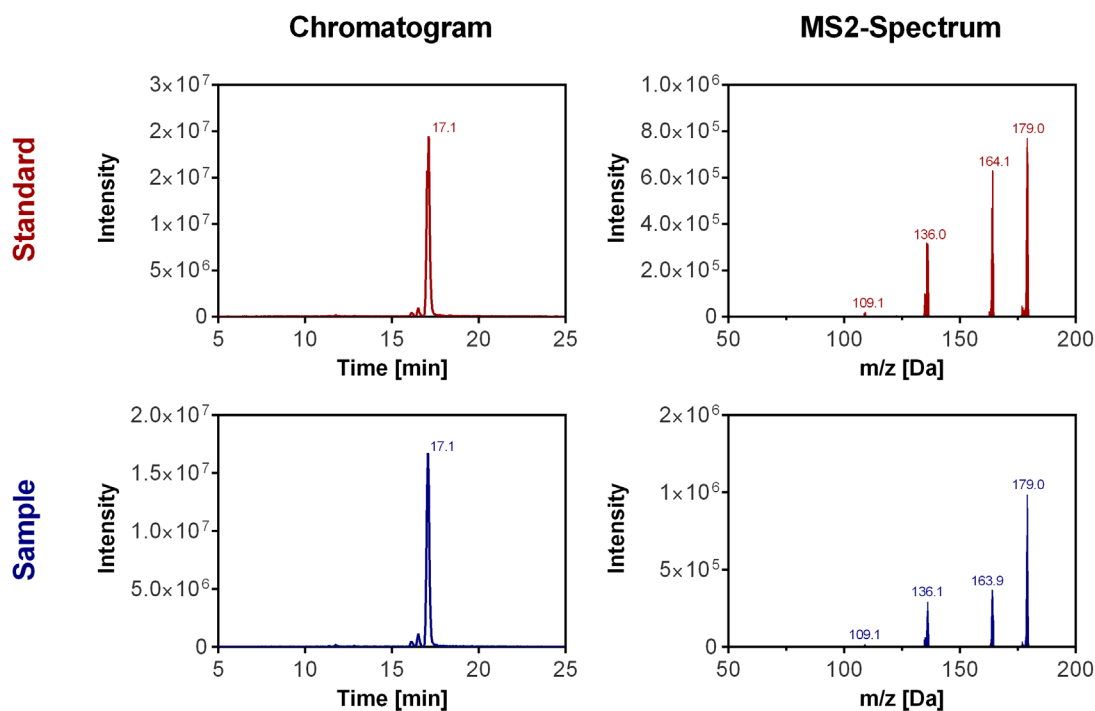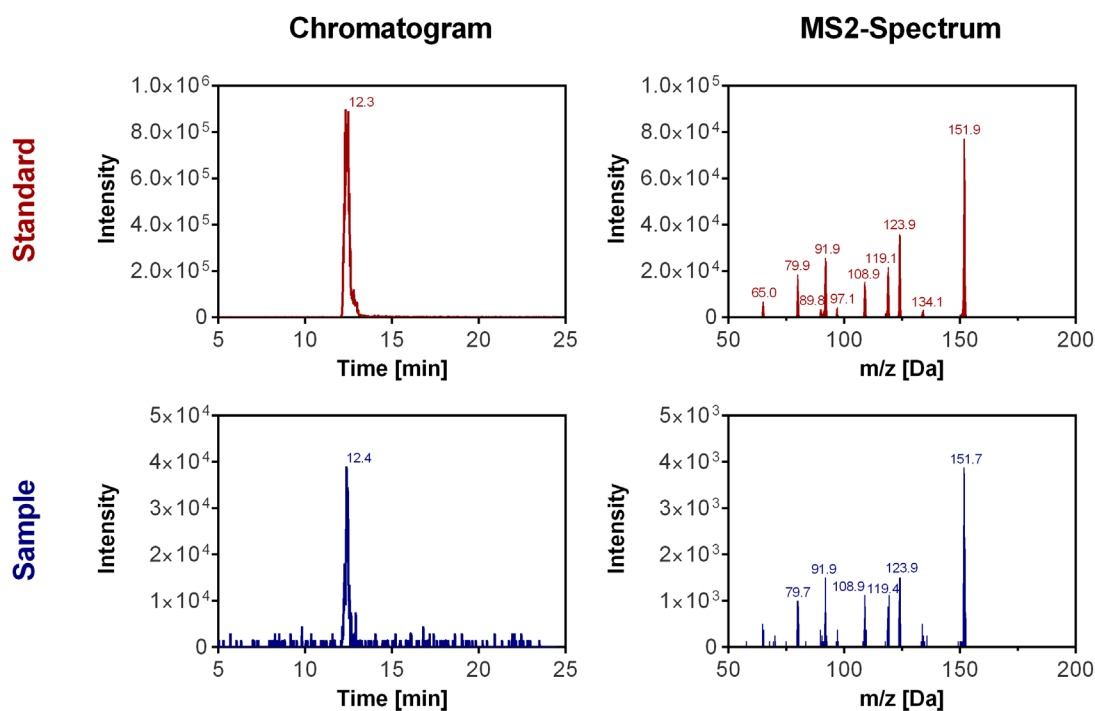
Chromatogram

MS2-Spectrum

Figure Appendix 3.4. Comparison of chromatogram and MS2 fragmentation of N'-(2-chloro-4-methyl-phenyl)-N,N-dimethylsulfuric diamide (CMSD) in standard (top) and samples (bottom).

Chromatogram

MS2-Spectrum
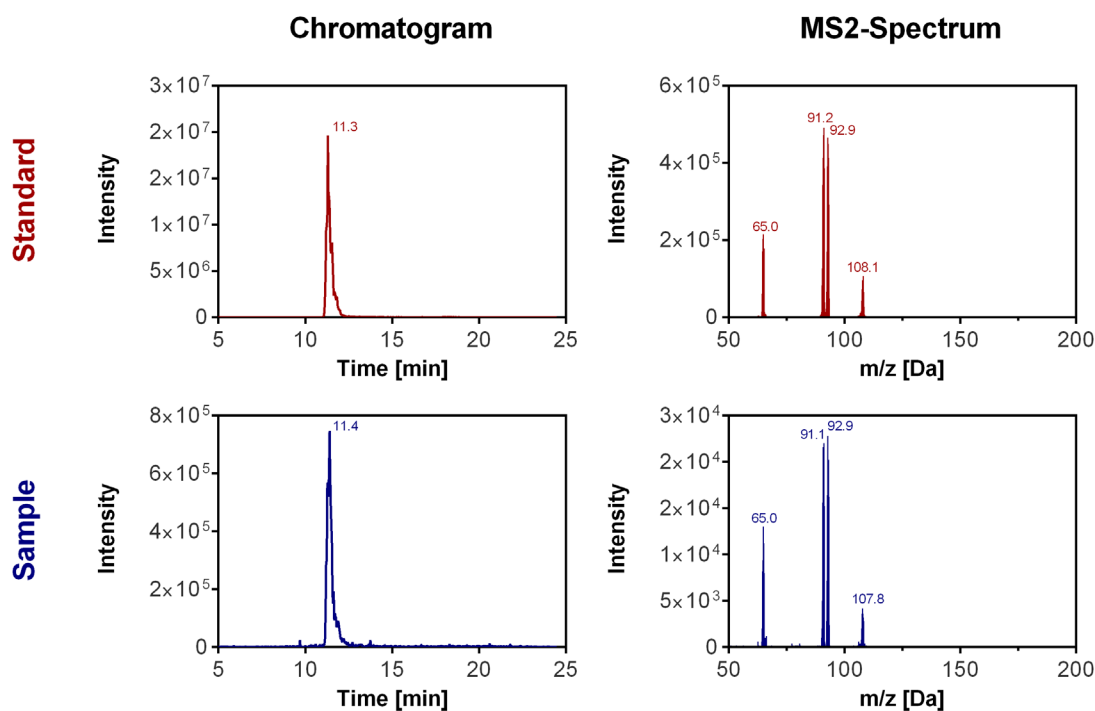
Figure Appendix 3.5. Comparison of chromatogram and MS2 fragmentation of p-toluidine in standard (top) and samples (bottom).

Figure Appendix 3.6. Comparison of chromatogram and MS2 fragmentation of N,N-dimethyl-1,3-benzothiazol-2-amine (DBZA) in standard (top) and samples (bottom).

Figure Appendix 3.7. Comparison of chromatogram and MS2 fragmentation of 1,3-Benzothiazol-2(3H)-one (2HBT) in standard (top) and samples (bottom).
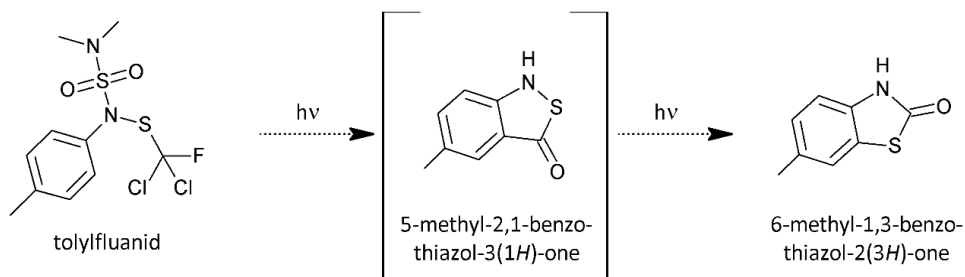
Figure Appendix 3.8. Proposed photoisomerization of tolylfluanid to 6-methyl-1,3-benzothia-zol-2(*3H*)-one.
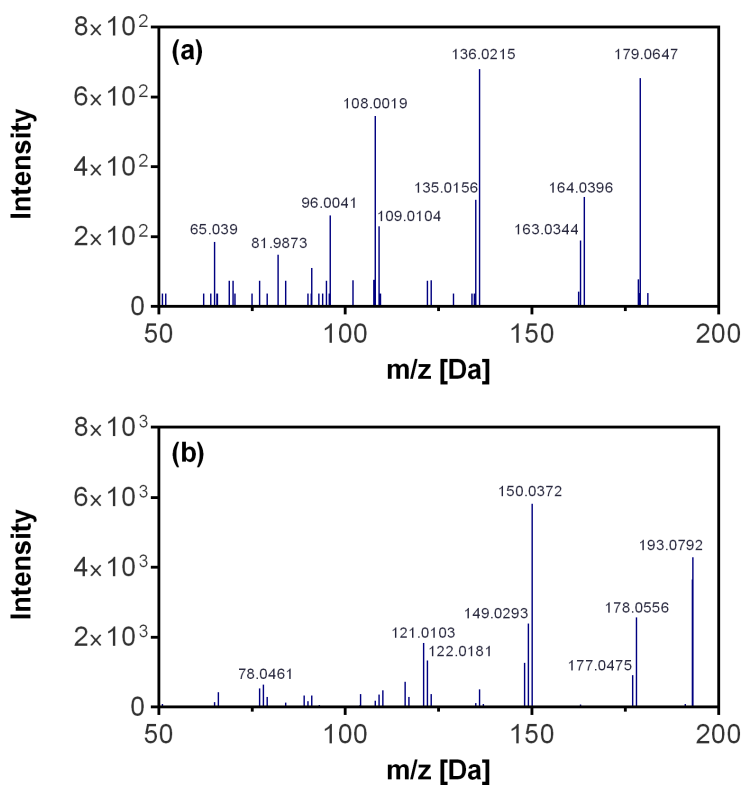
Figure Appendix 3.9. Comparison of the MS2-fragmentation of (a) N,N-dimethyl-1,3-benzo-thiazol-2-amine (DBZA, m/z: 179.0647) and (b) N,N,6-trimethylbenzo[d]thiazol-2-amine (m/z: 193.0794).
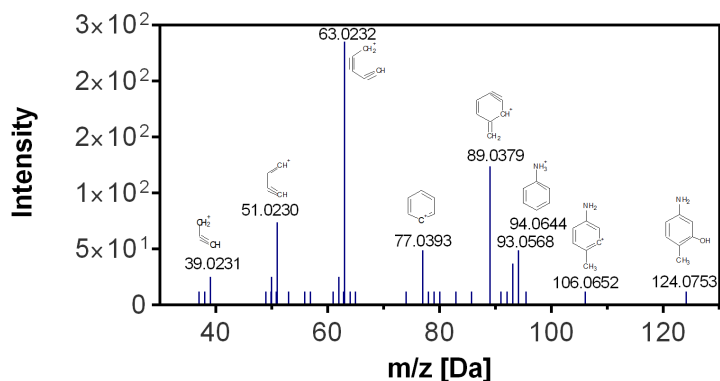
Figure Appendix 3.10. MS2-fragmentation pattern of TP124 from tolylfluanid, tentatively iden-tified as 5-Amino-2-methylphenol (5A2MP, m/z 124.0753).
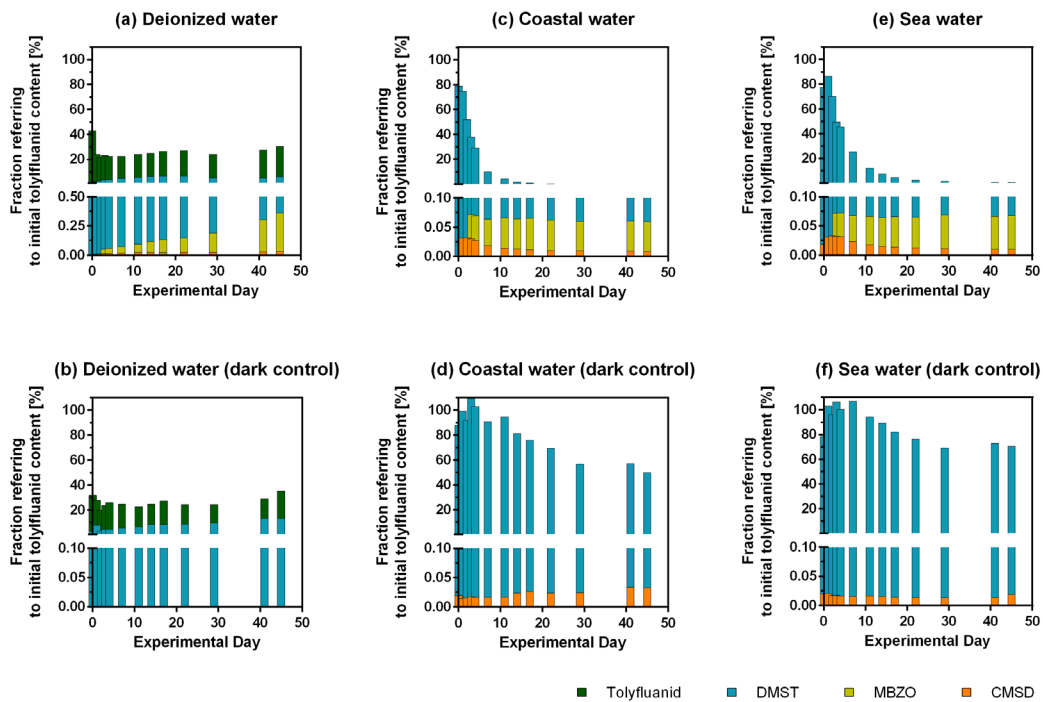
Figure Appendix 3.11. Mass balance of tolylfluanid in deionized water (a and b), coastal water (c and d), sea water (e and f); TDBS was not counted into the mass balance of tolylfluanid. Mind the different y-axis unit in a.
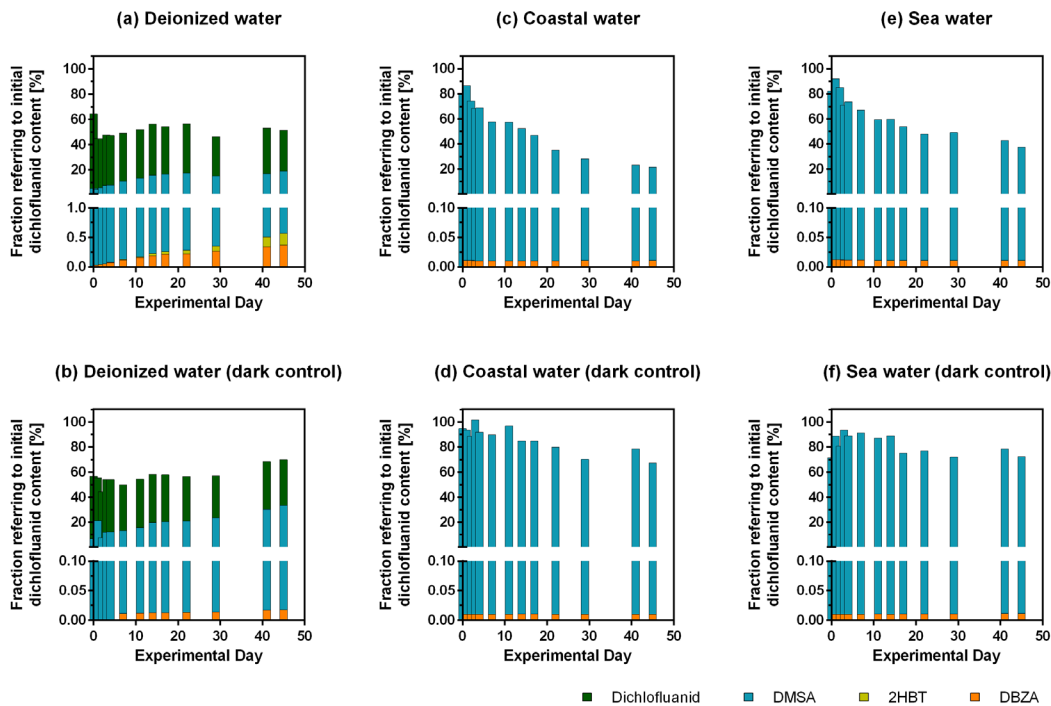
Figure Appendix 3.12. Mass balance of dichlofluanid in deionized water (a and b), coastal water (c and d), in sea water (e and f). Mind the different y-axis unit in a.
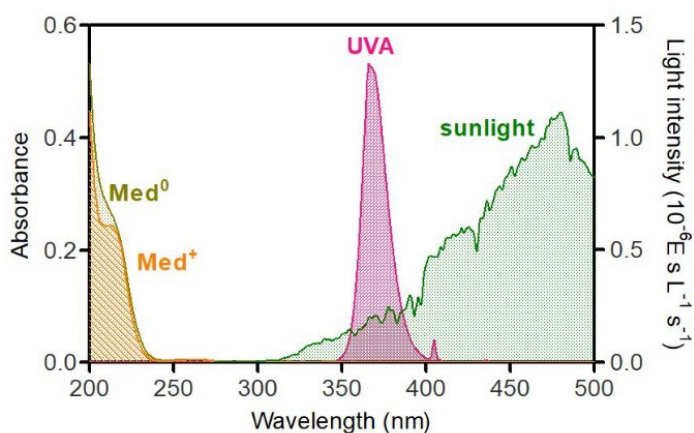
Figure Appendix 3.13. (Left y-axis) Absorbance spectra of deprotonated medetomidine (Med⁰, 20 µM at pH9.2), protonated medetomidine (Med⁺, 20 µM at pH5.1). (Right y-axis) Intensity of UVA and natural sunlight.
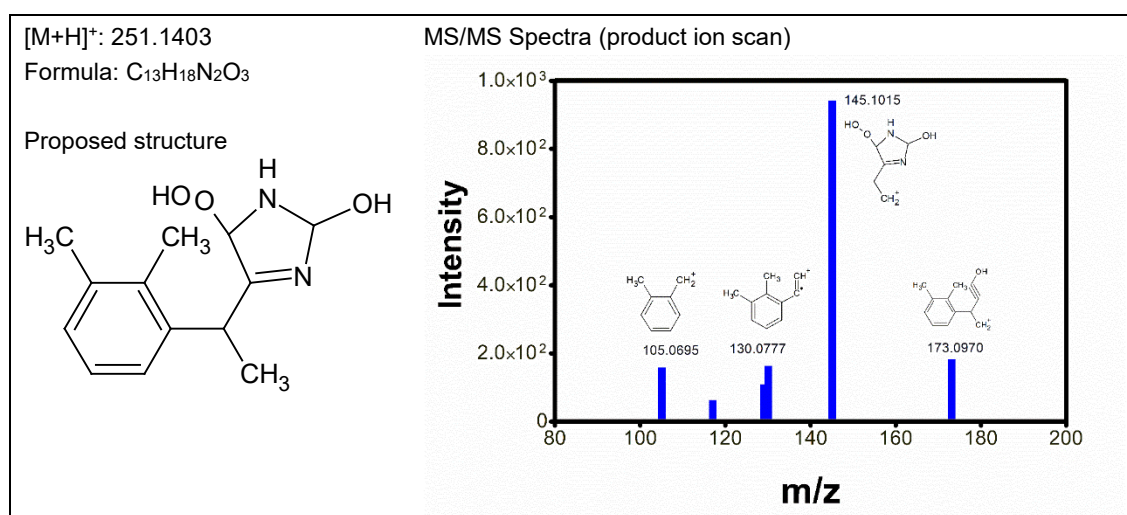

[M+H]⁺: 251.1403
Formula: $C_{13}H_{18}N_2O_3$

Proposed structure

MS/MS Spectra (product ion scan)

Figure Appendix 3.14. Structure elucidation based on the q-TOF MS/MS data of medetomidine´s photoproduct 2 (TP251).
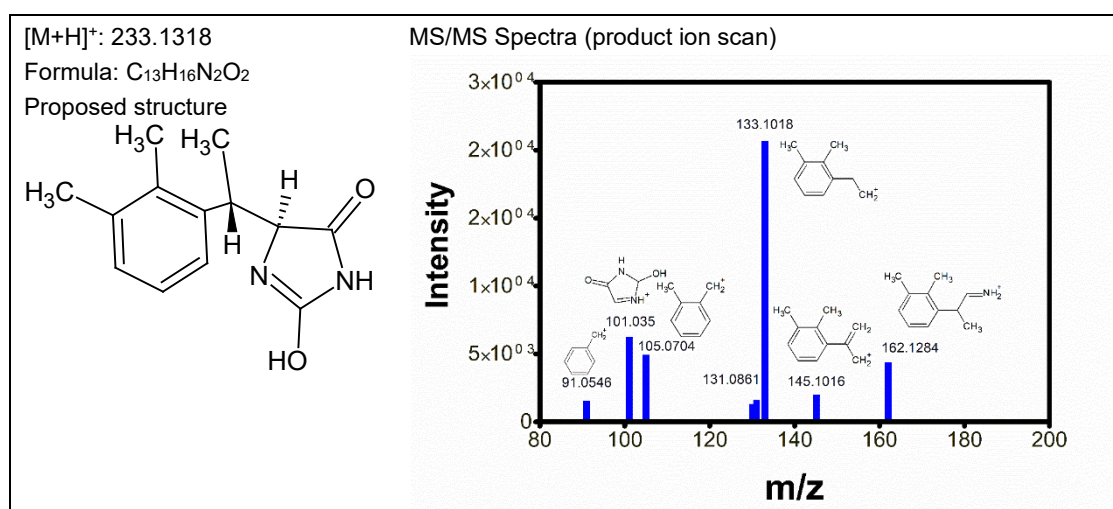

[M+H]⁺: 233.1318
Formula: $C_{13}H_{16}N_2O_2$
Proposed structure

MS/MS Spectra (product ion scan)

Figure Appendix 3.15. Structure elucidation based on the q-TOF MS/MS data of medetomidine´s photoproduct 5 (TP233-1).
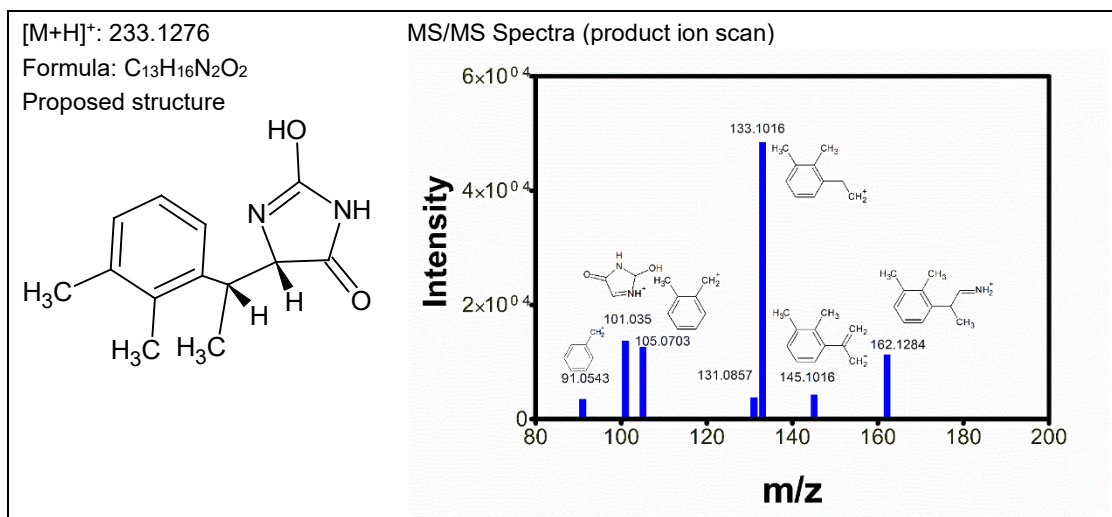
Figure Appendix 3.16. Structure elucidation based on the q-TOF MS/MS data of medetomidine´s photoproduct 6 (TP233-2).
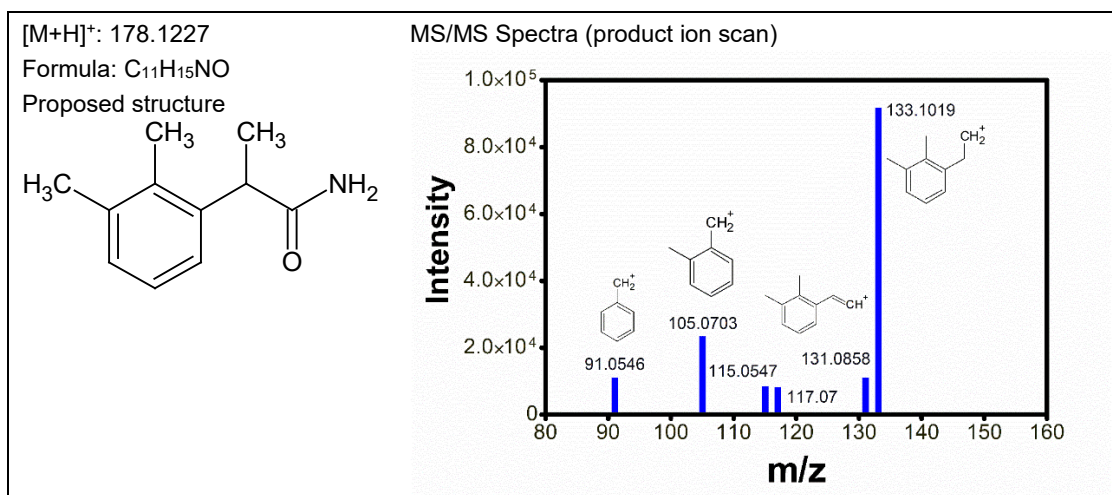

Figure Appendix 3.17. Structure elucidation based on the q-TOF MS/MS data of medetomidine´s photoproduct 10 (TP178).

Appendix 4. Leaching
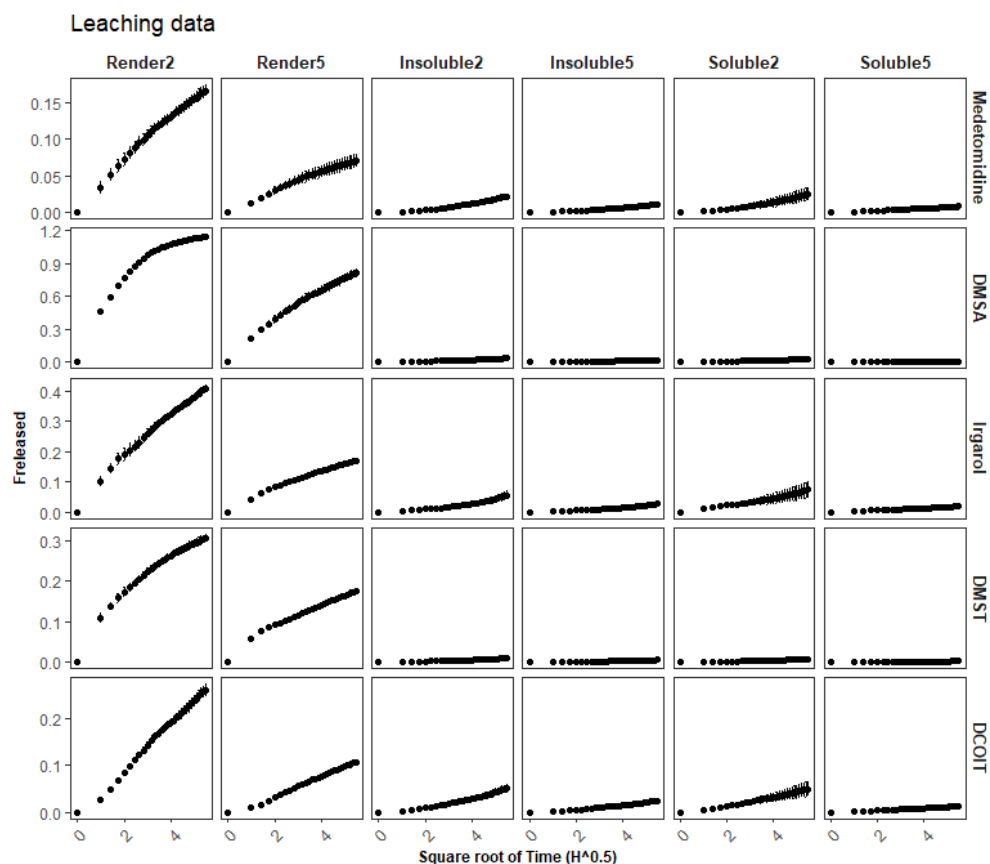
Leaching data

Figure appendix 4.1: Leaching of the other antifouling biocides. DMSA was chosen as an example under the leaching chapter. Render2 and Render5 refers to the amount of layers that was used for that paint type. All results between insoluble and soluble matrix paints were similar to those described under chapter 9. Leaching . The biocides with the fastest overall leaching rates from antifouling paints were DCOIT, Medetomidine, and Irgarol. Which stands in contrast to the leaching rates in façade (render) paints, where DMSA leached fastest. Difference might be caused due to the fact that DMSA and DMST are only formed after hydrolysis of Dichlofluanid and Tolylfluanid, therefore, leaching is measured indirectly. Nonetheless, the hydrolysis rates are fast enough so that, Dichlofluanid and Tolylfluanid hydrolyze rapidly upon release to the water.

Antifouling Biocides: Leaching, Degradation and Fate

Antifouling biocides have been used for several hundred years to protect underwater parts of ships and offshore installations against infestations of algae, fungi, mussels, and other organisms. They help to preserve the structures and they do decrease fuel consumption on ships. They also help to keep pleasure boats operational that are only operated few days a month.

Antifouling biocides are toxicants meant to adversely affect target organisms. However, they do leach into the surrounding water and also affect non-target organisms.

In general, both heavy metal-based (Copper, Chromium, Zinc) systems and organic (carbon-based) systems (TBT, Irgarol, SeaNine) are used. Opposite to the heavy metal-based systems that will stay in the environment forever, organic biocides can over time be degraded and thus rendered harmless.

While in ancient times copper plating was used, in the 20th-century organic biocides such as TBT became popular. TBT was banned as it had detrimental (estrogenic) effects on mollusks at very low concentrations. TBT was succeeded by Irgarol and SeaNine-based systems. However, with the Biocidal Product Directive of the EU also antifoulings were regulated in a new framework. Consequently, Irgarol was disputed and is no longer legally on the market.

Currently, there are Copper and Zinc-based systems, Zinc and Copper Pyrithione and a series of other new organic compounds (Dichlofluanid, Tolylfluanid, Tralopyril, and Medetomidine) on the market.

This project focused on the presence, stability, and leaching of these "new" compounds, while omitting Copper or Zinc-based systems.